Ph.D. Dissertation in Mechanical Engineering

Multi-Object Grasping Using Finger-to-Palm Translation for Pick-and-Place Tasks

손가락-손바닥 이동 동작 구현을 통해 다양한 파지 및 정렬 작업이 가능한 다물체 파지 그리퍼

February 2025

Department of Mechanical Engineering
Graduate School of Seoul National University

Jaemin Eom

Multi-Object Grasping Using Finger-to-Palm Translation for Pick-and-Place Tasks

Thesis Advisor: Kyu-Jin Cho

A dissertation submitted to the
Department of Mechanical Engineering
for the degree of
Doctor of Philosophy

October 2024

Graduate School of Seoul National University

The dissertation of Jaemin Eom
has been approved

December 2024

Chair Frank Chongwoo Park(Signature)
Vice Chair Kyu-Jin Cho (Signature)
Examiner Yong-Lae Park (Signature)
Examiner Amy Kyungwon Han (Signature)
Examiner Woongbae Kim (Signature)

Multi-Object Grasping Using Finger-to-Palm Translation for Pick-and-Place Tasks

Jaemin Eom
Department of Mechanical Engineering
Seoul National University

Abstract

Humans utilize their dexterous fingers and adaptable palm in various multi-object grasping strategies to efficiently move multiple objects together in diverse situations. In scenarios where picking and placing individual objects is crucial, humans often adopt a strategy of grasping objects one by one, temporarily storing them on the ulnar side of the palm. Subsequently, these stored objects are retrieved and placed at their intended locations one by one. This method effectively divides the hand into two functional sections: a ‘grasping section’ for picking and placing objects and a ‘storing section’ for temporary storing. The grasping section consists of fingers, and the storing section is composed of the palm and the remaining fingers. This segmentation facilitates the simultaneous handling of multiple objects while preserving the ability to perform precise pick-and-place tasks with individual objects. For functional segmentation of the hand to be effective, a method for transferring objects between the grasping and storing sections is necessary. Humans utilize in-hand translation techniques, such as finger-to-palm and palm-to-finger translations, to move objects between these sections. The finger-to-palm translation allows

the grasping section to transfer the grasped objects to the storing section for temporary storage, enabling the grasping section to freely perform various pick-and-place tasks while the storing section stores multiple objects. Moreover, the palm-to-finger translation allows the storing section to transfer stored objects to the grasping section one by one, enabling the grasping section to retrieve each object and place it in the desired position. However, conventional grippers, while able to handle multiple objects simultaneously, lack this integrated functionality, which combines the storing section's temporal storing ability with the grasping section's precise pick-and-place capability.

This dissertation introduces a multi-object gripper that applies human hand segmentation and in-hand translation to leverage the synergistic use of the grasping and storing sections for enhanced pick-and-place functionality. The proposed gripper consists of a grasping section made of four fingers and a storing section made of two pairs of adaptive conveyor belts. The fingers can pick single objects from various orientations and subsequently transfer them to the storing section through finger-to-palm translation for storing and moving them together. After moving the objects, the fingers retrieve the stored objects individually through palm-to-finger translation for placing them one by one in the desired position and orientation. Compared to the conventional single-object grasping process, the additional translating and storing processes may slow down the overall procedure. Therefore, a grasping section design for simple translation and a storing section design for simultaneous object storing and translating are proposed and analyzed. An experimental comparison shows that the proposed multi-object gripper can reduce the pick-and-place

process time by about 34% compared to single-object grasping. Furthermore, the pick-and-place versatility of the developed multi-object gripper was validated through a lab-scale domestic demonstration. Additionally, an algorithm for generating a near-optimal path was developed for real-world applications of the multi-object gripper. This algorithm was applied to the declutter problem, demonstrating the enhanced pick-and-place efficiency of the proposed gripper.

The multi-object gripper suggested in this dissertation highlights the potential of hand segmentation and in-hand translation in enhancing the functionality of multi-object grasping and broadens the applicability of multi-object grippers.

Keywords: Multi-Object Grasping, Human Hand, Robotic Gripper, Soft Robotics, Adaptive Mechanism

Student number: 2017-23593

Contents

List of Figures **v**

List of Tables **xxviii**

1 Introduction **1**

1.1 Background 1

1.1.1 Robotic Pick-and-Place Tasks 1

1.1.2 Multi-Object Grasping in Unstructured Environments . 6

1.1.3 Humans' Manipulation Skills 11

1.1.4 Underactuated Gripper and Robotic Hand 14

1.2 Problem Definition 15

1.3 Contributions 17

2 Design of Multi-Object Gripper Utilizing Finger-to-Palm Translation **19**

2.1 Gripper Design and Grasping Strategy 19

2.1.1 Background 19

2.1.2 Gripper Design 23

2.1.3 Grasping Strategy 26

2.2 Grasping Section Design 28

2.2.1 Background 28

2.2.2 Decoupling Linkage Design for Motion Decouple 30

2.3 Storing Section Design 32

2.3.1 Background 32

2.3.2 Conveyor Palm Design with Hairy Belt 33

2.3.3 Fabrication 33

2.3.4 Replaceable Design of the Conveyor Palm 36

3 Analysis of Grasping Section and Storing Section 38

3.1 Design Condition of Decoupling Links 38

3.1.1 Design Condition for Decoupling Grasping and Translation 38

3.1.2 Finger movements according to design variations in the decoupling links 44

3.1.3 Experimental Validation of Decoupling Links' Design Condition 50

3.2 Grasping Force Test 54

3.2.1 Maximum Grasping Force 54

3.2.2 Cyclic Grasping Test 57

3.3 Storing Force of Conveyor Palm 65

3.3.1 Parameter Selection 65

3.3.2 The Upper and Lower Limits of Storable Objects by the Conveyor Palm 68

3.3.3 Transverse Storing Force Varying Geometric Parameters 73

3.3.4 Longitudinal Storing Force Varying Geometric Parameters 78
3.3.5 Storing Force According to Material Parameter 85
3.3.6 Theoretical Analysis of Conveyor Palm Scalability . . . 91
3.3.7 Simultaneous Storing Capability 94
3.3.8 Design Guidelines of Conveyor Palm 97
3.4 Success Rate and Placement Error 100
3.4.1 Grasping with Center of Mass 100
3.4.2 Off-Centered Grasping 105
3.5 Position Error of Palm-to-Finger Translation 109
3.6 Validation through Lab-Scale Demonstrations 116
3.6.1 Comparison with Single-Object Gripper 116
3.6.2 Theoretical Efficiency Comparison with other Multi-Object Grasping Methods 121
3.6.3 Pick-and-Place Versatility 124

4 Path Planning for Proposed Multi-Object Gripper 128
4.1 Background 128
4.1.1 Real World Applications for Multi-Object Grasping . . 130
4.2 Problem Definition 138
4.2.1 Declutter Problem 138
4.2.2 Storing Capacity 141
4.2.3 Problem Definition of Declutter Problem using Proposed Multi-Object Gripper 146
4.3 Results 149
4.3.1 Path Planning Pipeline 149

4.3.2 Path Planning using Genetic Algorithm 152
4.3.3 Comparison with Paths Generated by Other Methods . 152
4.3.4 Comparison of Path Efficiency According to Storage Capacity 159
4.4 Summary 166

5 Conclusion 167

5.1 Summary 167
5.2 Limitation and Future Work 170

References 173

A Experiments for Analyzing Material Properties 191

B Another Fabrication Method: 3D Printed Conveyor Palm 198

C Methods for Storing Objects More Greedily 200

List of Figures

1.1 **Robotic applications in industry.** 3

1.2 **Detailed classification of robotic pick-and-place applications.** 4

1.3 **Conventional solution for efficient pick-and-place tasks: industrial multi-object grasping.** 5

1.4 **Open problems for multi-object grasping.** 7

1.5 **Types of conventional multi-object grippers.** These include grippers that sweep multiple objects on the same plane and then pick them up all at once [26], [37], and grippers that utilize the redundancy of the hand to sequentially pick up objects and move them all at once [39]. 8

1.6 **Human multi-object gripping strategy targeting more unstructured environments than the task environment of existing gripping solutions.** (**A**) Segmentation of the hand into the radial and ulnar sides. The radial side serves the role of grasping the object, while the ulnar side stably stores it [44]. Through object translation between these two sides, the radial side can sequentially store the grasped objects on the ulnar side, and after storage, the radial side can perform a new grip. (**B**) The process of human finger to palm translation [49]. 13

2.1 **Multi-object gripper inspired by humans' multi-object grasping utilizing in-hand translations.** (**A**) The sequence of human multi-object grasping method utilizing the translation movement of the finger allows for synergistic use of the finger and palm. (**B**) The concept of the proposed multi-object gripper corresponds to human strategy. The proposed gripper utilizes the pinch translation of the finger to store or retrieve objects for picking and placing each object. 21

2.2 **Proposed gripper design to address the issues with multi-object grasping using in-hand translation.** Firstly, a finger design capable of stable pinch translation is presented. Secondly, a hairy belt design is proposed, enabling active exchange of objects between the grasping section and allowing simultaneous storage of multiple objects. Finally, aligning the translation directions of both sections facilitates easy object transfer between them. 22

2.3 **Comparison of the manipulator's travel distances between single-object grasping and multi-object grasping.** 23

2.4 **Design of multi-object gripper utilizing in-hand translations.** (**A**) Overall design of the developed gripper. (**B**) Detailed design of a single finger. A finger made of a parallelogram linkage is placed on the slider, and a grasping tendon and a translating tendon are each connected with the finger and slider, creating rotation and translation of the finger. (**C**) Detailed design of the palm. The palm consists of two belts facing each other, and each belt has an array of elastomeric hairs on its surface. (**D**) The anchoring of the grasping tendon and the translating tendon. Four grasping tendons are underactuated using a moving pulley mechanism for adaptive grasping, while the four translating tendons are directly connected to the same pulley to ensure an equal translation distance for all four fingers. 25

2.5 **Grasping strategy of multi-object gripper utilizing in-hand translations.** The fingers grasp and transfer the object to the storage, and the palm inserts the object between the elastomeric hairs and stores it. By repeating the above procedure, the gripper can store multiple objects and transfer them at once and retrieve to place the objects with the reverse process. . . . 27

2.6 **Alternative finger designs for decoupling the finger rotation and translation.** (**A**) Directly connecting a motor to the revolute joint of the finger. (**B**) Using a soft pneumatic finger. 29

2.7 **The necessity of decoupling links** (**A**) One example of a simple planar RP linkages. (**B**) The proposed RP linkage with decoupling links. In the simple planar RP linkage design, the kinematics of the two tendons are coupled, causing coupled joint motions when a single tendon is pulled. In contrast, the decoupling links decouple the joint motions. (**C**) DDecoupling links capable of maintaining the length of the grasping tendon during the translation process of the finger. (**D**) Decoupling links that can withstand the pulling force of the grasping tendon, preventing translation of the finger when the grasping tendon is pulled. 31

2.8 **Comparison between hairless elastic belt storage and hairy elastic belt storage.** In the hairless elastic belt, the storage of an additional object results in additional deformation of the belt surfaces, (**A**) reducing the storing force of the stored objects and (**B**) leading to storage failure of small objects. When the object is inserted into the hairy belt storage, **(C)** the elastomeric hairs bend and independently push the object, allowing simultaneous storage of arbitrarily shaped objects. 34

2.9 **Fabrication process of the proposed hairy belt.** Hairy belts were manufactured by one-step injection molding: (**A**) the inner and outer molds were combined by bolts and nuts, and then (**B**) the elastomer (Dragon Skin 30) was injected into the mold. Air vents were incorporated to prevent air traps at the tips of the hairs. (**C**) The result after curing in an oven at 65℃ for 1 hour. (**D**) The hairy belt was obtained by attaching both ends of belt surface with elastomeric adhesive (Sil-poxy), following the removal of the thin cylinders formed by the air vents. 35

2.10 **The process of replacing the conveyor palm.** Hairy belts were manufactured by one-step injection molding: (**A, B**) Loosen the bolts connecting the conveyor palm to the fingers and the gripper body. (**C**) Replace the hairy belt of the conveyor palm. (**D**) Assemble the gripper by reversing the steps in (A). 37

3.1 **Analysis of decoupling links.** (**A**) Schematic of finger with decoupling links for kinematic analysis. The design parameter (l_1, l_2, r_1, r_2, r_3) condition for maintaining the length of the grasping tendon during finger translation was derived by kinematic analysis of the finger. (**B**) Free body diagram of the finger and slider. (**C**) Free body diagram of pulley 2. The design parameter condition for withstanding the pulling force of the grasping tendon was derived by kinetic analysis of the finger. . 39

3.2 **Effect of pulley radius variations on fingertip motion.** Except for the case where γ is 0, grasping and translation are coupled in all cases. 49

3.3 **Effect of decoupling link length variations on fingertip motion.** Except for the case where δ is 1, grasping and translation are coupled in all cases. 49

3.4 **Experiment setup for verifying motion decoupling of the finger.** (**A**) Measuring the change in grasping angle (θ) according to the translation distance (d). (**B**) Three red markers were attached to the finger, and their positions are tracked during finger translation. The grasping angle (θ) and translation distance (d) of the finger were measured by tracking the markers through image analysis with MATLAB. 52

3.5 **Experimental results for verifying motion decoupling of the finger.** (**A**) Experimental fingertip motion varying the radii of pulleys. (**B**) Experimental fingertip motion varying the lengths of decoupling links. The minimum and maximum values of each experimental data are indicated by the shaded region. . 53

3.6 **Analysis of the maximum grasping force.** (**A**) External forces exerted on the fingertip's three links (Link 3-5). (**B**) Free body diagrams of links 3-5. (**C**) Experimental setup of the maximum grasping force measurement. (**D**) Target objects with radius ranging from 5 to 17.5mm with 2.5mm increments in between. (**E**) The experimental results and theoretical grasping force according to the radius of target. 55

3.7 **Experimental setting for cyclic grasping test.** When the gripper grasps an object, the linear motor pulls the object while the load cell measures the grasping force. 63

3.8 **Experimental results of cyclic grasping test.** The grasping force remained nearly constant throughout 1,000 repeated grasping cycles. 63

3.9 **Explanation of the gripper's tendon-driven system.** (**A**) The gripper's fingers are operated by a total of four tendons. (**B**) One-fourth of the deformation in the tendon connected to the fingers (yellow) affects the total stroke, while half the deformation in the orange tendon and the full deformation in the red tendon affect it as well. 64

3.10 **Experimental parameters for analysis of storing force.** (**A**) Design parameters for investigating the storage force of the proposed conveyor palm. (**B**) Target objects were set as cylinders, and the radii of the targets ranged from 2.5 to 17.5mm with 2.5mm increments. 67

3.11 **Schematic of small and large objects being stored.** (**A**) When the smallest object is stored. (**B**) Hair bending when a large object is stored. 72

3.12 **Experimental setup for analysis of storing force.** (**A**) The target was placed between the storage on both sides, and then (**B**) sandwiched between both storages and stored. (**C**) The storing force was measured by pulling the object using a tensile testing machine. 73

3.13 **Finite element analysis (FEA) to predict the transverse storing force.** (**A**) Initial simulation setting considering gravitational force. (**B**) Simulation step 1: The object was stored in the palm by pushing the hairs. (**C**) Simulation step 2: The object moved in the transverse direction of the storage, and the maximum pulling force was obtained in this step. 75

3.14 **Experimental results and simulation results of the transverse storing force.** (**A**) Storing force in response to the radius of the target with storage designs of different radius of hairs (b was fixed at 20 mm). (**B**) Storing force in response to the radius of the target with storage designs of different distance between adjacent hairs (r was fixed at 20 mm). 77

3.15 **Experimental setup for measuring the longitudinal storing force of the conveyor palm.** A weight block is attached to the cylindrical object, and the belt is rotated to store the object (process (1)). Next, the belt is held stationary while a linear motor pulls the object in the longitudinal direction of the conveyor palm (process (2)). During this process, the maximum storing force is measured using a load cell. 79

3.16 **Experimental results and simulation results of the longitudinal storing force.** (**A**) Storing force in response to the radius of the target with storage designs of different radius of hairs (b was fixed at 20 mm). (**B**) Storing force in response to the radius of the target with storage designs of different distance between adjacent hairs (r was fixed at 20 mm). 80

3.17 **Detailed explanation of longitudinal storing force according to object diameter.** (**A**) The configuration of adjacent hairs changes depending on the size of the stored object. (**B**) When pulling a stored small object, the hairs in contact with the bottom surface of the object deform and stack on each other, as highlighted in the yellow box. This stacking effect increases the storing force for small objects. (**C**) For larger objects, the arrangement of adjacent hairs is already disrupted during the storing process, so the stacking effect does not occur. 82

3.18 **Longitudinal storing force of objects in relation to pulling distance.** (**A**) For small objects, the storing force drops sharply after reaching the maximum force as the stacking effect disappears. (**B**) In contrast, for large objects, the storing force decreases slowly after reaching the maximum force. 83

3.19 **Comparison of the transverse storing force and the longitudinal storing force for different conveyor palm designs.** In all tested conveyor palm designs, the longitudinal storing force was greater than the transverse storing force. 84

3.20 **Experimental setup for measuring storing force with material variation .** (**A**) Position the object between the two halves of the split conveyor palm. (**B**) Move the palms toward the center to store the object. (**C**) Finally, pull the object to measure the pulling force. 89

3.21 **Experimental results of storing force measurement with material variation.** (**A**) Storing force measured for conveyor palms composed of different materials. (**B**) To further investigate the effects of material properties on storing force, the storing force ratios of two conveyor palms were analyzed according to object size. 90

3.22 **Schematic related to the force exerted by hairs on an object.** (**A**) The combined restoring force exerted by multiple deformed hairs creates the normal force applied to the object. The product of this normal force and the coefficient of friction is the storing force. (**B**) Schematic of hairs bent due to the storage of the object. 93

3.23 **Experimental verification of individual storage capability of the hairy belt system.** (**A**) Experimental setup. The target (a black cylinder with a 7.5 mm radius) and an additional object (a white cylinder with radii of 7.5 mm and 17.5 mm) were stored together, spaced 30 mm apart. (**B**) The storing force of the target is measured through a tensile testing machine. (**C**) Relationships between the additional object's radius and the storing force of target. The standard deviation of each data point is presented with a black vertical line. 96

3.24 **Experimental setting for measuring the success rate and placement error of proposed multi-object grasping sequence.** (**A**) Experimental setup. The configuration of the object before grasping and after placement is captured using a camera to measure the placement error. The placement error consists of the displacement of the object's center of mass (d_o) and the tilting angle of the object (θ). (**B**) One example of a situation where the gripper fails to retrieve a cuboid occurs when the cuboid rotates during storage. (**C**) The target objects consist of cylinders and cuboids of various sizes. To prevent the cylinder from rolling during the placing process, a cylinder with one-tenth of its diameter sliced off was used. The diameter/width of the sliced cylinder/cuboid was set at intervals of 5 mm, ranging from 5 mm to 35 mm. 103

3.25 **Experimental results for the success rate and placement error of the proposed multi-object grasping sequence.** (**A** and **B**) The success rate for (A) sliced cylinders and (B) cuboids of various sizes. (**C** and **D**) The placement errors for (C) sliced cylinders and (D) cuboids of various sizes. 104

3.26 **Experimental setup and qualitative results for measuring the success rate and placement error when a long object is grasped off-center.** (**A**) The target objects were a 140 mm long sliced cylinder and a 140 mm long cuboid. The diameter of the sliced cylinder and the width of the cuboid were set to 20 mm, which is the median size of the storable objects. (**B**) The off-center distance is defined as the distance between the center of mass and the center of contact points. (**C**) The degree of tilting of each object when stored, depending on the off-center distance. 107

3.27 **Experimental results for measuring the success rate and placement error when a long object is grasped off-center.** (**A**) The success rate of the multi-object grasping sequence for each object depending on the off-center distance. (**B**) The placement error of the sliced cylinder depending on the off-center distance. (**C**) The placement error of the cuboid depending on the off-center distance. 108

3.28 **Analysis of the object's retrieval offset after palm-to-finger translation.** (**A**) Schematic of a tilted gripper grasping an object. (**B**) Free body diagram of the object. (**C**) Schematic of the finger grasping the object viewed from the gripper's longitudinal direction. (**D**) Free body diagram of fingers 1 and 3. (**E**) Free body diagram of fingers 2 and 4. (**F**) Equilibrium of moments at the fingertip, including the force exerted by the grasping tendon and the moment applied by the torsional spring. (**G**) Free body diagram of the slider connected to finger 1. 110

3.29 **Experimental study of the object's retrieval offset after palm-to-finger translation.** (**A**) Experimental setup. The tilt angle of the gripper was adjusted from 0 to 180 degrees in 30-degree increments. (**B**) Target objects. (**C**) Theoretical modeling results of retrieval offset varying with the mass of the grasped objects and the tilt angle of the gripper. (**D**) Experimental results of the retrieval offset varying with the tilt angle of the gripper and the mass of the grasped objects. 115

3.30 **Demonstration of the proposed multi-object gripper in a laboratory-scale logistics environment.** (**A**) Logistic demonstration to compare the travel distance of the manipulator's end-effector and the overall pick-and-place process time when using single-object grasping and multi-object grasping. (**B**) The comparison of travel distance and process time between single-object and multi-object grippers in a laboratory-scale logistics demonstration. Multi-object gripper can reduce the travel distance by about 71% and the overall process time by about 34% in this demonstration. 117

3.31 **Details of the proposed multi-object grasping sequence and a comparison of grasping process efficiency with single-object grasping.** (**A**) The grasping and placing sequence of the proposed multi-object gripper. (**B**) A detailed illustration of the proposed grasping and placing sequence. (**C**) Variables and assumptions for the comparison of manipulator's travel length and process time between multi-object and single-object grasping. (**D**) The schematic of the pick-and-place process.118

3.32 **Domestic demonstration to verify the placing ability of multi-object gripper.** (**A**) The gripper sequentially grasped a small lotion bottle, a travel toothbrush, and razor. And then, the gripper moved them together. After that, the gripper (**B**) placed the razor in a cup and retrieved the stored objects one by one to (**C**) hang the toothbrush set on the wall and (**D**) put the lotion bottle on the shelf. 126

3.33 **Grasping and placing capabilities of the proposed multi-object gripper.** Proposed gripper can grasp, store, retrieve and place 23 different objects, including the long cylinders, cubes, cuboids, spherical objects, thin objects, and porous objects. 127

4.1 **The classification of pick-and-place tasks among various manipulation tasks.** They are categorized based on goal specification and the level of labeling. 132

4.2 **Comparison of the path for the general TSP problem and the path for declutter problem using multi-object gripper.** (**A**) In the general TSP problem, the solution generates the shortest contour connecting the objects and the goal. (**B**) However, the multi-object gripper has a finite storing capacity, meaning it cannot follow the TSP-generated contour directly. Instead, it must return to the goal midway to place the stored objects before continuing. 140

4.3 **Definition of occupied space.** (**A**) The configuration of objects and hairs when multiple objects are stored on the proposed conveyor palm. (**B**) Examples of occupied spaces for different object sizes (for objects with diameters of 10 mm and 25 mm, respectively) are illustrated. The occupied space refers to the range of hairs that bend above or below the object when it is stored (green box). The range of hairs bending above the object is denoted as d_{up} (blue hairs), and the range of hairs bending below the object is denoted as d_{down} (red hairs). 142

4.4 **Occupied space based on the storage order of objects.** (**A**) uses storage capacity less efficiently compared to (**B**). In other words, minimizing the d_{up} and d_{down} of the first and last stored objects increases efficiency. (**C**) The first stored object can be stored stably even when placed near the top of the conveyor palm, as there are 4 hairs above it. (**D**) The last stored object, if light enough, can be supported by only 2 hairs beneath it. 145

4.5 **Schematic of the declutter problem for the proposed multi-object gripper.** As the gripper follows the path and stores objects, groups of objects that can be moved together are formed. 148

4.6 **The setup for declutter problem.** (**A**) Objects are placed on a desk, and the gripper recognizes and grasps them using a camera installed facing the workspace. (**B**). The camera view. (**C**) Target objects. All objects are black cylinders, each 100 in length, with diameters ranging from 5 mm to 30 mm in 5 mm intervals. 150

4.7 **The path planning pipeline of the declutter problem.** (**A**) The entire workspace is captured using an overhead camera. (**B**). Using OpenCV, the cylinders are approximated as rectangles, and the position, diameter, and tilt angle of each object are extracted. (**C**) Based on the object information, the manipulator's near-optimal path is obtained. 151

4.8 **The optimal path obtained through different methods.** (**A**) The common arrangement of objects for comparison. (**B**). Gripper path of SOG method. The manipulator performs 11 round trips to move all objects. (**C**) The shortest path obtained by solving the TSP problem. (**D**) Gripper path when grasping objects along the TSP route. The manipulator performs 4 round trips to move all objects. (**E**) Gripper path obtained using the TSP_Store method. The manipulator performs 3 round trips to move all objects. (**F**) Demonstration. 155

4.9 **Declutter demonstration using the path generated by solving the TSP problem.** (**A**) The gripper first moves 3 objects together, (**B**) then moves another 3 objects, (**C**) moves 4 objects, and (**D**) finally moves the last object. The manipulator performs 4 round trips to move all objects. 156

4.10 **Declutter demonstration using the path generated by solving the TSP_Store method.** (**A**) The demonstration setting with 11 objects. (**B**) The gripper first moves 4 objects together, (**C**) then moves another 3 objects, and (**D**) finally moves the last 4 objects. The manipulator performs 3 round trips to move all objects. 157

4.11 **Comparison of manipulator travel distance and declutter process time during demonstrations using the paths obtained through the SOG, TSP, and TSP_Store methods.** (**A**) The path obtained through the TSP_Store method was 65.7% shorter than the path obtained using the SOG method, and 15.9% shorter than the path obtained using the TSP method. (**B**) In terms of process time, the path obtained through the TSP_Store method reduced the process time by 40.5% compared to the SOG method, and by 10.3% compared to the TSP method. 158

4.12 **The test setup for comparing the efficiency of paths generated by TSP_Store, TSP, and SOG under varying storage capacities.** 160

4.13 **Comparison of the number of round trips for each algorithm's path based on storage capacity. (A)** Data covering the full range from the smallest storage capacity (0 mm) to the largest storage capacity (810 mm). **(B)** Enlarged graph for detailed comparison between TSP and TSP_Store (the storage capacity range: 0 to 135 mm). 160

4.14 **Paths under extreme storage capacities. (A)** When the storage capacity is 0 mm, all three algorithms, TSP_Store, TSP, and SOG, generate the same path. **(B)** When the storage capacity is 810 mm, allowing all objects to be transported in a single trip, there is no difference between the paths generated by TSP_Store and TSP. 162

4.15 **The cases of using storage most inefficiently and most efficiently when transporting 16 objects at once. (A)** Most inefficient case. The smallest object is grasped by the fingers, and the next smallest objects are stored at the very top and bottom of the storage. **(B)** Most efficient case. The largest object is grasped by the fingers, and the next largest objects are stored at the very top and bottom of the storage. 163

4.16 **Comparison of paths generated by TSP_Store and TSP when the storage capacity is 15 mm. (A)** TSP_Store matches a small object with a larger object to create an optimal path. **(B)** TSP suggests a path that grasps two small objects close to each other simultaneously. If the gripper follows the TSP path, it transports one of the storable objects without storing it, resulting in a higher number of round trips compared to when following the TSP_Store path. 165

4.17 **Comparison of travel lengths for paths generated by TSP_Store and TSP varying storage capacity. (A)** Absolute values of the travel lengths are compared. **(B)** The ratio between the travel lengths of the two paths is analyzed. 165

A.1 **Experimental setting for cyclic loading test of tendon.** 193

A.2 **Cyclic loading test results of tendon.** (**A**) The results of the cyclic loading test for Dyneema size 4 under a load of 2.9 kgf. (**B**) The degree of permanent deformation of each tendon based on the number of cycles. 193

A.3 **Measurement of 100% modulus for DragonSkin 30, Smooth-Sil 950, and Smooth-Sil 960.** (**A**) Specimens prepared according to ASTM D412 Type C standards. (**B**) Experimental setup for modulus measurement. (**C to E**) Stress-strain curves for (C) DragonSkin 30, (D) Smooth-Sil 950, and (E) Smooth-Sil 960. 195

A.4 **Measurement of static frictional coefficients for DragonSkin 30, Smooth-Sil 950, and Smooth-Sil 960.** (**A**) Prepared specimens. (**B to C**) Experimental setup for measuring the static frictional coefficients for each material. (**D to F**) Graphs of friction force versus normal force for (D) DragonSkin 30, (E) Smooth-Sil 950, and (F) Smooth-Sil 960. 197

B.1 **3D printed conveyor palm.** (**A**) Cross-sectional view of the conveyor palm during the printing process. (**B**). The conveyor palm immediately after printing. (**C**) The printed conveyor palm can be everted for use. (**D**) Feasibility of storing multiple objects. 199

C.1 **Non-interfering storing distance between two objects: The minimum distance that allows objects to be stored without interfering with each other's storage.** 201

C.2 **Experiment to determine the tolerable storing distance.** **(A)** The first object is stored, and the number of hairs beneath the object is adjusted. **(B)** The second object is brought into contact with the conveyor palm under a force of 200 gf. **(C)** The conveyor palm is rotated to verify if the second object can be successfully stored. 202

C.3 **Tolerable storing distance between two objects: The minimum distance at which two objects can be experimentally stored successfully, even if they interfere with each other's storage.** 203

C.4 **Storing force measurements for each object when two objects are stored based on the tolerable storing distance.** This result shows that they are stored with greater force compared to storing each object individually (green line). . . . 204

C.5 **The differences in the configuration of hairs beneath the first and second stored objects.** The tolerable storing distance between the first and second objects may differ from that between the second and third objects due to differences in the configuration of hairs beneath the stored objects. 205

List of Tables

1.1 Comparison of Multi-Object Grasping Methods 16

3.1 **Five decoupling link designs with different parameters.** The five designs include one proposed design, two with variations in the radii of the pulleys, and two with variations in the lengths of the links. 53

3.2 **Detailed experimental parameters of storing force.** The design parameters of conveyor palm were radius of the hair (r), distance between the hairs (a), and target sizes (R). 67

3.3 The upper and lower limits of storable objects based on the geometry of the conveyor palm. 72

3.4 **Detailed specifications of objects used in the demonstration of tidying up a cluttered desk.** 125

4.1 The criteria for classifying manipulation tasks [97]. 131

4.2 **Goal conditions and applicable multi-object grasping methods for each manipulation task.** The last column indicates cases where the multi-object grasping method proposed in this dissertation is more efficient compared to other methods. 137

4.3 **Experimentally measured $d_{\mathbf{up}}$ and $d_{\mathbf{down}}$ values for different object sizes.** 141

4.4 **Diameter variations of target objects for the declutter problem and the number of objects with each corresponding diameter.** 150

4.5 The diameter and quantity of the target objects for the experiment comparing path efficiency of three different algorithms varying storage capacity. 159

Chapter 1

Introduction

1.1 Background

1.1.1 Robotic Pick-and-Place Tasks

Robots have been increasingly used across various industries and environments [1]. Robots can be broadly categorized into industrial robots and service robots (Fig. 1.1). Industrial robots refer to robots used in factory settings, encompassing material handling, welding, assembling, packaging, and mobile systems like AGVs equipped with robotic manipulators [ISO 8373:2021]. Service robots, defined as robots for personal or professional use that perform useful tasks for humans or equipment, are employed in diverse applications such as transportation (logistics), hospitality (food or drink preparation), agriculture (farming, cultivation), cooking, and cleaning [ISO 8373:2021].

According to the "World Robotics 2024" statistics published by the International Federation of Robotics (IFR) [1], the operational stock of industrial robots increased by 10% in 2023. Moreover, research by Precedence Research [2] indicates that the service robotics market size is projected to continue growing (Fig. 1.1). Since this dissertation focuses on the robotic pick-and-place process, applications that do not involve object picking, such as welding and mobile platforms in industrial robots or transportation in service robots, are excluded from discussion.

The primary pick-and-place applications for industrial robots include manufacturing (automotive, electronics), logistics, and high-mix low-volume production, while those for service robots encompass hospitality, agriculture, and domestic tasks such as cleaning and cooking (Fig. 1.2). In the manufacturing industry, automation has been widely adopted for many years, facilitating standardized production lines and enabling innovations such as parallel manipulators [3–7], which increase robot arm speed by positioning heavy actuators away from the distal end.

Additionally, to improve the efficiency of packaging multiple objects, a grasping method has been proposed using multiple suction cup arrays attached to the end of a robotic arm [8] (Fig. 1.3). This setup allows the arm to grasp and move several objects simultaneously. Such grasping strategy, named multi-object grasping, can effectively decrease the entire pick-and-place process time by reducing the repetitive motion of the arm.

Recently, robotic pick-and-place applications have been expanding beyond structured settings into unstructured environments such as logistics and domestic tasks [9]. For instance, in manufacturing processes, there is a growing demand for automation in high-mix, low-volume production, while in the logistics industry, efforts to automate warehouse pick-and-place operations are required. Moreover, service robots designed for close human interaction are also being developed. To address these demands, advancements have been made in collaborative robot [10], sensing technologies like perception and SLAM [11], motion planning through learning-based approaches [12], underactuated grippers capable of handling diverse object shapes [13–17], and soft grippers suitable for handling fragile objects [18–22]. These innovations aim to develop manipulation technologies that adapt to unstructured environments.

Industrial Robots

Service Robots

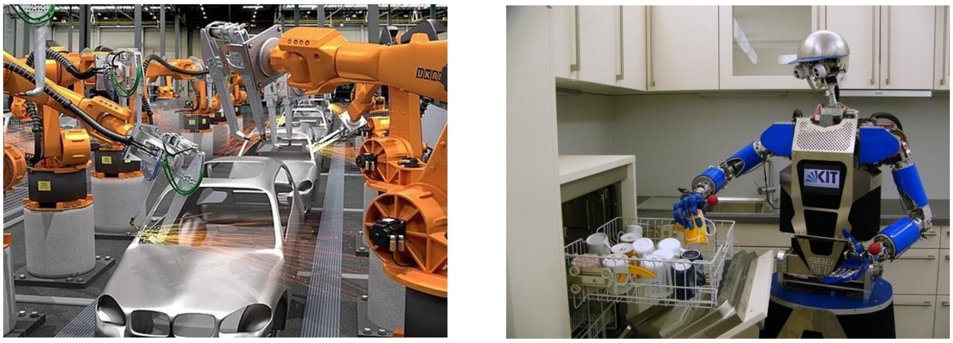

Operational Stock of Industrial Robots - World

Service Robotics Market Size 2023 to 2034

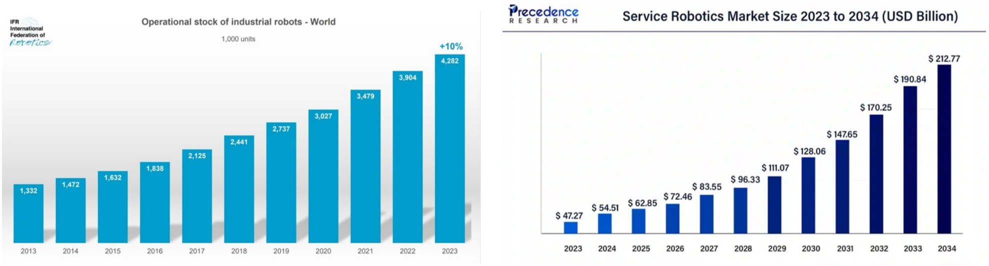

IFR [1]

Precedence [2]

Figure 1.1. Robotic applications in industry.

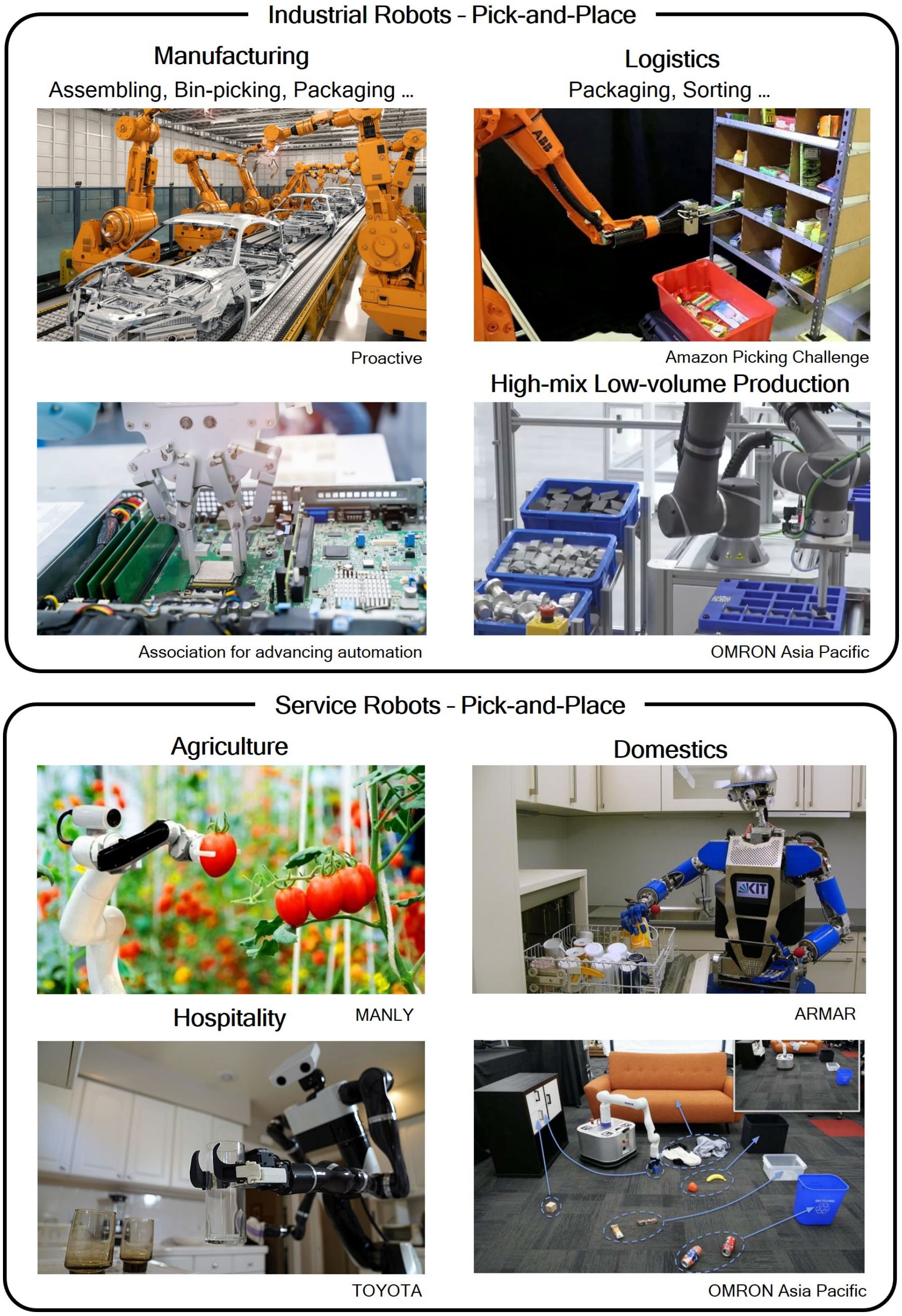
Industrial Robots - Pick-and-Place
Manufacturing
Assembling, Bin-picking, Packaging ...
Logistics
Packaging, Sorting ...
Proactive
Amazon Picking Challenge
High-mix Low-volume Production
Association for advancing automation
OMRON Asia Pacific
Service Robots - Pick-and-Place
Agriculture
Domestics
Hospitality
MANLY
ARMAR
TOYOTA
OMRON Asia Pacific

Figure 1.2. Detailed classification of robotic pick-and-place applications.

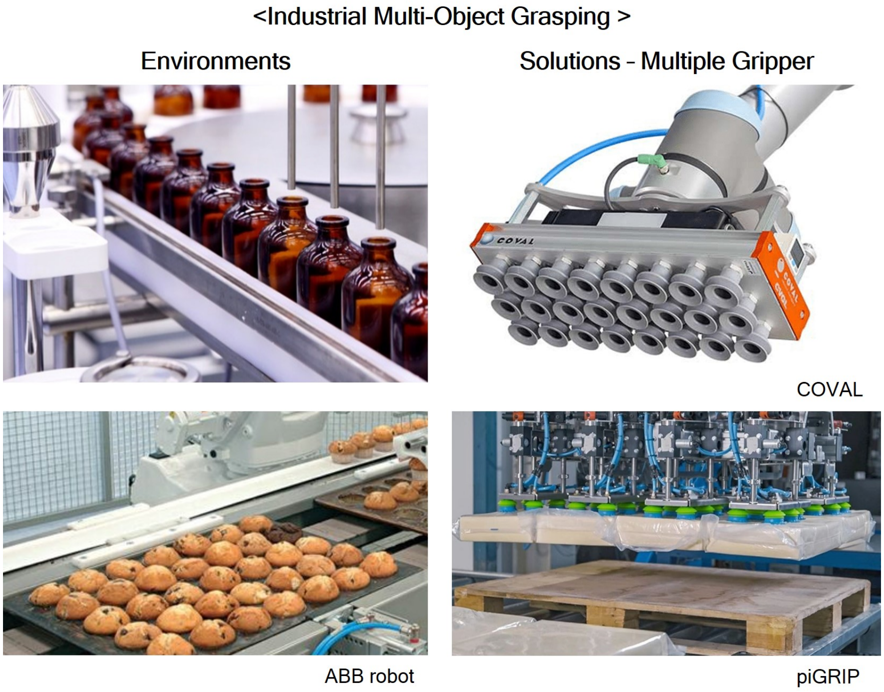
<Industrial Multi-Object Grasping >
Environments
Solutions – Multiple Gripper
COVAL
COVAL
ABB robot
piGRIP

Figure 1.3. Conventional solution for efficient pick-and-place tasks: industrial multi-object grasping.

1.1.2 Multi-Object Grasping in Unstructured Environments

Research on grasping in unstructured environments has primarily focused on improving the grasping success rate of single objects. However, for practical use of grippers in real-world settings, grasping methods to enhance the efficiency of the pick-and-place process should also be proposed. One of the most representative approaches is multi-object grasping (Fig. 1.3). However, conventional multi-object grasping methods are limited to situations where the arrangement of suction cups aligns with the objects, making them less effective in unstructured environments. The random positions of objects and the presence of environmental obstacles prevent the use of conventional multi-object grasping strategies (Fig. 1.4). In contrast, humans perform diverse multi-object grasping strategies depending on the task and environment, exploiting their dexterous hand skills, such as pinch grasp, power grasp, and other advanced manipulation skills; these include pinching objects between a pair of fingers or enveloping multiple objects using the palm and fingers [23]. Therefore, inspired by human multi-object grasping strategies, research has been conducted on grippers capable of performing multi-object grasping in unstructured environments. These grippers are referred to as multi-object grippers. Studies in multi-object grippers either have introduced new mechanical designs tailored to specific multi-object grasping strategies or have proposed algorithms for multi-object grasping that can be applied to conventional gripper designs (Fig. 1.5) [24–47].

First, multi-object grippers have been proposed for situations where objects are clustered in bins or on tables, allowing the simultaneous grasping of

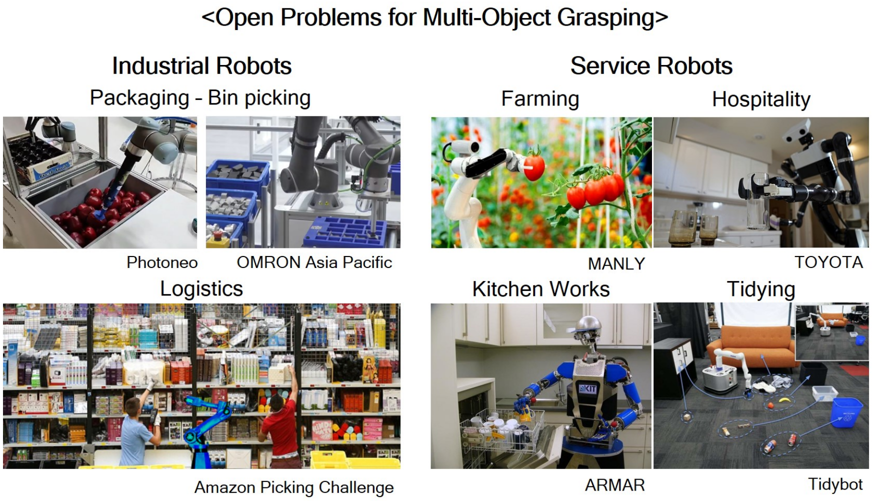
<Open Problems for Multi-Object Grasping>
Industrial Robots
Packaging - Bin picking
Photoneo
OMRON Asia Pacific
Logistics
Amazon Picking Challenge
Service Robots
Farming
Hospitality
MANLY
TOYOTA
Kitchen Works
Tidying
ARMAR
Tidybot

Figure 1.4. Open problems for multi-object grasping.

multiple items. For example, studies have proposed embedding elastic strings or elastic belts into curved rigid fingers to grasp multiple objects simultaneously [27, 41]. These grippers use the compliance of elastic strings and belts to effectively enclose and capture several objects at once. Additionally, research has been conducted on using conventional robot hands with rigid fingers to grasp multiple objects simultaneously [28, 30]. Specifically, a study demonstrated a 3-fingered gripper grasping multiple spherical objects in a bin at once, reducing the number of object transfers by the manipulator [28]. Another study used a commercial 5-fingered hand and a diffusion model to determine the hand's grasp posture for multiple clustered objects through reinforcement learning [30]. However, these studies often assume a specific scenario where objects are clustered together and have limitations in situations where objects are spread apart. In this dissertation, such methods will be referred to as

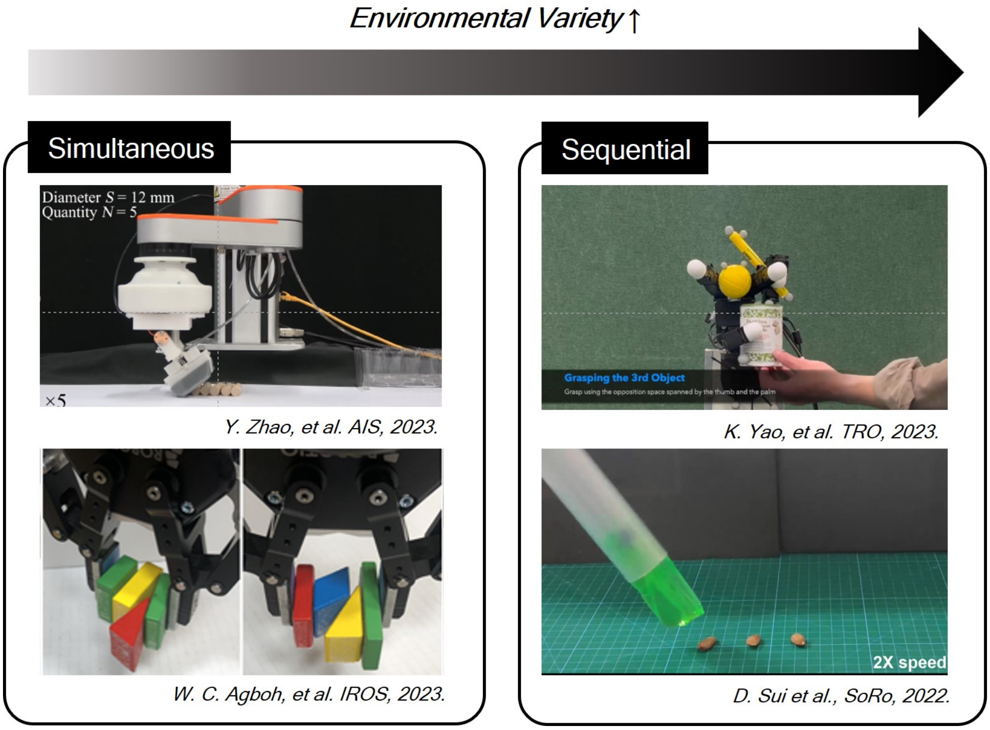
Environmental Variety ↑
Simultaneous
Diameter S = 12 mm
Quantity N = 5
×5
Sequential
Grasping the 3rd Object
Grasp using the opposition space spanned by the thumb and the palm
2X speed

Y. Zhao, et al. AIS, 2023.

W. C. Agboh, et al. IROS, 2023.

K. Yao, et al. TRO, 2023.

D. Sui et al., SoRo, 2022.

Figure 1.5. Types of conventional multi-object grippers. These include grippers that sweep multiple objects on the same plane and then pick them up all at once [26], [37], and grippers that utilize the redundancy of the hand to sequentially pick up objects and move them all at once [39].

"scooping." Scooping can be effective for tasks like packaging or bin picking, where precise placement is not critical. However, it is not suitable for tasks such as tidying, where the placement of individual objects is important.

Additionally, multi-object grippers which can sweep scattered objects on a table before grasping them simultaneously have been introduced. The gripper using pneumatic soft fingers to sweep and then envelop multiple objects easily [38] have been introduced. In addition, algorithms enabling conventional parallel grippers to collect and achieve force closure grasp of multiple objects have been proposed [29, 31, 37]. However, these strategies are limited to scenarios where objects are on the same surface (e.g., flat table) and without obstacles in between. Therefore, while sweeping can be effectively used for decluttering objects in a 2D space, it has limitations when applied to tasks in 3D spaces, such as logistics or farming, where objects are distributed along the 3D spaces.

Furthermore, multi-object grasping using the redundancy of dexterous robot hands to sequentially grasp multiple objects have been suggested [40]. However, this strategy has limitation in requiring human assistance for the gripper to grasp objects and needing too many degrees of freedom to grasp objects.

Lastly, a gripper capable of storing multiple objects through the rotation of an everting structure has been developed [34]. Known as the "swallowing gripper," it features a toroidal structure capable of infinite rotation along its longitudinal axis, allowing it to store and transport multiple objects at once. However, due to the absence of the fingers to directly grasp objects, this gripper requires external force to press objects during grasping, limiting its application to cases where objects can withstand such pressing forces. For example, it can effectively grasp objects on a table by pressing them downward but struggles to grasp objects laterally. Additionally, since it lacks fingers, the swallowing gripper cannot re-grasp stored objects, making it difficult to place them in a desired configuration. While it excels at grasping multiple objects simultaneously, even in the presence of obstacles, it has notable limitations in placing individual objects in specific orientations and directions. These constraints make the swallowing gripper effective for packaging tasks where precise placement is not critical, but unsuitable for applications such as tidying or hospitality, where accurate placing is essential.

In summary, as the target environments for grippers and manipulators have expanded [9], multi-object grippers that can be used in various environments have been developed. However, previously developed multi-object grippers have limitations in grasping arbitrarily placed objects and placing each object in desired configurations. Therefore, it is essential to investigate the fundamental manipulation skills for a multi-object grasping method with greater versatility in picking and placing. To address this issue, this dissertation aims to analyze human strategy for multi-object grasping in various unstructured environments and investigate the essential manipulation skills required for this strategy. This is a crucial step toward achieving multi-object grasping in more diverse environments in the future.

1.1.3 Humans' Manipulation Skills

In this chapter, a comprehensive review of human manipulation skills will be proposed, followed by a summary of the essential manipulation skills for multi-object grasping in unstructured environments. Humans can perform a variety of in-hand manipulations based on the dexterity of the hand, enabling them to accomplish diverse tasks. In-hand manipulation refers to the process of manipulating an object within the hand after grasping it [48]. There are several ways to classify in-hand manipulation skills. Specifically, in studies related to child development, in-hand manipulation is typically categorized into five types: finger-to-palm translation, palm-to-finger translation, shift, simple rotation, and complex rotation [49].

The process of finger-to-palm translation involves moving an object from the fingertips into the palm of the hand for short-term storage (e.g., picking up coins from a purse and transferring them to the hand). Palm-to-finger translation occurs when an object is moved from the palm to the fingertips (e.g., inserting multiple coins into a vending machine one by one). Shift refers to the linear traversal of an object along or across the fingertips. Examples of shift movements include spreading out plying cards or sliding the fingers down a pencil's shaft to get ready for writing. Simple rotation involves turning or rolling an object between the thumb and fingertips (e.g., elongating a small piece of play dough by rolling it). Complex rotation refers to the intricate and isolated finger movements required to turn an object between the 180° and 360°. For instance, rotating a pen end-over-end illustrates complex rotation [49].

Among these, in-hand translation skills are the first to develop in in-hand manipulation and are used to transfer objects between the fingertips and the palm [48]. In other words, in-hand translation skills allow a person to synergistically utilize the advantages of the fingertips and palm, which have different functions. This synergistic use of the human hand offers a more versatile object pick-and-place capability compared to other multi-object grasping methods while retaining the efficiency of moving multiple objects together.

To perform multi-object grasping in a greater variety of pick-and-place tasks than those targeted by previous multi-object grippers, humans use segmentation strategies of the hand and object translation strategies between hand segments (Fig. 1.2). For multi-object grasping, humans can use their radial and ulnar sides of the hand as different sections; the radial side for grasping objects, and the ulnar side for stable storage of one or multiple objects (stabilization) [50]. In this thesis, the radial side is referred to as the grasping section, and the ulnar side as the storing section. Humans translate objects between these two sections [51–53], leveraging the strength of both the grasping and storing sections, corresponding to the ability to pick and place a single object and the ability to store multiple objects simultaneously.

In detail, finger-to-palm translation allows objects pinched by the fingertips to be transferred into the palm for temporary and stable storage. This process frees the fingertips for grasping new targets and can be repeated to store multiple objects in the palm. Afterward, humans use palm-to-finger translation to transfer objects from the palm to the fingertips individually. This process enables the fingertips to retrieve the objects and perform various placement tasks, such as shelving or hanging objects in desired orientations. This strategy leverages hand segmentation and object translation in multi-object grasping, enabling a versatile pick-and-place process.

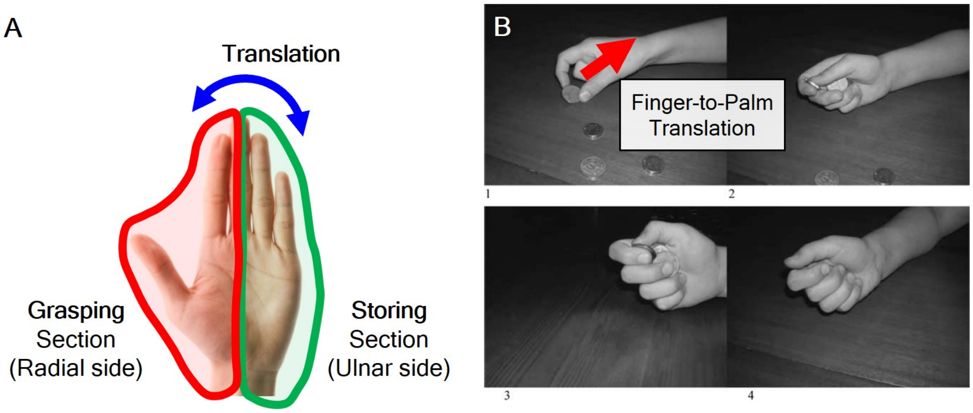
A
Translation
Grasping
Section
(Radial side)
Storing
Section
(Ulnar side)
B
Finger-to-Palm
Translation
1
2
3
4

Figure 1.6. Human multi-object gripping strategy targeting more unstructured environments than the task environment of existing gripping solutions. (**A**) Segmentation of the hand into the radial and ulnar sides. The radial side serves the role of grasping the object, while the ulnar side stably stores it [44]. Through object translation between these two sides, the radial side can sequentially store the grasped objects on the ulnar side, and after storage, the radial side can perform a new grip. (**B**) The process of human finger to palm translation [49].

1.1.4 Underactuated Gripper and Robotic Hand

Inspired by human hand functionalities, various robotic grippers have been developed, focusing on adopting specific capabilities rather than replicating the entire hand's functionalities. Most gripper research focuses on analyzing key principles of specific hand functions and integrating these insights into mechanical design. For example, underactuated grippers use differential mechanisms to achieve force closure, similar to human hands, enabling effective grasping of objects of diverse shapes [54–66]. Additionally, studies have been presented on grippers that automatically change the grasp mode between power grasp and pinch grasp depending on the type of object, using an adaptive mechanism [67–73]. Furthermore, research on adaptive palms, which have human-like stiffness to enhance adaptability during grasping, has been studied [74–78]. In the case of multi-object grippers, research has been introduced that uses elastic strings or soft materials to better envelop objects, simulating the human's adaptive enveloping strategy towards multiple objects [27, 38, 41].

The use of suitable adaptive mechanisms is also important in the object translation and storing processes in multi-object grasping. Compared to single-object grasping, the gripping sequence for multi-object grasping has been expanded to include object translation and storage. To ensure efficiency in multi-object grasping, these processes should be implemented as simply as possible.

1.2 Problem Definition

As the target environment for grippers expands to unstructured environments [9], research on multi-object grippers is also progressing to accommodate more diverse environments. The characteristics of currently developed multi-object grippers are summarized in Table 1.1. Early multi-object grippers [8], utilizing multiple suction arrays, were limited to well-structured industrial environments. However, advancements in compliant mechanisms [27, 38], dexterous hands [40], and learning-based control [30] have enabled multi-object grippers to handle objects in bins and those placed arbitrarily on planes, which are relatively more unstructured environments. Moreover, multi-object grippers have evolved from simultaneously grasping multiple objects to sequentially grasping objects [34, 40], though this process requires human assistance. Despite these advancements, there are still limitations in individually picking or placing objects without human intervention while holding multiple objects. Individual picking and placing of objects are essential capabilities for unstructured environment tasks such as logistics, food packaging, farming, and domestic applications. Therefore, a gripper capable of performing multi-object grasping while maintaining the ability to pick and place individual objects is necessary.

A review of how humans perform multi-object grasping in unorganized environments identified in-hand translation skills, including finger-to-palm and palm-to-finger translation, as critical manipulation techniques. Humans use the segmentation of the hand and in-hand translation skills, effectively utilizing the grasping and storing sections synergistically. This enables precise picking and placing of individual objects in the grasping section while simultaneously holding multiple objects in the storing section, making multi-object grasping possible for various pick-and-place tasks. However, existing multi-object grasping methods have not incorporated the functional segmentation of the hand or in-hand translation skills, limiting their applicability to a broader range of pick-and-place tasks.

Therefore, in this thesis, the multi-object gripper capable of performing various pick-and-place tasks was proposed through the functional separation of the fingers and palm, as well as in-hand translation. The proposed multi-object grasping technique is expected to be suitable for unstructured environments and tasks requiring precise placement. Additionally, a simple path planning algorithm tailored to the multi-object gripper, utilizing in-hand translation, was developed to enable more efficient use of the gripper. Consequently, this approach is expected to extend the applications of multi-object grasping, addressing the growing need for grippers that can not only effectively grasp and transfer multiple items simultaneously but also accurately place them.

Multi-Object Grasping Methods	**Picking**		**Placing**		**Overall Speed**
	Workspace	**Obstacle**	**Position**	**Orientation**	
Suction cup array [8]	1D	×	×	×	Relatively High
Scooping [27, 28]	1D	×	×	×	Relatively High
Pushing [29], Sweeping [38]	2D	△	×	×	Relatively Low
Swallowing [34]	3D	○	○	×	Relatively Low
This work	3D	○	○	○	Relatively Low

Table 1.1. Comparison of Multi-Object Grasping Methods

1.3 Contributions

The main contribution of this work is the proposal of a multi-object gripper for versatile pick-and-place tasks. For this purpose, human multi-object grasping strategies in unstructured environments were analyzed, leading to the identification of hand segmentation and in-hand translation between two hand sections as key strategies. Multi-object gripper using finger-to-palm translation and palm-to-finger translation is introduced.

Compared to the conventional single-object grasping process, the additional in-hand translation and storing processes may slow down the overall procedure. Therefore, to enhance the time efficiency of the proposed grasping method, it is necessary to design a simple translating and storing mechanism. To implement additional processes with simple control, fingers capable of stable pinching and in-hand translations, regardless of object size and type, were presented as the grasping section. As the storing section, an adaptive conveyor palm design was introduced, capable of storing multiple objects at once and facilitating translation with the grasping section. The proposed gripper can pick single objects from various orientations using the under-actuated fingers and subsequently transfer them to the storing section through finger-to-palm translation for storing and moving them together. After moving the objects, the fingers retrieve the stored objects individually with the fingertips through palm-to-finger translation for precise object placement. Finally, a simple path planning algorithm was proposed to enhance the efficiency of the developed gripper, and its effectiveness was validated by applying the gripper to the declutter problem.

The main accomplishments of this dissertation research are:

- Presentation of a multi-object grasping method using hand segmentation and in-hand translation.
- Designs of multi-object gripper for various pick-and-place tasks using in-hand translation.
- Prove the efficiency and potential of the multi-object grasping method using in-hand translation in various pick-and-place tasks.
- Classification of the real-world tasks where the proposed multi-object grasping is effective and suggestion of path planning algorithm for declutter problems

Chapter 2

Design of Multi-Object Gripper Utilizing Finger-to-Palm Translation

2.1 Gripper Design and Grasping Strategy

2.1.1 Background

To define the issues associated with multi-object grasping using in-hand translation, the sequence of human multi-object grasping was analyzed (Fig. 2.1A). Humans first pinch object with 2 or 3 fingers and translate it to the palm. After transferring the object to the palm, they are moved to the ulnar side, the storing section, for temporary storage. If the length of the object matches the width of the hand, it can be directly stored in the storing section. However, if it is shorter than the width of the hand, the thumb pushes the object into the storing section. Next, while the storing section stores the object, the grasping section prepares to grasp a new object. After storing all objects and moving them to the desired place, human utilizes palm-to-finger translation to place the objects one by one into the desired place. To perform palm-to-finger translation, humans use the dexterous movement of the thumb to retrieve the object from the storing section and grasp it again.

Inspired by human's multi-object grasping strategy utilizing in-hand translation, a gripper design was proposed (Fig. 2.1B). Firstly, a finger design capable of translating objects while pinching is necessary (Fig. 2.2). To address this, a finger design decoupling the pinching and translating of objects was proposed. Secondly, a design for a storing section capable of holding multiple objects and enabling palm-to-finger translation is needed. To facilitate simple finger-to-palm and palm-to-finger translation, the storing section must also actively translate objects. For this purpose, a belt-shaped storing section was developed. Thirdly, to simplify the object transfer process, the object translation directions of the grasping section and storing section were aligned. Human object transfer from the grasping section to the storing section is complex, but by mechanically aligning the translation directions, object exchange between the two sections can be facilitated. The developed multi-object gripper can reduce the overall travel length of the manipulator compared to single-object gripper, enhancing the time efficiency of the pick-and-place tasks (Fig. 2.3).

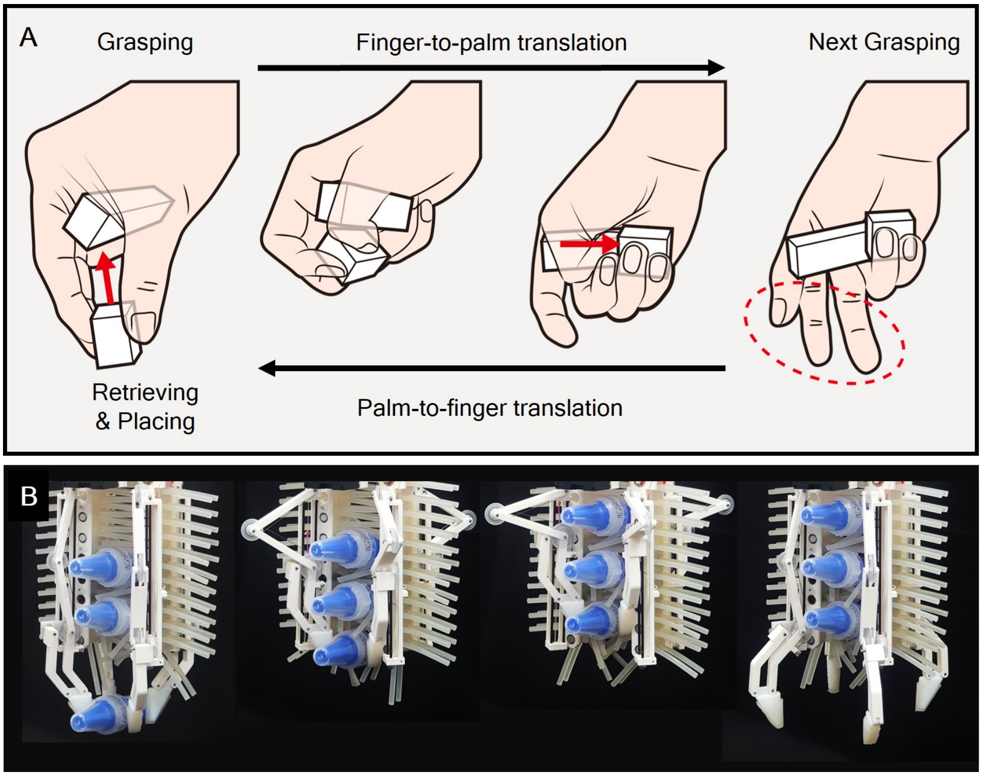
A
Grasping
Finger-to-palm translation
Next Grasping
Retrieving
& Placing
Palm-to-finger translation
B

Figure 2.1. Multi-object gripper inspired by humans' multi-object grasping utilizing in-hand translations. (**A**) The sequence of human multi-object grasping method utilizing the translation movement of the finger allows for synergistic use of the finger and palm. (**B**) The concept of the proposed multi-object gripper corresponds to human strategy. The proposed gripper utilizes the pinch translation of the finger to store or retrieve objects for picking and placing each object.

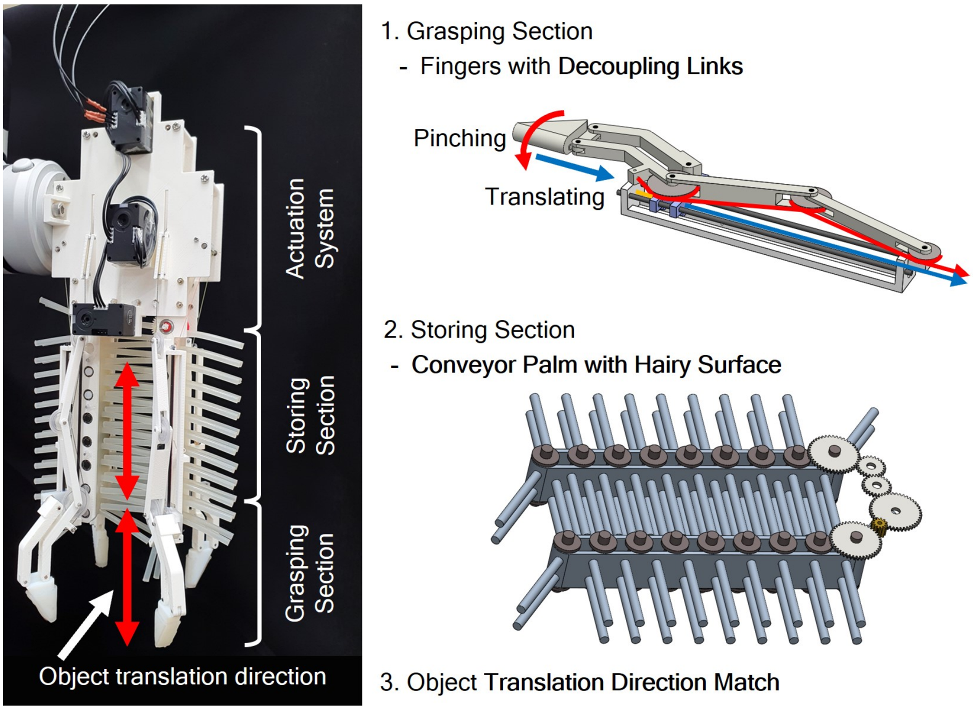
Actuation System
Storing Section
Grasping Section
Object translation direction
1. Grasping Section
- Fingers with Decoupling Links
Pinching
Translating
2. Storing Section
- Conveyor Palm with Hairy Surface
3. Object Translation Direction Match

Figure 2.2. Proposed gripper design to address the issues with multi-object grasping using in-hand translation. Firstly, a finger design capable of stable pinch translation is presented. Secondly, a hairy belt design is proposed, enabling active exchange of objects between the grasping section and allowing simultaneous storage of multiple objects. Finally, aligning the translation directions of both sections facilitates easy object transfer between them.

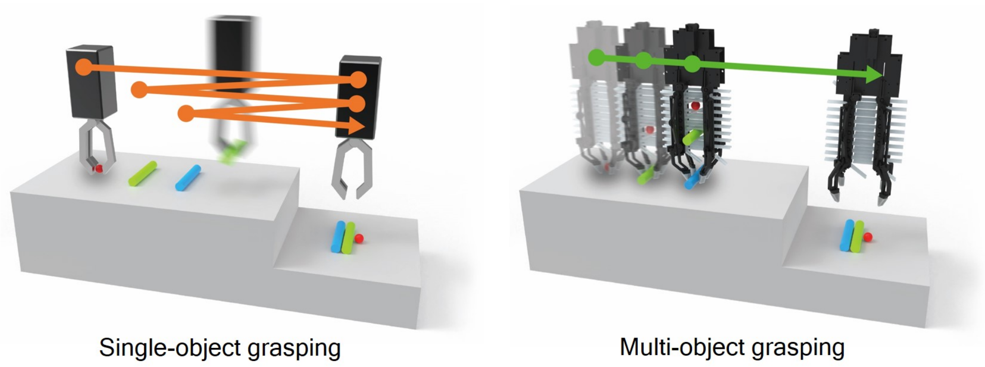

Figure 2.3. Comparison of the manipulator's travel distances between single-object grasping and multi-object grasping.

2.1.2 Gripper Design

Inspired by the human multi-object grasping strategy employing translational movements of the fingers, we have developed a multi-object gripper that utilizes fingers capable of finger-to-palm translation and palm-to-finger translation, along with a palm suitable for simultaneous storage. The developed gripper is illustrated in Fig. 2.4. The proposed gripper consists of four fingers and a conveyor palm (Fig. 2.4A). Four fingers are placed on each slider and are driven by two tendons called the "grasping tendon" and the "translating tendon" (Fig. 2.4B). The grasping tendon produces the grasping motion of the finger, and the translating tendon actuates the finger-to-palm translation of the finger. The grasping tendon wraps around the free-rotating pulleys, centered on the three revolute joints of the decoupling links, and attaches to the parallelogram linkage finger. The translating tendon is directly connected to a slider. A torsional spring is inserted between the finger and the slider, and a linear spring is embedded between the slider and the linear guide. These passive elements generate a restoring force that returns the finger to its initial state without the need for additional tendons. For the storage, a motor and a gear system are utilized to rotate the belts with polymer hairs embedded on their surfaces (Fig. 2.4C). The grasping motion of the four fingers is underactuated by a single motor using a floating moving pulley system, which was introduced by the several underactuated grippers [79–81] like SDM Hand [79], to adaptively grasp objects with simplified control (Fig. 2.4D). The four translating tendons are also driven by a single motor and are connected on the same pulley, allowing the fingers to move an equal distance from each other. By using an appropriate underactuation mechanism suitable for grasping and translating tendons, the number of required motors and the complexity of the system are reduced.

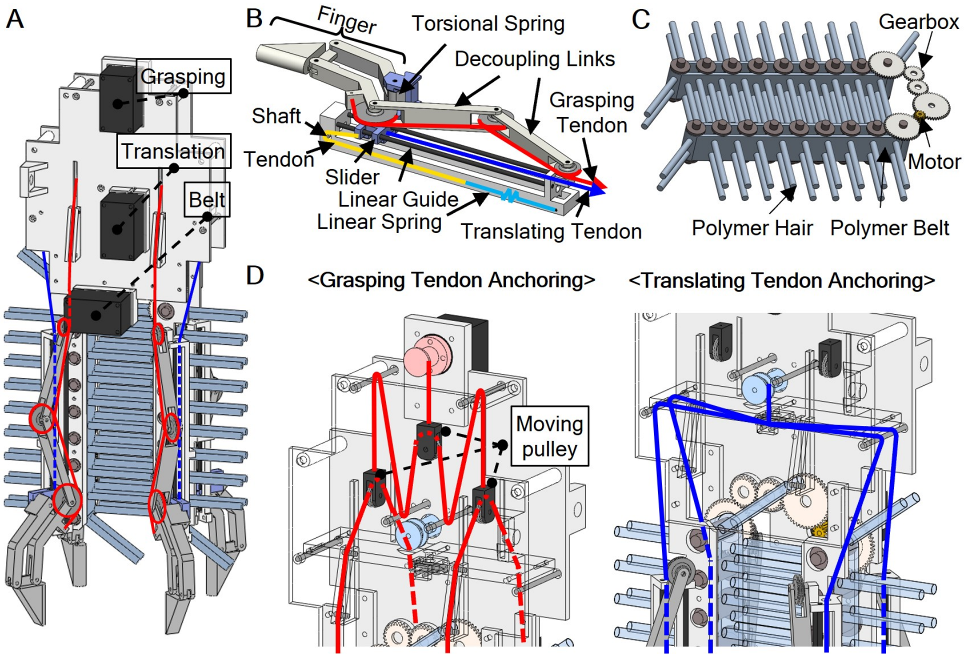
A
Grasping
Translation
Belt
B
Finger
Torsional Spring
Decoupling Links
Grasping Tendon
Shaft
Tendon
Slider
Linear Guide
Linear Spring
Translating Tendon
C
Gearbox
Motor
Polymer Hair
Polymer Belt
D
<Grasping Tendon Anchoring>
<Translating Tendon Anchoring>
Moving pulley

Figure 2.4. Design of multi-object gripper utilizing in-hand translations. (**A**) Overall design of the developed gripper. (**B**) Detailed design of a single finger. A finger made of a parallelogram linkage is placed on the slider, and a grasping tendon and a translating tendon are each connected with the finger and slider, creating rotation and translation of the finger. (**C**) Detailed design of the palm. The palm consists of two belts facing each other, and each belt has an array of elastomeric hairs on its surface. (**D**) The anchoring of the grasping tendon and the translating tendon. Four grasping tendons are underactuated using a moving pulley mechanism for adaptive grasping, while the four translating tendons are directly connected to the same pulley to ensure an equal translation distance for all four fingers.

2.1.3 Grasping Strategy

Figure 2.5 illustrates the multi-object grasping sequence of the developed gripper. When the grasping tendon is pulled, the fingers rotate to grasp an object (Fig. 2.5, i-ii). Subsequently, actuating the translating tendon causes the fingers to translate the object into the storage while maintaining the grasp (Fig. 2.5, ii-iii). When the object arrives at the entrance of the storage, the belts start to rotate at the same speed as the translational movement of fingers and store the object between their hairs (Fig. 2.5, iii-iv). Finally, once the grasping and translating tendons are released, the fingers return to their initial position due to the restoring force of the torsional spring and the linear spring. By reversing the aforementioned grasping and storing processes, the gripper can individually retrieve and place objects in the desired orientation.

Compared to the conventional single-object grasping process, the additional translating and storing processes may slow down the overall procedure. Therefore, to enhance the time efficiency of the proposed grasping method, it is necessary to design a simple translating and storing mechanism. Decoupling links simplify the object grasping and translating processes of the fingers, and a conveyor palm with elastomeric hairs enables the straightforward translation and storage of multiple objects using a single motor.

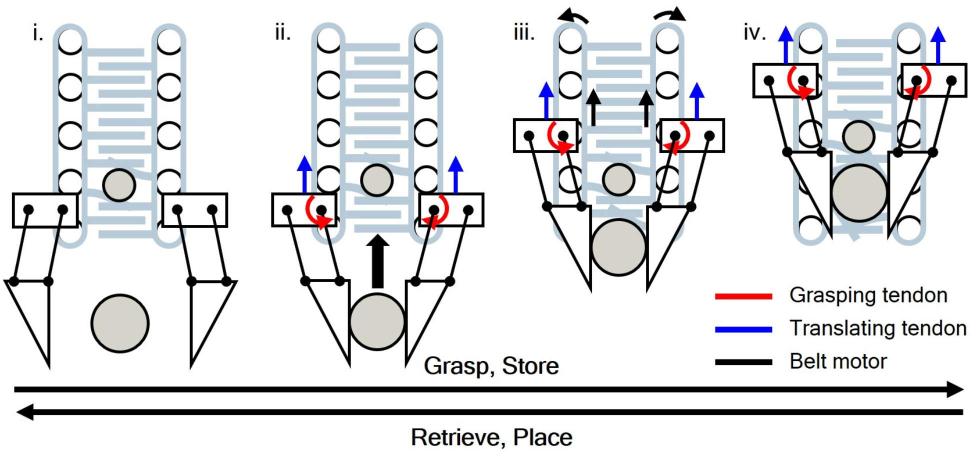
i.
ii.
iii.
iv.
Grasping tendon
Translating tendon
Belt motor
Grasp, Store
Retrieve, Place

Figure 2.5. Grasping strategy of multi-object gripper utilizing in-hand translations. The fingers grasp and transfer the object to the storage, and the palm inserts the object between the elastomeric hairs and stores it. By repeating the above procedure, the gripper can store multiple objects and transfer them at once and retrieve to place the objects with the reverse process.

2.2 Grasping Section Design

2.2.1 Background

Each gripper finger consists of a revolute joint and a prismatic joint for directly grasping and translating objects. To reduce the complexity of control, it is necessary to decouple the rotational and translational movements of the fingers. The simplest solution to achieve this is to mount the fingers on sliders for linear motion, embedding motors between the sliders and fingers to enable finger rotation (Fig. 2.6A). By driving the sliders of all four fingers simultaneously using one tendons, the decoupled rotation and translation movements can be easily achieved. However, directly attaching motors to the fingers increases their inertia and requires dynamic motor control. Additionally, controlling each finger individually for object grasping further complicates the control process. Another approach is to design the fingers as pneumatically driven soft fingers, embed them on sliders, and use tendons to achieve translation (Fig. 2.6B). This method simply separates grasping and translational motions but is limited in tasks where pneumatic actuation can be used. To address these challenges, tendon-driven mechanisms were employed instead of directly attaching motors to the finger joints. This approach reduces the inertia of the fingers while enabling all finger movements to be powered by compact motors.

To address these challenges, tendon-driven mechanisms were employed instead of directly attaching motors to the finger joints. This approach reduces the inertia of the fingers while enabling all finger movements to be powered

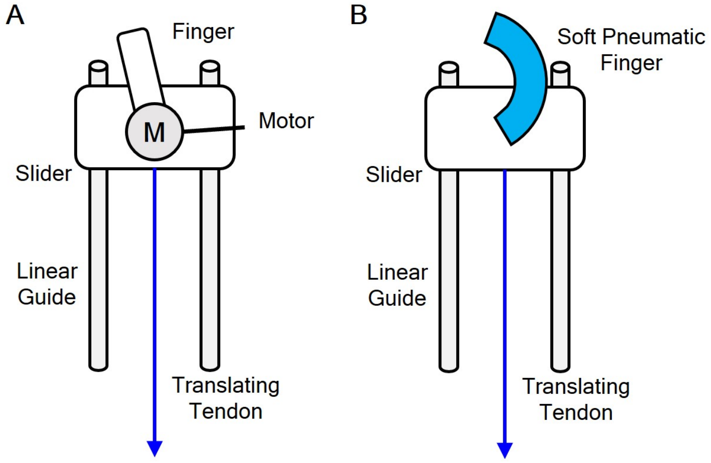

Figure 2.6. Alternative finger designs for decoupling the finger rotation and translation. (**A**) Directly connecting a motor to the revolute joint of the finger. (**B**) Using a soft pneumatic finger.

by compact motors. Figure 2.7A shows a finger constructed with one of the intuitive RP joints; the finger is connected to the slider by a revolute joint, and the slider moves linearly along a linear guide. In this design, pulling the grasping tendon not only rotates the finger but also translates the finger. Similarly, pulling the translating tendon loosens the grasping tendon, causing grasping failure of the finger. This problem generally occurs in a multi-joint robotic system driven by multiple tendons [82]. To address this issue, studies for controlling coupled tendons [83, 84] or designing systems that mechanically decouple the kinematics of tendons [85–91] have been proposed. Especially, tendon decoupling designs enable direct motion control, reducing control costs for each finger. The fundamental principle of tendon decoupling design is that when the length of one tendon changes, the lengths of other tendons must remain constant. As an example, the RUTH Hand (35) utilizes a constant tendon system to maintain the grasp on an object while the tendon-driven finger translates the object in a direction parallel to the palm

2.2.2 Decoupling Linkage Design for Motion Decouple

Based on this principle, we proposed a finger design incorporating two decoupling links that can decouple grasping and translation motions, which has not been explored previously. Figure 2.7B shows the finger made of RP planar linkage with a decoupling linkage. When the finger is pulled toward the palm, the grasping tendon is released at pulley 2, and further wound at pulleys 1 and 3 (Fig. 2.7C). The amount of winding and unwinding of the grasping tendon can be equalized by choosing appropriate radii of the pulleys and lengths of decoupling links, allowing finger translation without changing the length of the grasping tendon. Therefore, the decoupling linkage maintains the finger's rotation angle during finger translation and prevents grasping failure. In addition, the decoupling linkage can withstand the pulling force of the grasping tendon, preventing translation of the finger when the grasping tendon is pulled (Fig. 2.7D). As a result, adding a decoupling linkage to the RP planar linkage creates a decoupled movement of the joints, allowing direct control of each joint.

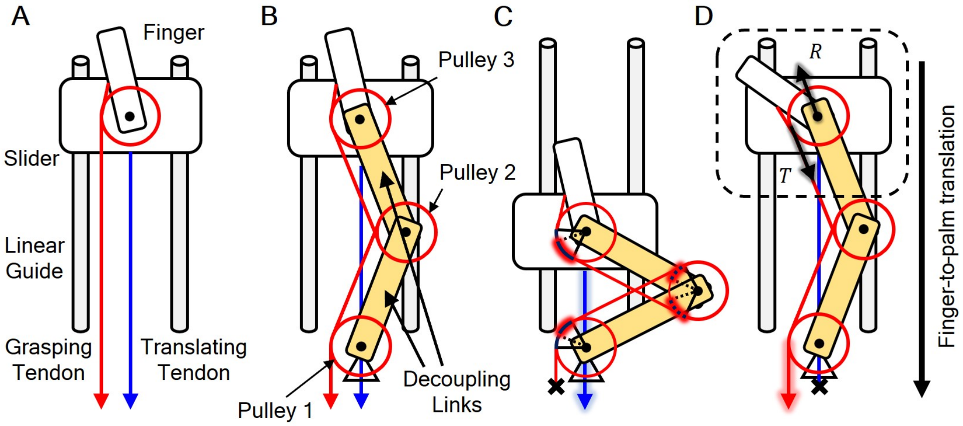
A
Finger
Slider
Linear Guide
Grasping Tendon
Translating Tendon
B
Pulley 3
Pulley 2
Pulley 1
Decoupling Links
C
D
R
T
Finger-to-palm translation

Figure 2.7. The necessity of decoupling links (**A**) One example of a simple planar RP linkages. (**B**) The proposed RP linkage with decoupling links. In the simple planar RP linkage design, the kinematics of the two tendons are coupled, causing coupled joint motions when a single tendon is pulled. In contrast, the decoupling links decouple the joint motions. (**C**) DDecoupling links capable of maintaining the length of the grasping tendon during the translation process of the finger. (**D**) Decoupling links that can withstand the pulling force of the grasping tendon, preventing translation of the finger when the grasping tendon is pulled.

2.3 Storing Section Design

2.3.1 Background

A storing section that can translate multiple objects between the storage and fingers and simultaneously store various objects was proposed. To simplify the object translating process, the proposed storing section was designed to actively translate objects. This is because passive storages, such as a basket, may result in more difficult grasping issues when getting objects out of the storage, often seen in bin-picking problems. Therefore, a belt system that can easily manipulate multiple objects with a single actuator is proposed as a storage. Objects are sandwiched between the two belts, stored in order, and delivered to the fingers in the reverse order of storage. Such active surfaces, like belts or rollers, have been widely used by conventional grippers to manipulate objects in desired directions while maintaining the grasp [92–95]. Particularly, the BACH Hand [92] and the Velvet Hand [93] demonstrated that fingers embedded within belt surfaces could perform various in-hand manipulation tasks successfully. While this flat belt design is powerful for in-hand manipulation of single objects, it faces challenges in simultaneously translating multiple stored objects. When storing multiple objects together, the flat elastic belt storage lacks the surface area in contact with small objects, resulting in the unstable storage of differently sized objects (Fig. 2.8A) and the storage failure of small objects (Fig. 2.8B).

2.3.2 Conveyor Palm Design with Hairy Belt

To stably store different-sized objects simultaneously between the two belts with a simple storing system, elastomeric hairs were embedded on the surface of the belts. Inserting objects between the hairy belts causes deformation in the hairs, generating a restoring force that stores the objects in place (Fig. 2.8C). The storage of the palm is simplified by using this passive storing mechanism, which only utilizes the rotation of the belts to translate and store objects. In addition, the hairy belt design allows simultaneous storage of different-sized objects, as the hairs can ensure the contact area for each object and the deformed hairs in contact with the object do not hinder the storage of other objects.

2.3.3 Fabrication

The fabrication process of the hairy belts is shown in Fig. 2.9. The proposed belts were molded with an elastomer (Dragon Skin 30, Smooth-On Inc.) using inner and outer molds (Fig. 2.9A). To simplify the fabrication process, the belt and hairs are manufactured in one step through injection molding (Fig. 2.9B). Air vents with a diameter of 0.5 mm were applied to prevent air traps at the tips of the hairs. After curing in an oven at 65℃ for 1 hour, a long rectangular surface with embedded hairs was obtained (Fig. 2.9C). After removing the thin cylinders made by the vents, an elastomeric adhesive (Sil-poxy, Smooth-On Inc.) was applied to attach both ends of surface (Fig. 2.9D). Finally, the belt attached by Sil-poxy was cured in an oven at 65℃ for 10 minutes.

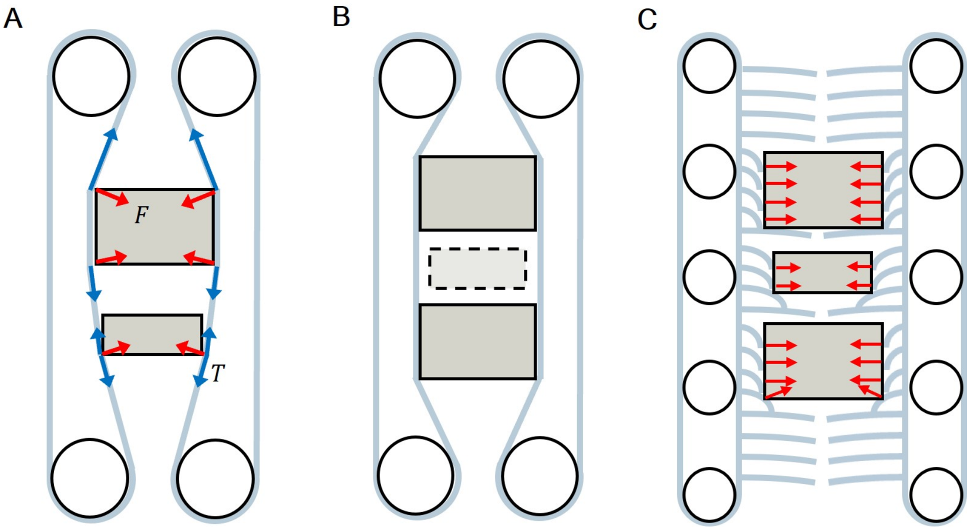

Figure 2.8. Comparison between hairless elastic belt storage and hairy elastic belt storage. In the hairless elastic belt, the storage of an additional object results in additional deformation of the belt surfaces, (**A**) reducing the storing force of the stored objects and (**B**) leading to storage failure of small objects. When the object is inserted into the hairy belt storage, (**C**) the elastomeric hairs bend and independently push the object, allowing simultaneous storage of arbitrarily shaped objects.

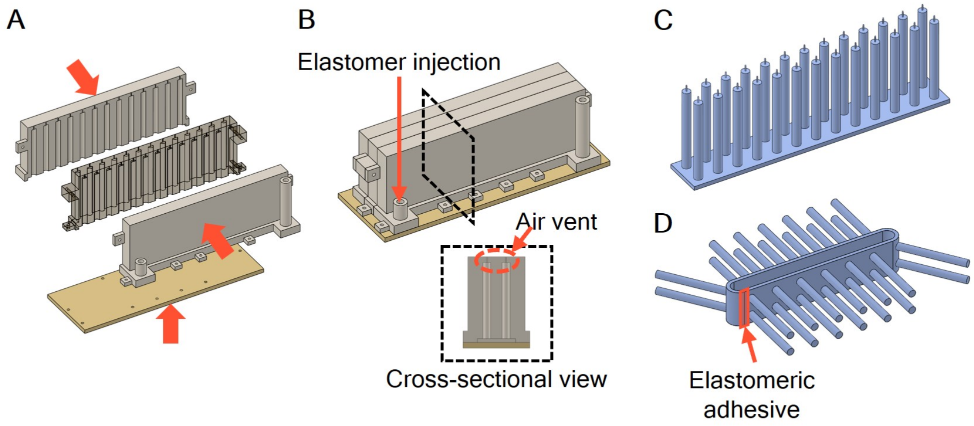
A
B
Elastomer injection
Air vent
Cross-sectional view
C
D
Elastomeric adhesive

Figure 2.9. Fabrication process of the proposed hairy belt. Hairy belts were manufactured by one-step injection molding: (**A**) the inner and outer molds were combined by bolts and nuts, and then (**B**) the elastomer (Dragon Skin 30) was injected into the mold. Air vents were incorporated to prevent air traps at the tips of the hairs. (**C**) The result after curing in an oven at 65℃ for 1 hour. (**D**) The hairy belt was obtained by attaching both ends of belt surface with elastomeric adhesive (Sil-poxy), following the removal of the thin cylinders formed by the air vents.

2.3.4 Replaceable Design of the Conveyor Palm

The proposed conveyor palm has the advantage of storing multiple objects with a single motor, but it has the drawback that the storing force is passively determined. Therefore, a replaceable conveyor palm design is necessary to ensure the appropriate conveyor palm can be used depending on the gripper's target task. The fingers are connected to the gripper body with tendons, making them difficult to detach. In contrast, the conveyor palm uses gears for motor torque transmission, allowing for easy separation from the body.

The process of replacing the conveyor palm is detailed in Figure 2.10. First, loosen the bolts connecting the conveyor palm to the fingers and the gripper body (Figure 2.10A and B). This allows the conveyor palm to be detached while keeping the fingers connected to the tendons. Next, disassemble the conveyor palm to replace the hairy belt (Figure 2.10C). The hairy belt, made of elastomer, is tensioned and fixed to the rollers. It can be easily removed by pulling the belt and replaced with the desired one. Once the replacement is complete, reassemble the parts in reverse order to finalize the new gripper (Figure 2.10D).

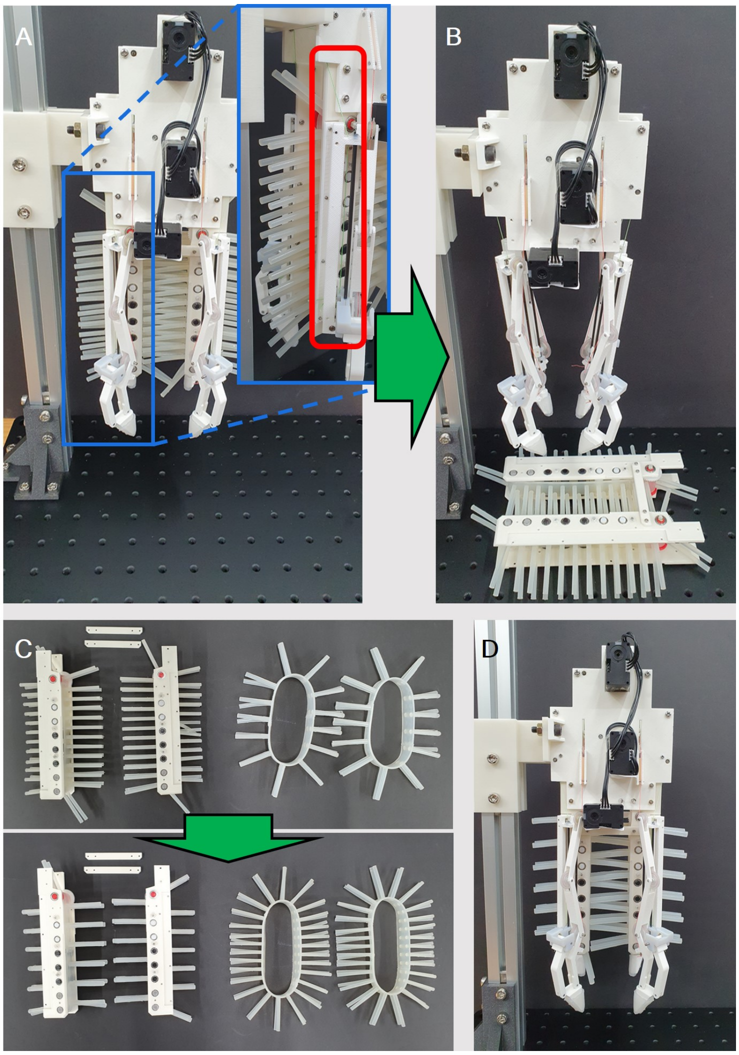

Figure 2.10. The process of replacing the conveyor palm. Hairy belts were manufactured by one-step injection molding: (**A, B**) Loosen the bolts connecting the conveyor palm to the fingers and the gripper body. (**C**) Replace the hairy belt of the conveyor palm. (**D**) Assemble the gripper by reversing the steps in (A).

Chapter 3

Analysis of Grasping Section and Storing Section

3.1 Design Condition of Decoupling Links

3.1.1 Design Condition for Decoupling Grasping and Translation

To successfully decouple the joints' movement, proper design conditions for the length of the decoupling links and the size of the pulleys are required. The required functions of the decoupling links are as follows:

- Preventing slack on the grasping tendon during translation
- Preventing translation of the finger during grasping

The condition for the first function is derived by the kinematic analysis of the finger (Fig. 3.1A). During finger translation after grasping the object, the

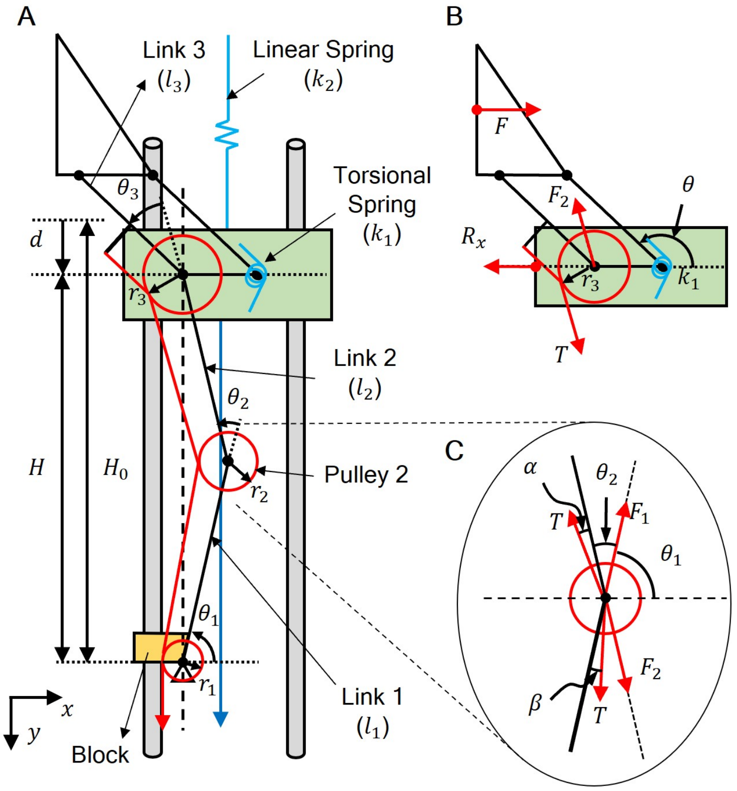
A
Link 3
(l_3)
Linear Spring
(k_2)
Torsional
Spring
(k_1)
θ_3
d
r_3
Link 2
(l_2)
θ_2
H
H_0
Pulley 2
r_2
θ_1
r_1
Link 1
(l_1)
x
y
Block
B
F
θ
F_2
R_x
r_3
k_1
T
C
α
θ_2
T
F_1
θ_1
F_2
β
T

Figure 3.1. Analysis of decoupling links. (**A**) Schematic of finger with decoupling links for kinematic analysis. The design parameter (l_1, l_2, r_1, r_2, r_3) condition for maintaining the length of the grasping tendon during finger translation was derived by kinematic analysis of the finger. (**B**) Free body diagram of the finger and slider. (**C**) Free body diagram of pulley 2. The design parameter condition for withstanding the pulling force of the grasping tendon was derived by kinetic analysis of the finger.

change in length of the grasping tendon (Equation 3.1) and the constraints due to the linear guide (Equations 3.2 and 3.3) and the grasped object (Equation 3.4) are given as follows:

$$\Delta L_T = -r_1\Delta\theta_1 - r_2\Delta\theta_2 - r_3\Delta\theta_3 = 0 \tag{3.1}$$

$$l_1 \cos\theta_1 + l_2 \cos(\theta_1 + \theta_2) = 0 \tag{3.2}$$

$$l_1 \sin\theta_1 + l_2 \sin(\theta_1 + \theta_2) = H \tag{3.3}$$

$$\Delta(\theta_1 + \theta_2 + \theta_3) = 0 \tag{3.4}$$

where l_1 and l_2 are lengths of decoupling links, and r_1, r_2 and r_3 are radii of pulleys, θ_1, θ_2 and θ_3 are angles between the adjacent links and H is the distance between the slider and storage. From Equations 3.1 and 3.4, the relation between $\Delta\theta_1$ and $\Delta\theta_2$ are derived as:

$$\Delta\theta_2 = -\frac{r_3 - r_1}{r_3 - r_2}\Delta\theta_1 \tag{3.5}$$

By substituting Equation 3.5 into the derivative of Equation 3.2, we can obtain the relationship of l_1 and l_2 as:

$$l_1 \sin\theta_1 = \left(\frac{r_2 - r_1}{r_3 - r_2}\right) l_2 \sin(\theta_1 + \theta_2), \quad \left(0 < \theta_1 < \frac{\pi}{2}, \quad \frac{\pi}{2} < \theta_1 + \theta_2 < \pi\right) \tag{3.6}$$

where θ_1 and θ_2 are confined with geometrical constraints. Equation 3.6 is valid for arbitrary θ_1 which satisfies its confinement, so the conditions for preventing slack on the grasping tendon are derived as:

$$l_1 = \left(\frac{r_2 - r_1}{r_3 - r_2}\right) l_2 \tag{3.7}$$

$$\pi - \theta_1 = \theta_1 + \theta_2 \tag{3.8}$$

By substituting Equation 3.8 into Equation 3.2, the lengths relationship of the decoupling links is derived as follows:

$$l_1 = l_2 \tag{3.9}$$

By combining Equation S7 and S9, the design condition of the three pulleys is obtained as:

$$r_2 = \frac{r_1 + r_3}{2} \tag{3.10}$$

The design conditions to achieve the second function of the decoupling links are derived through kinetic analysis of the finger (Figs. 3.1B and 3.1C). Since the decoupling links, pulleys, and joints are connected by bearings, the friction between the links and joints is negligible. In addition, since there are no springs on the joints, the links can only exert axial force to other links. Additionally, when the translating tendon is not pulled ($d = 0$), the pretension of the linear spring applies a force in the -y direction on the slider, but the block on link 1 prevents the slider from moving in the -y direction from the initial position. Assuming that the weight of the link and pulley is negligible and d=0, the y-axis force equilibrium of the finger (Fig. 3.1B, Equation 3.11) and x, y-axis force equilibrium of pulley 2 (Fig. 3.1C, Equations 3.12 and 3.13) are derived as follows:

$$\sum F_y = -F_2 \sin(\theta_1 + \theta_2) + T \sin(\theta_1 + \theta_2 + \alpha) = 0 \tag{3.11}$$

$$\sum F_x = F_1 \cos\theta_1 - F_2 \cos(\theta_1 + \theta_2) + T \cos(\theta_1 + \theta_2 + \alpha) - T \cos(\theta_1 + \beta) = 0 \tag{3.12}$$

$$\sum F_y = -F_1 \sin\theta_1 + F_2 \sin(\theta_1 + \theta_2) - T \sin(\theta_1 + \theta_2 + \alpha) + T \sin(\theta_1 + \beta) = 0 \tag{3.13}$$

where α is the angle between link 2 and the grasping tendon, β is the angle between link 1 and the grasping tendon, T is the tension of grasping tendon, k_2 is the stiffness of the linear spring attached to slider, d is the translation distance of the finger, and F_1 and F_2 are the axial forces applied to link 1 and 2, respectively. α and β are determined geometrically as follows:

$$\sin\alpha = \frac{r_3 - r_2}{l_2}, \quad \sin\beta = \frac{r_2 - r_1}{l_1} \tag{3.14}$$

From Equations 3.11 to 3.13, the relation between θ_1 and θ_2 is derived as follows:

$$\frac{\sin(\theta_1 + \beta)\cos\theta_1 - \cos(\theta_1 + \beta)\sin\theta_1}{\sin\theta_1} - \frac{\sin(\theta_1 + \theta_2 + \alpha)\cos(\theta_1 + \theta_2) - \cos(\theta_1 + \theta_2 + \alpha)\sin(\theta_1 + \theta_2)}{\sin(\theta_1 + \theta_2)} \tag{3.15}$$

$$\frac{\sin(\theta_1 + \theta_2)}{\sin\theta_1} = \frac{\sin\alpha}{\sin\beta} = c_1 \text{ (constant)} > 0 \tag{3.16}$$

From Equation 3.2, another relation between θ_1 and θ_2 is derived as follows:

$$\frac{\cos(\theta_1 + \theta_2)}{\cos\theta_1} = -\frac{l_1}{l_2} = c_2 \text{ (constant)} < 0 \tag{3.17}$$

From Equations 3.16 and 3.17, we can obtain the following conditions:

$$(c_2^2 - c_1^2)\cos^2\theta_1 = 1 - c_1^2 \quad \text{(for all } \theta_1\text{)} \tag{3.18}$$

$$c_1 = 1, \quad c_2 = -1 \tag{3.19}$$

$$c_1 = 1 \rightarrow \sin\alpha = \sin\beta \rightarrow \frac{r_3 - r_2}{l_2} = \frac{r_2 - r_1}{l_1} \tag{3.20}$$

$$c_2 = -1 \rightarrow \theta_2 = \pi - 2\theta_1 \tag{3.21}$$

By substituting Equation 3.21 into Equation 3.2, and substituting the result into Equation 3.20, the conditions for the design parameter to prevent the finger's movement along the linear guide can be obtained as follows:

$$l_1 = l_2, \quad r_2 = \frac{r_1 + r_3}{2} \tag{3.22}$$

As a result, the derived conditions of the design parameters, Equations 3.9, 3.10, and Equation 3.22, are the same. The derived design conditions for motion decoupling are based on the ideal case with no friction between the bearing of the pulley and the joint. In practice, friction between the bearing and the joint may slightly affect the motion decoupling of the finger. To prevent this, pretension can be applied to the spring connected to the slider, ensuring that the slider does not move when the grasping tendon is pulled.

3.1.2 Finger movements according to design variations in the decoupling links

To better understand the design condition of decoupling links (Equation 3.9, 3.10, and 3.22), the effect of varying the pulley radii and link lengths was analyzed. It is assumed that each tendon is controlled through position control of its corresponding motor. Initially, the change of grasping angle was analyzed when actuating the translating tendon, with the grasping tendon held stationary. Due to the torque provided by the torsional spring to the finger, it is assumed there is no slack in the grasping tendon throughout the process. When the translating tendon pulls the slider to translate by distance d, the following equation is applicable:

$$H = H_0 - d \tag{3.23}$$

where H_0 is the initial distance between the slider and storage. By solving the Equations 3.1 to 3.4 and 3.23, the grasping angle (θ) is expressed as follows:

$$\begin{aligned}\theta = \theta_{3,0} &+ \frac{1}{r_3}(r_1\theta_{1,0} + r_2\theta_{2,0}) \\ &+ \frac{r_3 - r_1}{r_3}\left(\frac{\pi}{2} - \cos^{-1}\left(\frac{(H_0 - d)^2 + l_1^2 - l_2^2}{2l_1(H_0 - d)}\right)\right) \\ &+ \frac{r_3 - r_2}{r_3}\left(\pi - \cos^{-1}\left(\frac{l_1^2 + l_2^2 - (H_0 - d)^2}{2l_1l_2}\right)\right) = f(d)\end{aligned} \tag{3.24}$$

where θ is the grasping angle of the finger (Fig. 3.1) and $\theta_{1,0}$, $\theta_{2,0}$, and $\theta_{3,0}$ are the initial value of θ_1, θ_2, and θ_3 (Fig. 3.1A). When the decoupling links satisfy only the length condition (Equation 3.9), the centers of three pulleys form an isosceles triangle, causing θ_1 and θ_2 to vary according to the following equation:

$$2\theta_1 + \theta_2 = \pi \tag{3.25}$$

By substituting Equation 3.25 to 3.24, $f(d)$ is expressed as follows:

$$\begin{aligned} f(d) = \theta_{3,0} &+ \frac{1}{r_3}(r_1\theta_{1,0} + r_2\theta_{2,0}) \\ &+ \frac{2r_2 - (r_1 + r_3)}{2r_3}\left(\pi - 2\cos^{-1}\left(\frac{(H_0 - d)^2 + l_1^2 - l_2^2}{2l_1(H_0 - d)}\right)\right) \end{aligned} \tag{3.26}$$

If $\frac{2r_2-(r_1+r_3)}{2r_3} = 0$, then $f(d)$ maintains a constant value with respect to d. Conversely, when the decoupling links satisfy only the radius condition (Equation 3.10), substituting Equation 3.10 into 3.24 results in the following expression for $f(d)$:

$$\begin{aligned} f(d) = C_d + \frac{r_2 - r_1}{r_3}\Bigg(2\pi &- 2\cos^{-1}\left(\frac{(H_0 - d)^2 + l_1^2 - l_2^2}{2l_1(H_0 - d)}\right) \\ &- \cos^{-1}\left(\frac{l_1^2 + l_2^2 - (H_0 - d)^2}{2l_1 l_2}\right)\Bigg) \end{aligned} \tag{3.27}$$

$$C_d = \theta_{3,0} + \frac{1}{r_3}(r_1\theta_{1,0} + r_2\theta_{2,0}) \tag{3.28}$$

If $\frac{l_2}{l_1} = 1$, $f(d)$ maintains a constant value with respect to d.

Next, the change of the translation distance was analyzed when pulling the grasping tendon with the translating tendon held stationary. From Equations 3.11 to 3.13, the relationship between d and T is derived as follows:

$$k_2 d = T\left(\sin(\theta_1 + \theta_2 + \alpha) - \frac{\sin(\theta_1 + \theta_2)}{\sin\theta_2}(\sin(\theta_2 + \alpha) - \sin\beta)\right) \tag{3.29}$$

In addition, the tension of the grasping tendon (T) is expressed as below by the moment equilibrium of link 3 (Fig. 3.1B):

$$T = \frac{k_1 \Delta\theta}{r_3}, \quad \theta = \theta_1 + \theta_2 + \theta_3 \tag{3.30}$$

where k_1 represents the torsional stiffness of torsional spring embedded between the finger and the slider. By substituting Equation 3.30 into 3.29, the relationship between d and is obtained:

$$d = \frac{k_1(\theta - \theta_0)}{k_2 r_3} \Bigg(\sin(\theta_1 + \theta_2 + \alpha) - \frac{\sin(\theta_1 + \theta_2)}{\sin\theta_2} (\sin(\theta_2 + \alpha) - \sin\beta) \Bigg) = g(\theta) \tag{3.31}$$

where θ_0 is the initial angle of link 3 relative to x-axis. In Equation 3.31, $g(\theta)$ can be negative; however, in practice, the translating tendon directly connected to the slider blocks d from becoming negative. Therefore, the actual translation distance when only the grasping tendon is pulled is positive as follows:

$$d = \max(g(\theta), 0) \tag{3.32}$$

When the decoupling links satisfy only the length condition (Equation 3.9), substituting Equations 3.25 and 3.14 into 3.31 results in the following expression for $g(\theta)$:

$$g(\theta) = \frac{k_1(\theta - \theta_0)}{k_2 \cos\theta_1} \cdot \frac{1}{r_3} \left(r_2 - \frac{r_1 + r_3}{2} \right) \tag{3.33}$$

If $\frac{2r_2 - (r_1 + r_3)}{2r_3} = 0$, $g(\theta)$ equals 0. Conversely, when the decoupling links satisfy only the radius condition (Equation 3.10), substituting Equation 3.10 into 3.31 yields the following equation for $g(\theta)$:

$$g(\theta) = \frac{k_1(r_2 - r_1)(\theta - \theta_0)}{k_2 r_3 \cos\theta_1} \sqrt{\frac{1}{l_1^2} + \frac{1}{l_2^2} + \frac{2\cos(2\theta_1 + \theta_2)}{l_1 l_2}} \tag{3.34}$$

If $l_2/l_1 = 1$, $g(\theta)$ equals 0.

In summary, when the decoupling links do not satisfy the design condition's radius criteria, $f(d)$ and $g(\theta)$ change in accordance with $\frac{2r_2-(r_1+r_3)}{2r_3}$. Similarly, when the length condition is not satisfied, $f(d)$ and $g(\theta)$ varies according to l_2/l_1. Consequently, the radii of pulleys and the lengths of links were non-dimensionalized as shown in the equations below (Equation 3.35), and these parameters were used to model changes in the finger's movement.

$$\gamma = \frac{2r_2 - (r_1 + r_3)}{2r_3}, \quad \delta = \frac{l_2}{l_1} \tag{3.35}$$

When the radius condition is not satisfied, finger's movements are directly related to γ as shown in Equations 3.26 and 3.33. In contrast, when the length condition is not satisfied, $f(d)$ and $g(\theta)$ change complexly with respect to l_1 and l_2 (Equations 3.27 and 3.34), making it difficult to define appropriate non-dimensional variables related to the lengths of the links. Therefore, a simplified non-dimensional variable (δ) was defined, and constraint was applied to the lengths of the links as shown in the equation below:

$$l_1 + l_2 = 110 \text{ mm} \tag{3.36}$$

Since H_0 is 100 mm, the total length of the decoupling links must be greater than 100 mm. However, if the lengths of the links become too long, the space occupied by the decoupling links becomes too large. Therefore, the total length of the links was set to 110 mm.

The detailed modeling results on the finger's movement with changes in γ and δ are illustrated in Figs. 3.2 and 3.3. The solid line represents the change in the finger's movements when only the grasping tendon is pulled, while the dotted line indicates the finger's movements when only the translating tendon is actuated. Specifically, when γ equals 0 and δ equals 1 (red lines in Fig. 3.2 and magenta lines in Fig. 3.3), pulling the translating tendon only affects the translation distance, while pulling the grasping tendon exclusively alters the finger's grasping angle. Additionally, when γ is above 0 (green lines in Fig. 3.2), or δ is greater than 1 (orange lines in Fig. 3.3), actuating the translating tendon reduces the grasping angle, and actuating the grasping tendon induces the translation of the finger. In contrast, when γ is below 0 (blue lines in Fig. 3.2), or δ is less than 1 (cyan lines in Fig. 3.3), actuating the translating tendon increases the grasping angle, and actuating the grasping tendon does not lead to finger translation. The prevention of translation occurs because the translating tendon, which is directly connected to the slider, inhibits the translational movement of finger in the negative y-direction ($d < 0$).

To successfully separate the finger's grasping and translation, the lengths of links 1 and 2 were determined to be 55 mm, and r_1, r_2, and r_3 are set to be 4, 6, and 8 mm, respectively, in accordance with Equation 3.22. r_3 is set to be the largest to increase the gripper's grasping force. In addition, the resulting decoupled motions of the proposed fingers enable the decoupled control of each

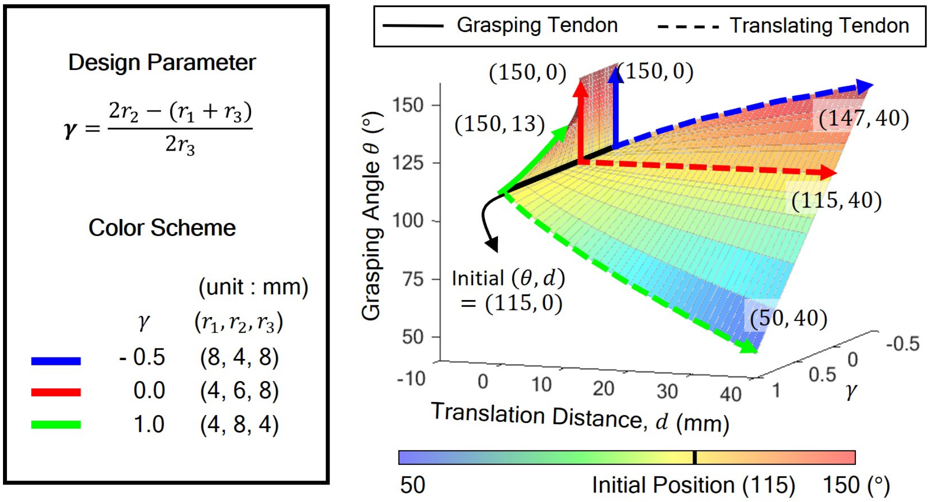

Figure 3.2. Effect of pulley radius variations on fingertip motion. Except for the case where γ is 0, grasping and translation are coupled in all cases.

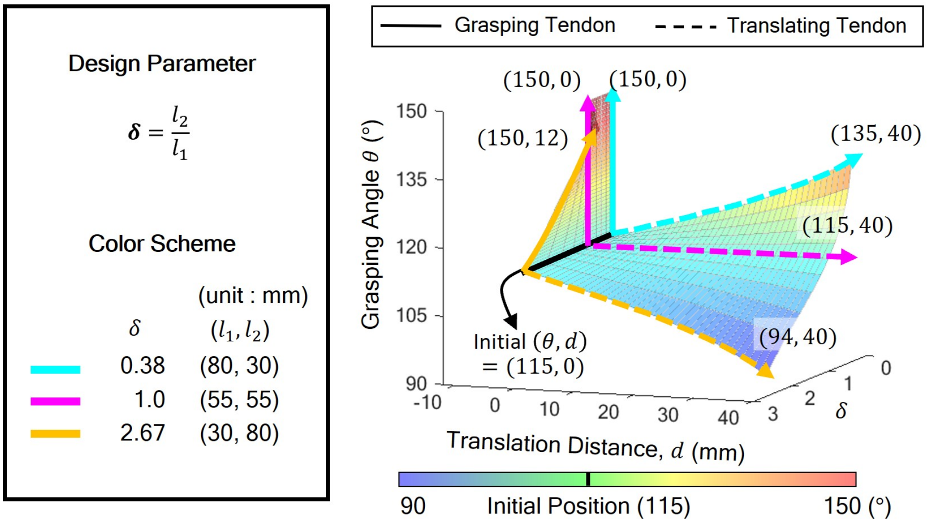

Figure 3.3. Effect of decoupling link length variations on fingertip motion. Except for the case where δ is 1, grasping and translation are coupled in all cases.

motion through underactuation (Fig. 2.4D).

3.1.3 Experimental Validation of Decoupling Links' Design Condition

To experimentally validate the design conditions of decoupling links, the rotational and translational motions of fingers with various decoupling linkage designs were examined. Five different designs were proposed: one satisfied the proposed design conditions, two did not satisfy the radius condition of pulleys, and the other two did not satisfy the length condition of links (Table 3.1). For designs not satisfying the radius condition, the radii of pulleys 1, 2, and 3 were set at combinations of 4, 6, and 8 mm, selecting the smallest (design 2) and largest (design 3) γ values. Also, for the designs that did not satisfy the length condition, lengths of links were chosen such that they significantly differed while satisfying Equation 3.36, with the ratio of link lengths being more than double (designs 4 and 5).

In order to verify the decoupling of the two motions (grasping and translation), the change in the grasping angle of the finger according to its translation distance was measured while pulling the translating tendon (Fig. 3.4). The initial grasping angle of the finger was set to 115° by pulling the grasping tendon with a motor (100:1 Micro Metal Gearmotor HPCB 6V, Pololu). Three markers were attached to the finger (Fig. 3.4A) and the movements of the finger joints were recorded on video. Subsequently, the grasping angle (θ) and translation distance (d) of the finger were measured by tracking the markers through image analysis with MATLAB (MathWorks) (Fig. 3.4B). The MAT-

LAB function “imfindcircle” was utilized to find the red markers, and through the positions of these three markers, the rotation angle and translation distance of the finger were calculated. Five decoupling linkages with different design parameters were fabricated and experiments for each decoupling link design were repeated five times (Table 3.1).

The experimental results for the five designs are shown in Fig. 3.5. The movement of the fingers with the five different designs closely matched the predictions of the analytic model. When $\gamma = 0$ and $\delta = 1$ (design 1), the angle of the finger was almost maintained during translation (red line in Fig. 3.5A and magenta line in Fig. 3.5B). The slight change in grasping angle was due to manufacturing tolerances in the 3D printed linkage. However, applying other designs to the finger leads to significant changes of the grasping angle during translation, which means the finger’s motions are coupled. Specifically, when $\gamma < 0$ (design 2) or $\delta < 1$ (design 4), the grasping tendon tightened during translation, increasing the grasping angle of the finger. In contrast, when $\gamma > 0$ (design 3) or $\delta > 1$ (design 5), the grasping tendon loosened, decreasing the grasping angle of the finger. The translation distance of the finger varies with the design, as finger movement is geometrically constrained by the link lengths and interference from adjacent links.

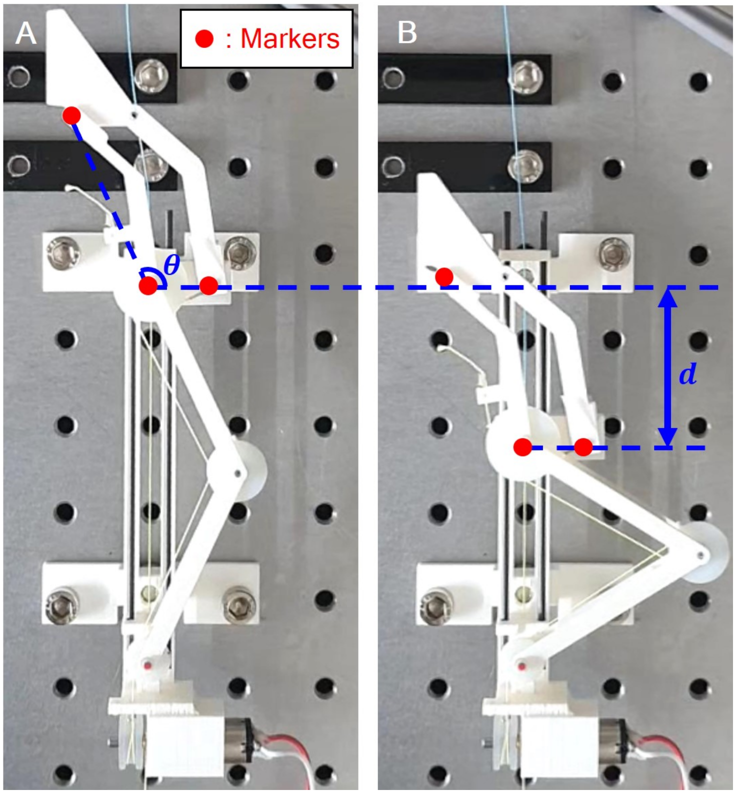

Figure 3.4. Experiment setup for verifying motion decoupling of the finger. (**A**) Measuring the change in grasping angle (θ) according to the translation distance (d). (**B**) Three red markers were attached to the finger, and their positions are tracked during finger translation. The grasping angle (θ) and translation distance (d) of the finger were measured by tracking the markers through image analysis with MATLAB.

Design #	Description	*Parameters* (mm)				
		l_1	l_2	r_1	r_2	r_3
1	Proposed design	55	55	4	6	8
2	Radius variation	55	55	8	4	8
3	Radius variation	55	55	4	8	4
4	Length variation	80	30	4	6	8
5	Length variation	30	80	4	6	8

Table 3.1. Five decoupling link designs with different parameters. The five designs include one proposed design, two with variations in the radii of the pulleys, and two with variations in the lengths of the links.

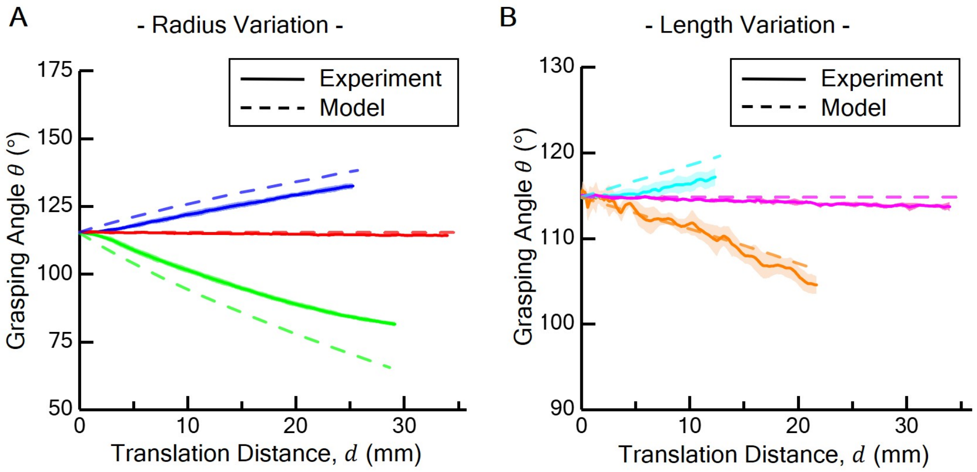

Figure 3.5. Experimental results for verifying motion decoupling of the finger. (**A**) Experimental fingertip motion varying the radii of pulleys. (**B**) Experimental fingertip motion varying the lengths of decoupling links. The minimum and maximum values of each experimental data are indicated by the shaded region.

3.2 Grasping Force Test

3.2.1 Maximum Grasping Force

The maximum grasping force of the gripper is obtained through analyzing the forces exerted on the fingertip's three links (Fig. 3.6A, links 3 to 5), while assuming quasi-static state. Since the gripper pinches an object using frictional force, the maximum grasping force is equal to the sum of the maximum static friction applied by four fingers to the object. The free body diagram of the three links is shown in Fig. 3.6B. The maximum static frictional force exerted on the finger is derived through the force equilibrium equations (3.37, 3.38) at link 5, and the moment equilibrium equations (3.39, 3.40) of link 3 and 4, as shown below:

$$-R_{1,x} - R_{2,x} + F = 0 \tag{3.37}$$

$$-R_{1,y} - R_{2,y} + \mu_s F = 0 \tag{3.38}$$

$$r_3 T - R_{1,x} l_3 \sin\theta + R_{1,y} l_3 \cos\theta = 0 \tag{3.39}$$

$$-k_1 \Delta\theta - R_{2,x} l_3 \sin\theta + R_{2,y} l_3 \cos\theta = 0 \tag{3.40}$$

where R_1 is the reaction force between links 3 and 5, R_2 is the reaction force between links 4 and 5, and μ_s is the static friction coefficient between the object and finger. By solving the system of equations (3.37–3.40), the normal

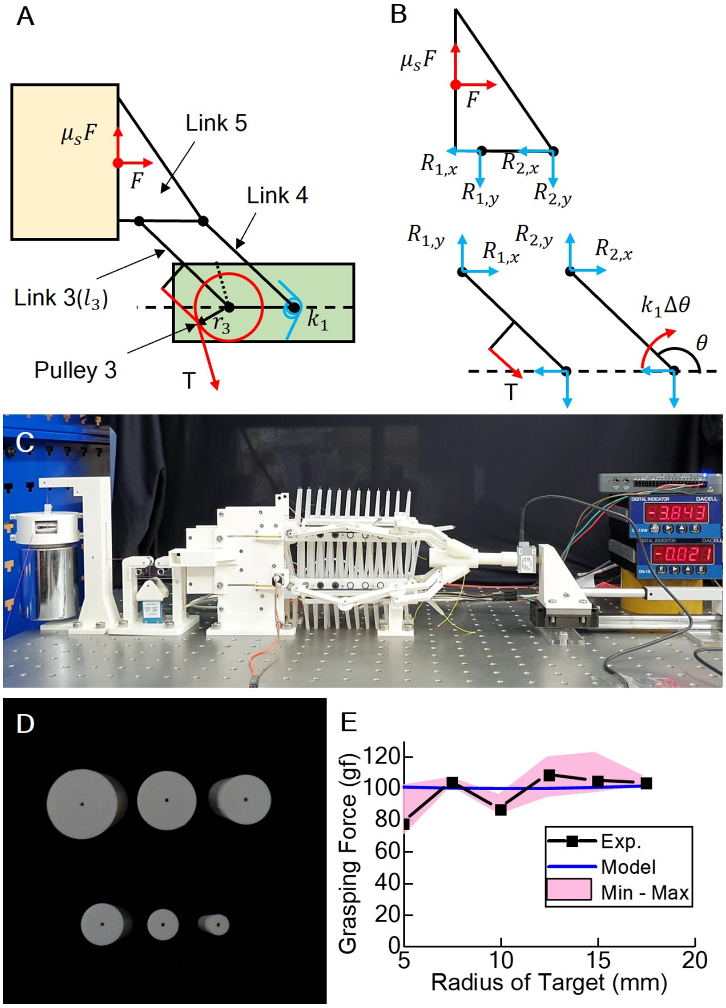
A
$\mu_s F$
F
Link 5
Link 4
Link 3(l_3)
r_3
k_1
Pulley 3
T
B
$\mu_s F$
F
$R_{1,x}$
$R_{2,x}$
$R_{1,y}$
$R_{2,y}$
$R_{1,y}$
$R_{1,x}$
$R_{2,y}$
$R_{2,x}$
$k_1\Delta\theta$
θ
T
C
-3.843
-0.021
D
E
Grasping Force (gf)
0
20
40
60
80
100
120
5
10
15
20
Radius of Target (mm)
Exp.
Model
Min - Max

Figure 3.6. Analysis of the maximum grasping force. (**A**) External forces exerted on the fingertip's three links (Link 3-5). (**B**) Free body diagrams of links 3-5. (**C**) Experimental setup of the maximum grasping force measurement. (**D**) Target objects with radius ranging from 5 to 17.5mm with 2.5mm increments in between. (**E**) The experimental results and theoretical grasping force according to the radius of target.

force applied by the finger to the object is derived as:

$$F = \frac{r_3 T - k_1 \Delta\theta}{l_3(\sin\theta - \mu_s \cos\theta)} \tag{3.41}$$

and the maximum grasping force is obtained as:

$$F_{\text{grasp\_max}} = 4\mu_s \left(\frac{r_3 T - k_1 \Delta\theta}{l_3(\sin\theta - \mu_s \cos\theta)} \right) \tag{3.42}$$

Derived Equation 3.42 implies that a larger r_3 generates a larger grasping force, so the radius of pulley 3 was set to be the largest among the pulleys.

The maximum grasping force of the gripper was also measured experimentally to evaluate its grasping capabilities. Figure 3.6C shows the experimental setup of the maximum grasping force measurement. The maximum grasping force was measured as the object was pulled away from the gripper. A rubber band was attached between the load cell (333FB, Ktoyo Co. Ltd.) and the linear actuator (P16-P, Equinox) to prevent the object from slipping before reaching the maximum static friction. By measuring the force just before the object starts to move, the maximum static friction, which is equal to the maximum grasping force, was obtained.

A weight of 2 kg was hung on the grasping tendon so that the tension of the grasping tendon was maintained throughout the experiment. The tension of the grasping tendon was measured using a load cell (333FDX, Ktoyo Co. Ltd.). The sizes of the target objects were chosen according to the geometric limitations of the gripper and storage. Since the diameter of the fingertip was 11 mm, the gripper could grasp objects with diameters larger than 4.6 mm.

Also, since the distance between the two belts' surfaces was 45 mm, an upper diametric limit of the target objects was set at 45 mm. The diameters of the target objects were determined with a margin of approximately 5 mm from the maximum and minimum storable object diameters. In detail, the target objects were chosen to be cylinders with radii ranging from 5 to 17.5 mm with 2.5 mm increments in between (Fig. 3.6D). The experimental results and theoretical grasping force were compared in Fig. 3.6E. Since the tension at which the fingers start to move was about 1040 gf, the sum of the frictional forces of the system components such as the moving pulley, slider, and joint of the finger is estimated to be about 1040 gf. Therefore, the theoretical maximum forces were calculated by substituting the total tension of 960 gf (subtracting total frictional force of 1000 gf at a total weight of 2000 gf) and the static friction coefficient into Equation 3.42. The static friction coefficient between the fingertip (wrapped up by Dragon Skin 30, Smooth-On Inc.) and target (3D printed with ABS material) was 0.8. The experimental and theoretical results have similar trends, as the diameter of the target object increases.

3.2.2 Cyclic Grasping Test

The proposed gripper's four fingers are tendon-driven, and its grasping force can vary due to slack caused by the permanent deformation of tendons during repeated operations. To evaluate this, a cyclic pulling force test was conducted to measure the gripper's grasping force according to the number of repeated operations. The experimental setup is illustrated in Fig. 3.7. An object was fixed to the slide of a linear guide that moves vertically, while a load cell (KTOYO 333FDX) was attached to the end of a linear motor (Actuonix P16-150-256-12-P). The load cell and the object were connected via tendons.

The object used for grasping test was a cylinder with a diameter of 20 mm, corresponding to the median size of the target objects used in both previous and future experiments. To better observe the effects of permanent deformation in the tendon, the gripper's tendon was replaced with a new, unused tendon for the experiment. The gripper was driven by current control of the motor (Dynamixel XC330-M288-T), and the current was set to 220 mA.

The experiment consisted of several steps. First, the gripper grasped the object and held it for 1 second, and after that, the grasping force was measured using a load cell while the objects were pulled by a linear motor at a speed of 4.2 mm/s. The object was pulled 10 mm downward while grasped by the gripper, and the maximum pulling force during this process was measured as the grasping force. After the object was pulled 10 mm downward, the gripper released the object, and the linear motor returned to its initial position, bringing the object back to its starting point. However, since the tendon cannot exert a pushing force, an external force in the opposite direction of gravity is required to return the object to the initial position. To address this, a method was proposed to automatically return the object to the initial position: a weight block (200 g) was hung to apply force in the opposite direction of gravity. The experiment was repeated 1,000 times.

The experimental results are shown in Fig. 3.8. During 1,000 cycles of operation, the grasping force exhibited slight fluctuations but remained largely consistent. The maximum measured value was 233.88 gf, and the minimum was 218.22 gf, with all observed values falling within 7% of the maximum. The change in the required stroke due to the permanent deformation of the tendon after 1,000 cycles was measured to be approximately 20 mm. This value represents the sum of the changes in the tendons that make up the moving pulley tendon system and was calculated using the following equation (Fig. 3.9):

$$\Delta L_{\text{stroke}} = \Delta L_{T_1} + \frac{1}{2}\Delta L_{T_2} + \frac{1}{4}\left(\Delta L_{T_3} + \Delta L_{T_4}\right) \tag{3.43}$$

where ΔL_{stroke} is the change in the total required stroke length, ΔL_{T_1} is the length change of tendon 1, ΔL_{T_2} is the length change of tendon 2, ΔL_{T_3} is the length change of tendon 3, and ΔL_{T_4} is the length change of tendon 4.

The gripper is driven by a moving pulley system consisting of four tendons to differentially drive the four fingers. In this system, the ends of tendon 3 and tendon 4 are fixed to the fingers, and these two tendons receive force transmitted through the moving pulleys at both ends of tendon 2. Tendon 2 transmits motor force through the moving pulley at the end of tendon 1. The permanent deformation of the tendons affects the total stroke length as follows: one-fourth of the permanent deformation length of tendons 3 and 4, one-half of the permanent deformation length of tendon 2, and the entire permanent deformation length of tendon 1 contribute to the overall stroke length change.

Even if permanent deformation occurs in the tendons and changes the stroke length required to drive the gripper, the grasping force is maintained because the gripper's fingers are driven through current control. Current control maintains tension in all times when grasping occurs, even when deformation occurs in the tendons. Therefore, as long as the fingers are driven through current control, no significant degradation in grasping force was observed over repeated use.

However, a sufficient condition for preventing degradation of grasping force is that the motor must be able to pull the entire tendon system by the stroke length required for grasping. If the system's available stroke is smaller than the required stroke, the motor will not be able to pull the tendon sufficiently, failing to grasp the object. Therefore, it is crucial to predict the amount of permanent deformation in tendons 1, 2, 3, and 4 and design the tendon system with sufficient additional stroke in advance to ensure proper gripper operation.

In order to design the stroke margin of the tendon system, it is necessary to predict the amount of permanent deformation in each tendon. Therefore, the permanent deformation of each tendon was measured under the same load conditions as those used in the cyclic pulling force test. Two types of tendons were used in this study: Dyneema (SAPA) size 2 and size 4. Dyneema size 2 was used for tendons 3 and 4, which experience relatively lower forces, while Dyneema size 4 was used for tendons 1 and 2, which need to withstand higher forces. These tendons are synthetic fibers, and permanent deformation of synthetic fibers can be predicted by performing a cyclic loading test, which involves repeatedly applying and releasing loads. Since the process of grasping and placing objects involves applying and releasing loads on the tendons, cyclic loading tests are suitable for measuring the permanent deformation of tendons during repeated grasping. Accordingly, cyclic loading tests were conducted 5,000 times under the load conditions for each tendon, and the details are summarized in Appendix A. When the motor was controlled at 220 mA, the tension on tendon 1 was 2.9 kgf, tendon 2 was 1.45 kgf, and tendons 3 and 4 were 0.725 kgf. The experiment was conducted under these load conditions.

The experimental results are shown in Fig. A.2. Regardless of the load condition, the permanent deformation ratio of each tendon converged as the number of cycles increased. For tendon 1, under a load of 2.9 kgf, the permanent deformation converged to 7.56% after 5,000 cycles (blue line in Fig. A.2B). This means that repeatedly applying and releasing a load of 2.9 kgf to Dyneema size 4 causes its neutral length to increase, stabilizing at 7.56% deformation. Similarly, for tendon 2, under a load of 1.45 kgf, the deformation converged to 3.45% (red line in Fig. A.2B). For tendons 3 and 4, under a load of 0.725 kgf, the deformation converged to 4.54% (green line in Fig. A.2B).

Now, the stroke margin required for the gripper to repeatedly grasp objects can be calculated using the measured permanent deformation of the tendons. Assume the gripper is controlled at 220 mA. The initial lengths of the tendons in the gripper design are approximately 60 mm for tendon 1, 250 mm for tendon 2, and 650 mm each for tendons 3 and 4. If the permanent deformation ratio of each tendon is defined as $\epsilon_{\mathrm{per},i}$, the permanent deformation length of each tendon is expressed as follows:

$$\Delta L_{T_i} = \epsilon_{\mathrm{per},i} L_{T_i} \tag{3.44}$$

where ΔL_{T_i} is the permanent deformation length of tendon i, and L_{T_i} is the original length of tendon i. Substituting the permanent deformation lengths of all tendons into Equation 3.43, the total stroke length required for the tendon system ($\Delta L_{\mathrm{stroke}}$ is calculated as 23.61 mm. This indicates that, as long as no other parts of the tendons or fingers are damaged, a stroke length margin of approximately 23.61 mm is sufficient to maintain the grasping force.

After 1,000 grasping cycles, a tendon length change of approximately 20 mm was observed, which appears smaller than 23.61 mm as the tendon deformation had not yet converged. Additionally, comparing the blue and red lines in Fig. A.2B shows that using the same type of tendon results in greater deformation under higher loads. Comparing the red and green lines demonstrates that smaller Dyneema sizes result in greater deformation, even under lower loads. Therefore, to minimize the stroke margin and achieve a more compact design, it is recommended to use larger Dyneema sizes with higher load capacities.

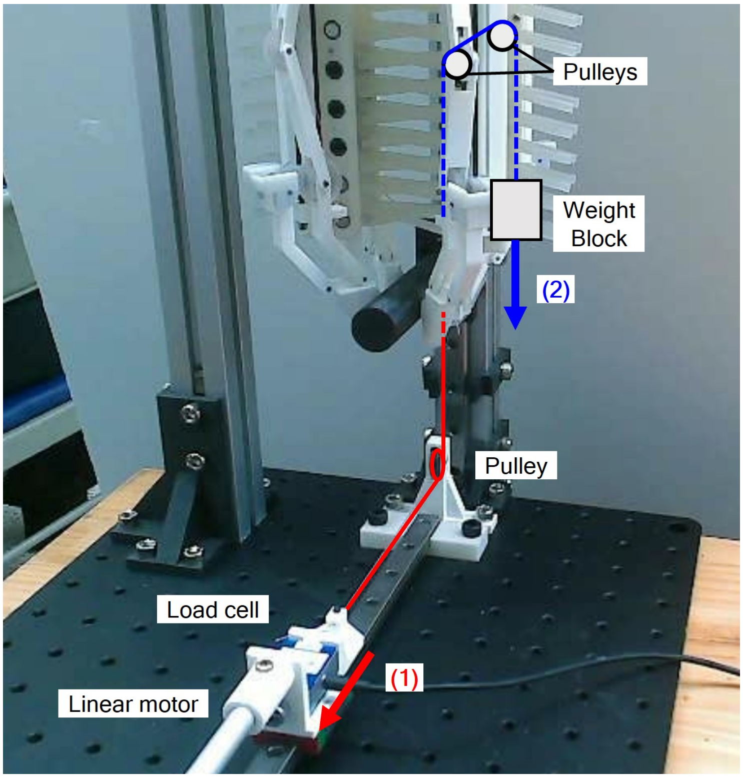
Pulleys
Weight Block
(2)
Pulley
Load cell
Linear motor
(1)

Figure 3.7. Experimental setting for cyclic grasping test. When the gripper grasps an object, the linear motor pulls the object while the load cell measures the grasping force.

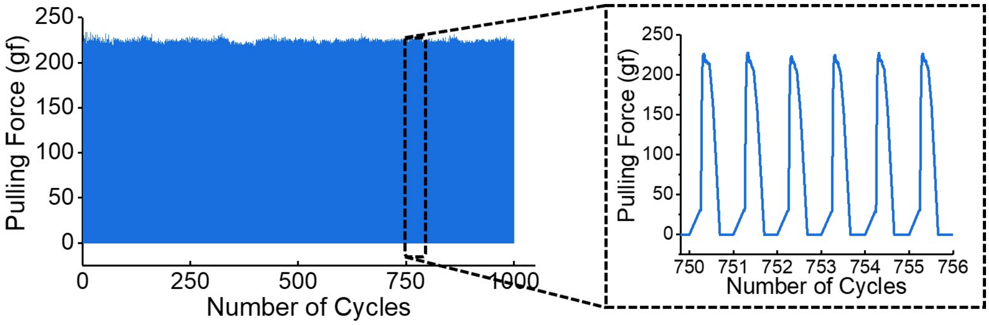

Figure 3.8. Experimental results of cyclic grasping test. The grasping force remained nearly constant throughout 1,000 repeated grasping cycles.

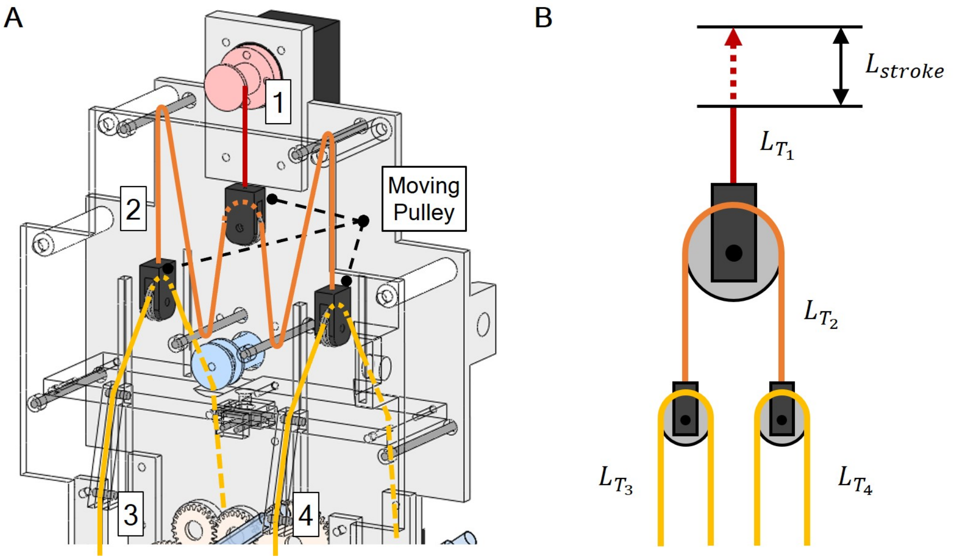
A
B
1
2
3
4
Moving Pulley
L_{stroke}
L_{T_1}
L_{T_2}
L_{T_3}
L_{T_4}

Figure 3.9. Explanation of the gripper's tendon-driven system. (**A**) The gripper's fingers are operated by a total of four tendons. (**B**) One-fourth of the deformation in the tendon connected to the fingers (yellow) affects the total stroke, while half the deformation in the orange tendon and the full deformation in the red tendon affect it as well.

3.3 Storing Force of Conveyor Palm

3.3.1 Parameter Selection

The maximum weight of the object that can be stored in the palm was analyzed. When an object is inserted into the palm, the object deforms the hairs significantly, and the hairs stochastically contact each other, making analytical modeling difficult. Therefore, the maximum storable weight was experimentally measured and analyzed by the finite element analysis (FEA).

The storing force is determined by the frictional force between the hairs and the object, which is generated by the restoring force of the hair. The restoring force is calculated by the product of the hair's deformation and its bending stiffness. The main parameters that affect the deformation of the hair are the distance between the hairs (b) and the size of the target (R) (Fig. 3.10A). The main parameters that affect the bending stiffness of the hair are the radius of the hair (r) and the Young's modulus of its material (E). In detail, according to the moment-curvature equation of hair (Equation 3.44), the second moment of inertia and the curvature of the hair affect the restoring force. Changing r affects not only the second moment of inertia but also the curvature of the hairs because the distance between the surfaces of adjacent hairs varies depending on r. In contrast, changing E does not affect the deformation of the hairs.

These design parameters can be divided into the geometric parameters and material parameters of the conveyor palm. The geometric parameters of the conveyor palm include the distance between the hairs (b) and the size of the target (R), while the material parameter is the Young's modulus of the material composing the hair (E). The changes in the storing force of the conveyor palm were experimentally measured based on variations in each parameter. The shapes of the targets were set as a cylinder, and the radius was used to represent size. The target objects' radii were ranging from 2.5 to 17.5 mm with 2.5 mm increments in between (Fig. 3.10B). The detailed method for determining the size of the target object will be discussed in Chapter 3.3.2. The distance between the two belt surfaces on either side of storage was designed as 45 mm. The details of the experimental parameters are shown in Table 3.2.

In summary, four parameters were selected to analyze the storing force of the conveyor palm: the radius of the hair (r), the distance between the hairs (b), the size of the target (R), and Young's modulus of hairs' material (Fig. 3.10A). The maximum storable weight of the palm varies depending on the direction of the gravitational force applied to the object. Therefore, both the storable weight along the y-axis and the storable weight along the x-axis were analyzed (Fig. 3.10A). In this thesis, the storing force in each direction is defined as the maximum storable weight in that direction. In addition, storing force along the y-axis was defined as transverse storing force, and along the x-axis as longitudinal storing force.

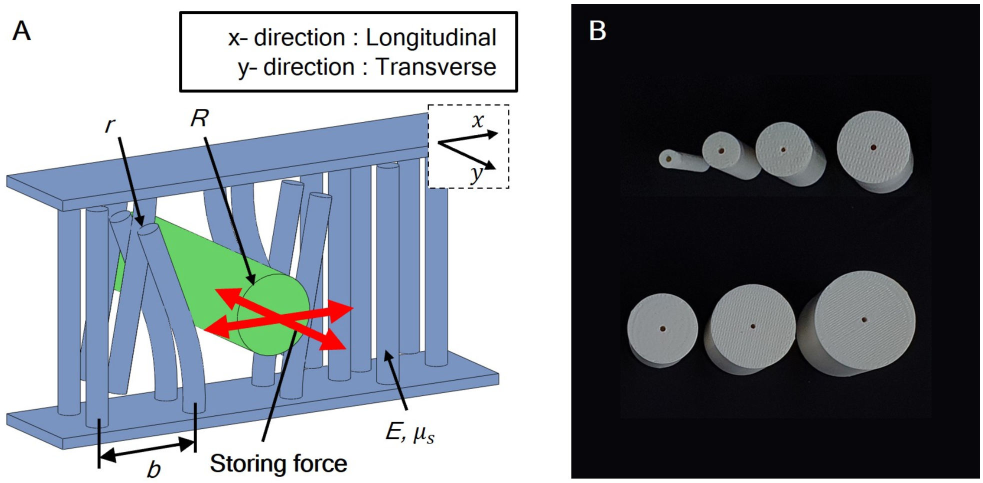
A
x- direction : Longitudinal
y- direction : Transverse
r
R
x
y
E, μ_s
b
Storing force
B

Figure 3.10. Experimental parameters for analysis of storing force. (**A**) Design parameters for investigating the storage force of the proposed conveyor palm. (**B**) Target objects were set as cylinders, and the radii of the targets ranged from 2.5 to 17.5mm with 2.5mm increments.

Parameters	**Variations**
Radius of the hair (r)	1.5, 2.0, 2.5, 3.0 mm
Distance between the hairs (b)	10.0, 20.0, 30.0 mm
Target size (R)	2.5, 5.0, 7.5, 10.0, 12.5, 15.0, 17.5 mm
Fabrication material	DragonSkin 30, Smooth-Sil 950, Smooth-Sil 960

Table 3.2. Detailed experimental parameters of storing force. The design parameters of conveyor palm were radius of the hair (r), distance between the hairs (a), and target sizes (R).

3.3.2 The Upper and Lower Limits of Storable Objects by the Conveyor Palm

Before measuring the storing force according to changes in the parameters of the conveyor palm, it is necessary to first analyze the size of objects that can be stored by the conveyor palm. Therefore, this chapter presents a theoretical analysis on the size of objects that the conveyor palm can store. Since the conveyor palm stores objects through the passive deformation of its hairs, the size of objects that can be stored depends on the palm's geometric parameters (r and b) and material property (elongation at break). Accordingly, a theoretical model has been proposed to analyze how the hair radius (r), the distance between hairs (b), and the material's elongation at break affect the upper and lower size limits of storable objects.

Although the upper and lower size limits may also vary depending on the shape of the objects, the analysis was conducted focusing on cylindrical objects for simplicity. The lower limit of object size storable by the conveyor palm is defined simply by the geometry of the object and the conveyor palm (Fig. 3.11A). For an object to be stored in the palm, it must contact at least two hairs. Therefore, the lower limit of storable object size is defined as the distance between the surfaces of two adjacent hairs:

$$R_{\text{min}} = \frac{b}{4} - r \tag{3.45}$$

where R_{min} is the lower limit of the radius of storable objects.

The upper limit of storable object size depends on how extremely the hairs can deform. Accordingly, the elongation at break of the material composing the hairs is the most important parameter. For example, if the hairs are made of brittle glass, even a slightly larger object than the distance between the surfaces of two adjacent hairs would cause the hairs to break. Therefore, it is necessary to model how much deformation the hairs undergo when storing an object. Since the hair closest to the surface of the object experiences the greatest deformation, the deformation of the nearest hair was analyzed theoretically. When an object is stored, the deformation of the closest hair can be schematically represented as shown in Figure 3.11B. Let us assume that the hair bends with constant curvature. In this case, the following equation can be derived using the Pythagorean theorem:

$$\left(x + \frac{b}{4}\right)^2 + \left(\frac{d_{\text{surf}}}{2}\right)^2 = (x + R + r)^2 \tag{3.46}$$

where d_{surf} is the distance between the two belt surfaces of the conveyor palm, and x is the radius of the imaginary circle created by the bending of the hair. By rearranging Equation 3.46, the expression for x can be derived as follows:

$$x = \frac{1}{2(R+r) + \frac{b}{2}} \left(\frac{d_{\text{surf}}^2}{4} + \frac{b^2}{16} - (R+r)^2\right) \tag{3.47}$$

When the hair is bent as shown in Figure 3.11B, the maximum strain of the hair (ϵ_{hair}) can be calculated as follows:

$$\epsilon_{\text{hair}} = \frac{(x+r)\theta - x\theta}{x\theta} = \frac{r}{x} < \epsilon_{\text{max}} \tag{3.48}$$

where θ is the bending angle of the hair, and ϵ_{max} is the elongation at break of the material composing the hair. To ensure robustness during the actual use of the conveyor palm, it is advisable to avoid deforming the material to its full elongation at break. Instead, a safety factor is applied as follows:

$$\epsilon_{\text{allow}} = \frac{\epsilon_{\text{max}}}{SF} \tag{3.49}$$

where ϵ_{allow} is the usable range of elongation, and SF is the safety factor. Although safety factors are typically used to determine working stress, in this dissertation, they are employed to define the usable range of elongation due to the high dependence of conveyor palm deformation on geometric factors. The safety factor was also applied because the actual bending of the hairs during object storage may exceed the theoretically calculated values. For instance, Equation 3.48 is derived under the assumption of pure bending, but in practice, longitudinal elongation may occur. Additionally, out-of-plane bending could result in strains greater than the strain values calculated in a two-dimensional model. Finally, to ensure robustness during actual use of the conveyor palm, it is advisable not to deform the material to its full elongation at break.

By substituting Equation 3.49 into Equation 3.48, the following relationship is obtained:

$$\frac{r}{x} = \frac{\epsilon_{\text{max}}}{SF} \tag{3.50}$$

By substituting Equation 3.50 into Equation 3.47, the following equation for the maximum radius of storable objects is obtained:

$$R_{\text{max}} = -\left(1 + \frac{SF}{\epsilon_{\text{max}}}\right) r + \sqrt{\left(\frac{SF \cdot r}{\epsilon_{\text{max}}} - \frac{b}{4}\right)^2 + \frac{d_{\text{surf}}^2}{4}} \tag{3.51}$$

Now, the lower and upper radius limits of storable cylindrical objects can be determined based on the design of the conveyor palm. The radius of storable objects according to the storage design is summarized in Table 3.3. For example, if the radius of the hair (r) is 2 mm, the distance between hairs (b) is 10 mm, and the hair material is DragonSkin 30, then using a safety factor of 2 for the calculation, the maximum storable radius is calculated to be 19.4 mm, and the minimum storable radius is calculated to be 0.5 mm. According to Smooth-On Inc., the elongation at break of DragonSkin 30 is 3.64, and this value was used in the calculations.

As shown in Table 3.3, the smallest radius of objects that can be stored by various conveyor palm designs is 0.5 mm, while the largest radius is 20.6 mm. When conducting experiments with a common target object across various designs, it is safe to attempt to store objects smaller than the lower limit of storable objects for a specific design, but it is risky to store objects larger than the upper limit. Therefore, the radius range for target objects was set between 0.5 mm and 18.1 mm. To ensure equal intervals between radii, the size increment size was set to 2.5 mm. Consequently, the radii of target objects for the storing force experiments were determined to increase from 2.5 mm to 17.5 mm in increments of 2.5 mm.

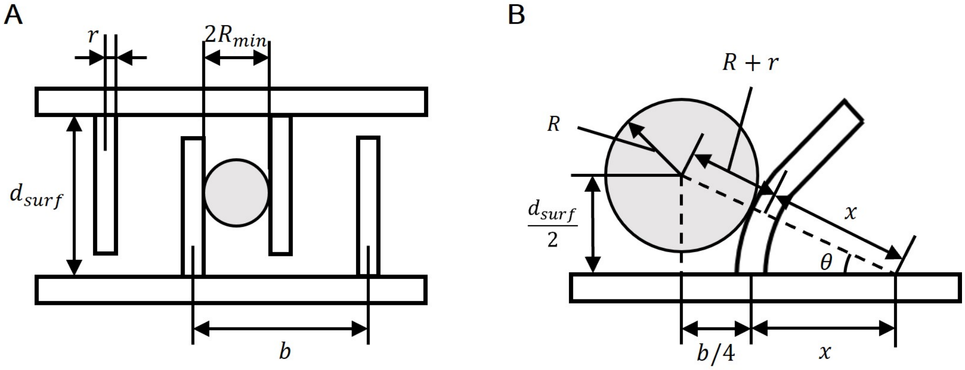

Figure 3.11. Schematic of small and large objects being stored. (**A**) When the smallest object is stored. (**B**) Hair bending when a large object is stored.

(unit: mm)

Material: DragonSkin 30						
(r, b)	(1.5, 20)	(2.0, 20)	(2.5, 20)	(3.0, 20)	(2.0, 10)	(2.0, 30)
Minimum Storable Radius	3.5	3.0	2.5	2.0	0.5	5.5
Maximum Storable Radius	20.6	19.7	18.9	18.1	19.4	20.3

Table 3.3. The upper and lower limits of storable objects based on the geometry of the conveyor palm.

3.3.3 Transverse Storing Force Varying Geometric Parameters

The transverse storing force was measured by a tensile testing machine (INSTRON 5948 Microtester), varying the experimental parameters (Table 3.2). To ensure repeatability in the process of inserting the object into the storage, the storage was divided in half and placed on both sides of the rail (Fig. 3.12A and B). Then, the target was placed between the storages, and stored by moving both storages to the center. Each stored target was pulled 5 times through a tensile testing machine at a speed of 30 mm/min, and the maximum pulling force was measured as the storing force (Fig. 3.12C).

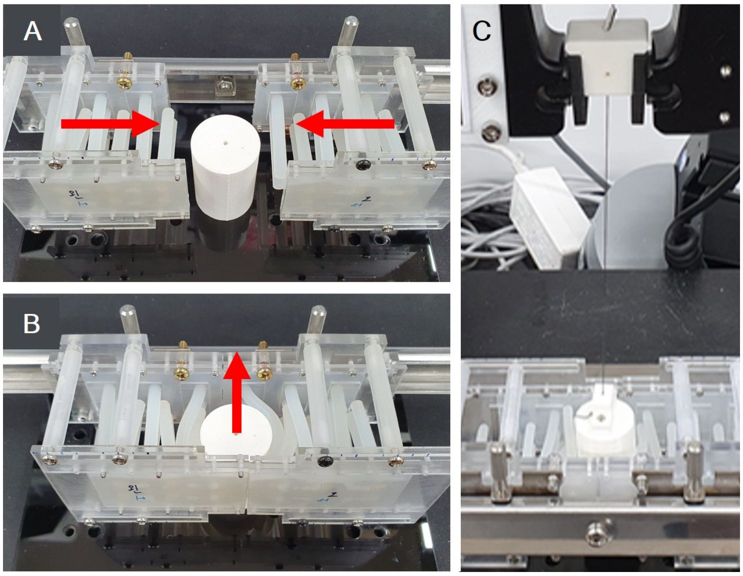

Figure 3.12. Experimental setup for analysis of storing force. (**A**) The target was placed between the storage on both sides, and then (**B**) sandwiched between both storages and stored. (**C**) The storing force was measured by pulling the object using a tensile testing machine.

Finite element analysis (FEA) was also conducted using the FEA software ABAQUS (ABAQUS 2023, Dassault systems) to predict the transverse storing force. All simulation conditions were set to be identical to the experimental conditions. The belt surfaces opposite to the hair were set as a fixed boundary condition, and the gravitational force applied to the hair was also considered (Fig. 3.13A). In addition, by dividing the simulation steps, the object was stored in the storage by pushing the hairs (Fig. 3.13B), and after the storing process was finished, the maximum pulling force was obtained by pulling the object (Fig. 3.13C). The objects were considered as a rigid body, and all contacts between the object and hairs and the hairs with each other were considered as “general contact condition.” Since dynamic motion occurs as the hair is pushed, static analysis is challenging; therefore, the simulation was conducted through dynamic analysis. For the quasi-static assumption, both mass scaling and time period were set to 1, and the kinetic energy of the hair belt was less than 3% of the internal energy at every step until the maximum storing force was measured.

The mean transverse storing force of an object, its standard deviation, and the FEA simulation results of each design are shown in Fig. 3.14. In Figure 3.14, the simulation results show good agreement with the experimental results. Figure 3.14A shows the transverse storing force according to the changes of R and r when b was fixed at 20mm. In both the experiment and simulation, as R increased, the storing force and the increment of storing force gradually increased. This is because the larger object induces more significant deformations in the contacting hairs, and the number of hairs in contact is higher

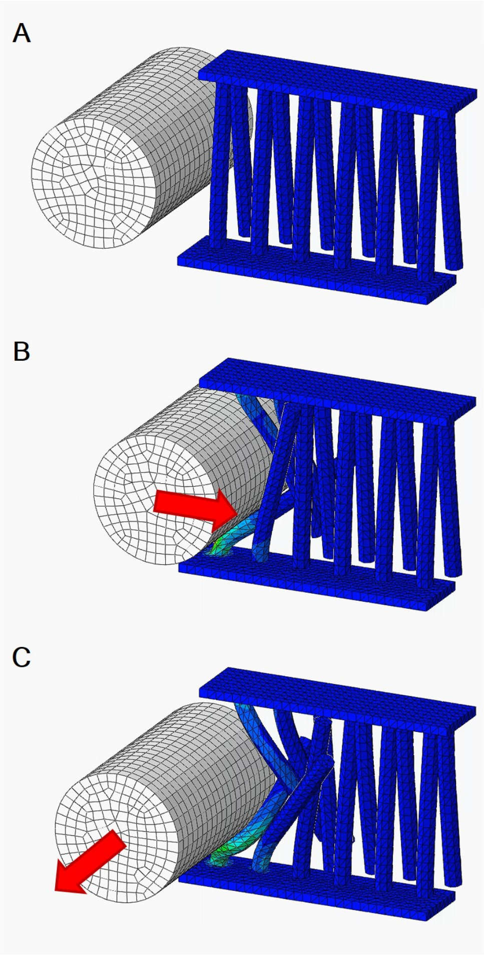

Figure 3.13. Finite element analysis (FEA) to predict the transverse storing force. (**A**) Initial simulation setting considering gravitational force. (**B**) Simulation step 1: The object was stored in the palm by pushing the hairs. (**C**) Simulation step 2: The object moved in the transverse direction of the storage, and the maximum pulling force was obtained in this step.

compared to smaller objects. As r increased, the moment exerted on the hair by the object increased with the fourth power of r (Equation 3.44). This implies that the force exerted by the hair on the object also increases with the fourth power of r. Furthermore, the curvature of the hair increases because the surfaces of the hair and the cylinder became closer. Therefore, the change in storing force according to the change of r was predicted to follow a slightly larger value than the fourth power of r, but the result was smaller. For example, the storing force of a cylinder with a radius 17.5 mm was 35.3 gf when r was 1.5 mm, and 323.5 gf when r was 3 mm. The difference between the two values is approximately 9.2 times and does not exceed 16 times. This result is because the cylindrical-shaped hairs are unable to stack up perfectly, leading them to slide past each other. This sliding causes a change in the direction of hair bending, resulting in a decrease in the restoring force exerted by the hairs on the object in the normal direction.

Figure 3.14B shows the measured transverse storing force and simulation result according to the change of R and b when r was fixed at 2 mm. Similar to the results in Fig. 3.14A, the increment of storing force gradually increased as R increased. Also, it was noteworthy that the change in b significantly shifts the storing force. This is because as b decreases, not only the distance between the object and the hair gets closer, but also the number of hairs touching the object increases. This also explains that the slope of the storing force increases significantly according to the change of r when b is small.

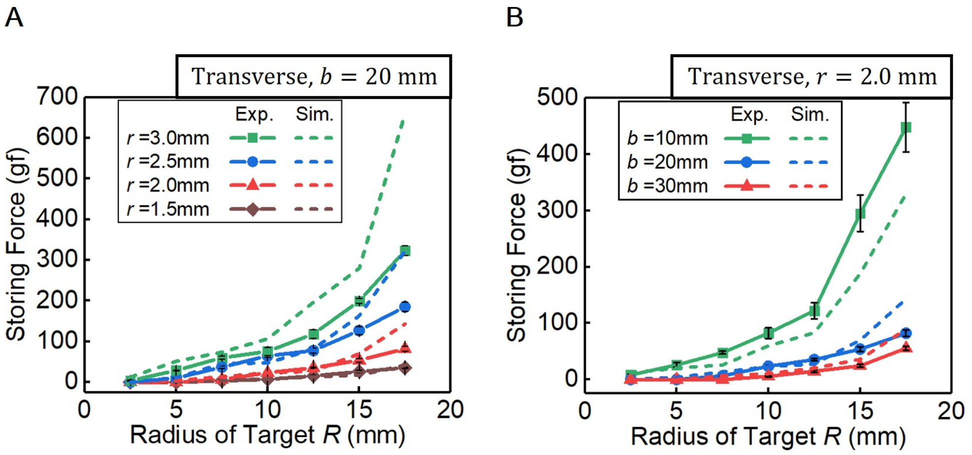

Figure 3.14. Experimental results and simulation results of the transverse storing force. (**A**) Storing force in response to the radius of the target with storage designs of different radius of hairs (b was fixed at 20 mm). (**B**) Storing force in response to the radius of the target with storage designs of different distance between adjacent hairs (r was fixed at 20 mm).

3.3.4 Longitudinal Storing Force Varying Geometric Parameters

The mean storing force of an object along the longitudinal direction was also analyzed. The experimental setup for measuring the longitudinal storing force is illustrated in Fig. 3.15. The longitudinal storing force was measured by a load cell (KTOYO 333FDX) while pulling the objects using a linear motor (Actuonix P16-150-256-12-P) at a speed of 4.2 mm/s (Fig. 3.15). For repeated experiments, a method for automatically feeding the object into the conveyor palm was proposed: a weight block was hung to apply force to insert the cylindrical object into the storage while rotating the belt. The experiment for measuring the longitudinal storing force consists of two steps. First, a weight block provides the force to insert the target object into the palm. When the belt is rotated, the object is fed into the conveyor palm for storage. Next, the belt is held stationary while a linear motor pulls the object in the longitudinal direction of the conveyor palm. When calculating the storing force, the weight of the block was subtracted from the measurement obtained by the load cell. All experiments for each parameter were repeated five times.

The experimental results for the longitudinal storing force are shown in Fig. 3.16. In contrast to the transverse storing force, the longitudinal storing force tends to increase, then decrease, and then increase again as the object's radius increases. For example, the storing force of a palm design with $r = 3.0$ mm and $b = 20$ mm (green line in Fig. 3.16A) increases until R reaches 5 mm, then decreases until R reaches 10 mm, and then increases again.

This phenomenon occurs because the configuration of the hairs adjacent

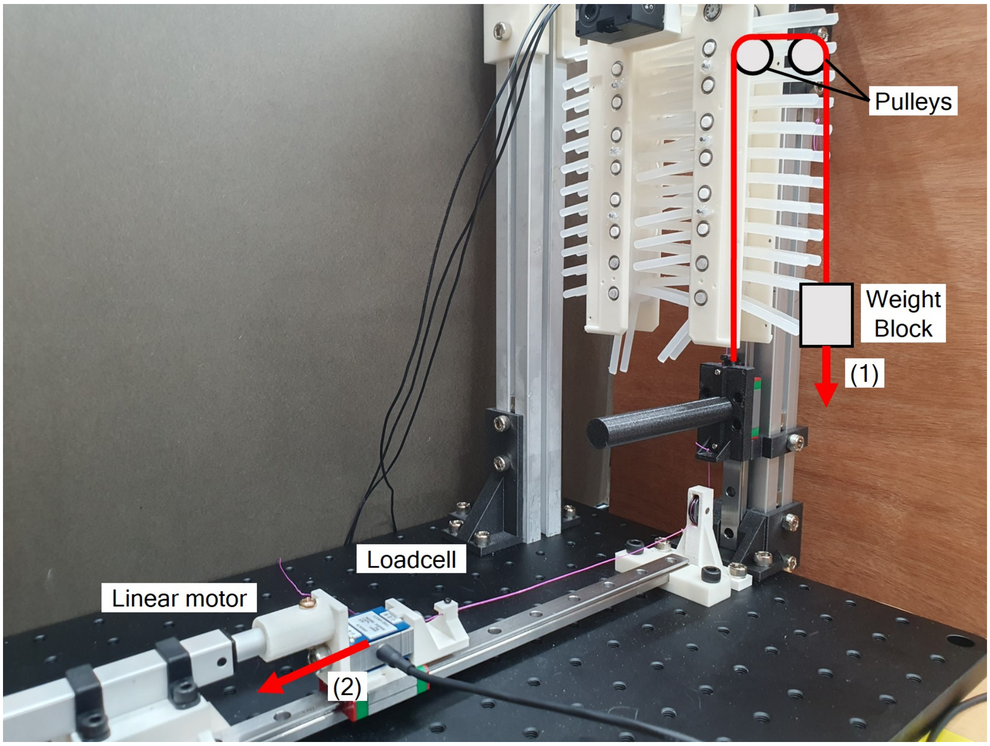

Figure 3.15. Experimental setup for measuring the longitudinal storing force of the conveyor palm. A weight block is attached to the cylindrical object, and the belt is rotated to store the object (process (1)). Next, the belt is held stationary while a linear motor pulls the object in the longitudinal direction of the conveyor palm (process (2)). During this process, the maximum storing force is measured using a load cell.

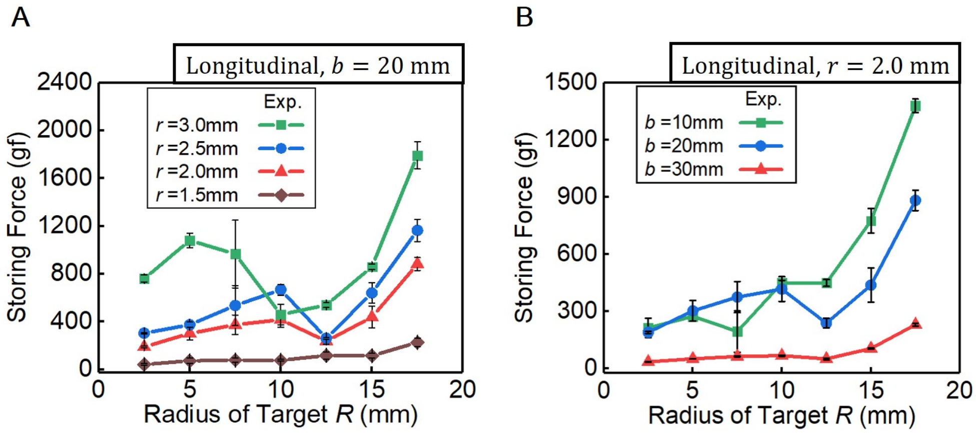

Figure 3.16. Experimental results and simulation results of the longitudinal storing force. (**A**) Storing force in response to the radius of the target with storage designs of different radius of hairs (b was fixed at 20 mm). (**B**) Storing force in response to the radius of the target with storage designs of different distance between adjacent hairs (r was fixed at 20 mm).

to the object changes with the size of the object while storing it (Fig. 3.17A). For smaller objects, the storage of the object does not significantly affect the alignment of the hairs, allowing the hairs to remain well-aligned along the length of the belt (Fig. 3.17A, i). In this case, when the object is pulled along the longitudinal direction, the hairs in contact with the bottom surface of the object deform and stack on each other (Fig. 3.17B). The stacked hairs can withstand a significantly greater force than the sum of the forces each hair can individually endure until the hairs begin to slip against each other. When the object size increases, the storage of the object begins to affect the alignment of the hairs, causing slip among the hairs as the object is stored in the palm (Fig. 3.17A, ii and iii). In this case, the stacking effect of the hairs disappears, and the storing force is determined by the sum of the individual hairs' restoring forces (Fig. 3.17C). The absence of the stacking effect leads to a decrease in the storing force. If the object size increases further, the energy required for the hairs to bend also increases, resulting in an increased storing force.

The stacking effect can also be observed in the storing force graph relative to the pulling distance of object (Fig. 3.18). For small objects, the storing force drops sharply after the maximum force as the stacking effect disappears (Fig. 3.18A), whereas for large objects, the storing force decreases slowly after the maximum (Fig. 3.18B). The critical radius at which the stacking effect disappears depends on the palm design parameters (r and b). In Figure 3.16A, the critical radius was 5 mm for r = 3.0 mm and 10 mm for r = 2.5 mm, indicating that the critical radius decreases as r increases. In Figure 3.16B, the critical radius was 5 mm for b = 10 mm and 10 mm for b = 20 mm,

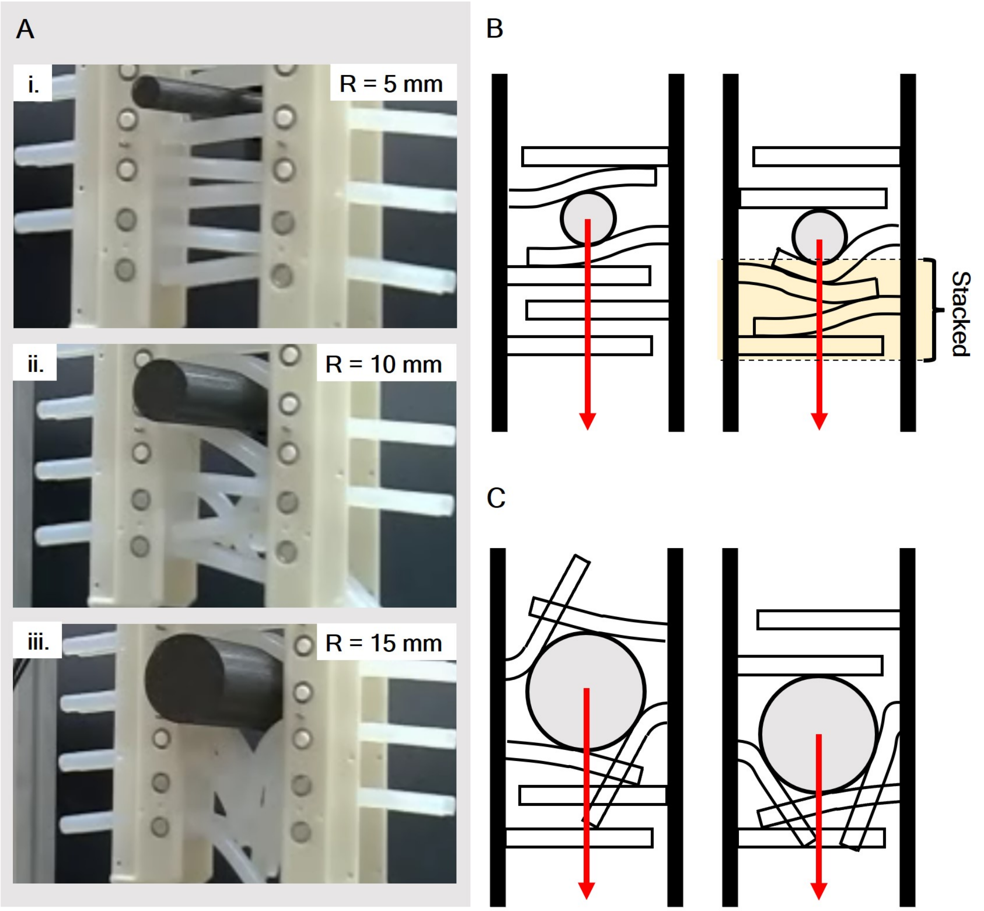

Figure 3.17. Detailed explanation of longitudinal storing force according to object diameter. (**A**) The configuration of adjacent hairs changes depending on the size of the stored object. (**B**) When pulling a stored small object, the hairs in contact with the bottom surface of the object deform and stack on each other, as highlighted in the yellow box. This stacking effect increases the storing force for small objects. (**C**) For larger objects, the arrangement of adjacent hairs is already disrupted during the storing process, so the stacking effect does not occur.

indicating that the critical radius increases as b increases. The stacking effect occurs during the process of storing the object by rotating the belt, and it is dependent on the size of the object. Since it is difficult to apply this effect in FEA simulations, the storing force in the longitudinal direction was analyzed exclusively through experiments.

As mentioned in Chapter 3.3.1, the storing force of the conveyor palm is defined as the maximum storable weight in the weakest direction. Therefore, comparisons between transverse and longitudinal storing forces were conducted for all palm designs (Fig. 3.19). The results showed that the longitudinal storing force was greater than the transverse storing force in all tested conveyor palm designs. Consequently, the transverse storing force was selected as the representative storing force of the conveyor palm.

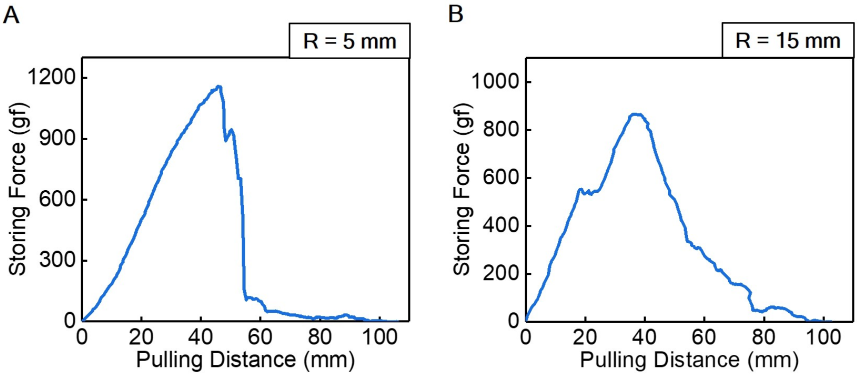

Figure 3.18. Longitudinal storing force of objects in relation to pulling distance. (**A**) For small objects, the storing force drops sharply after reaching the maximum force as the stacking effect disappears. (**B**) In contrast, for large objects, the storing force decreases slowly after reaching the maximum force.

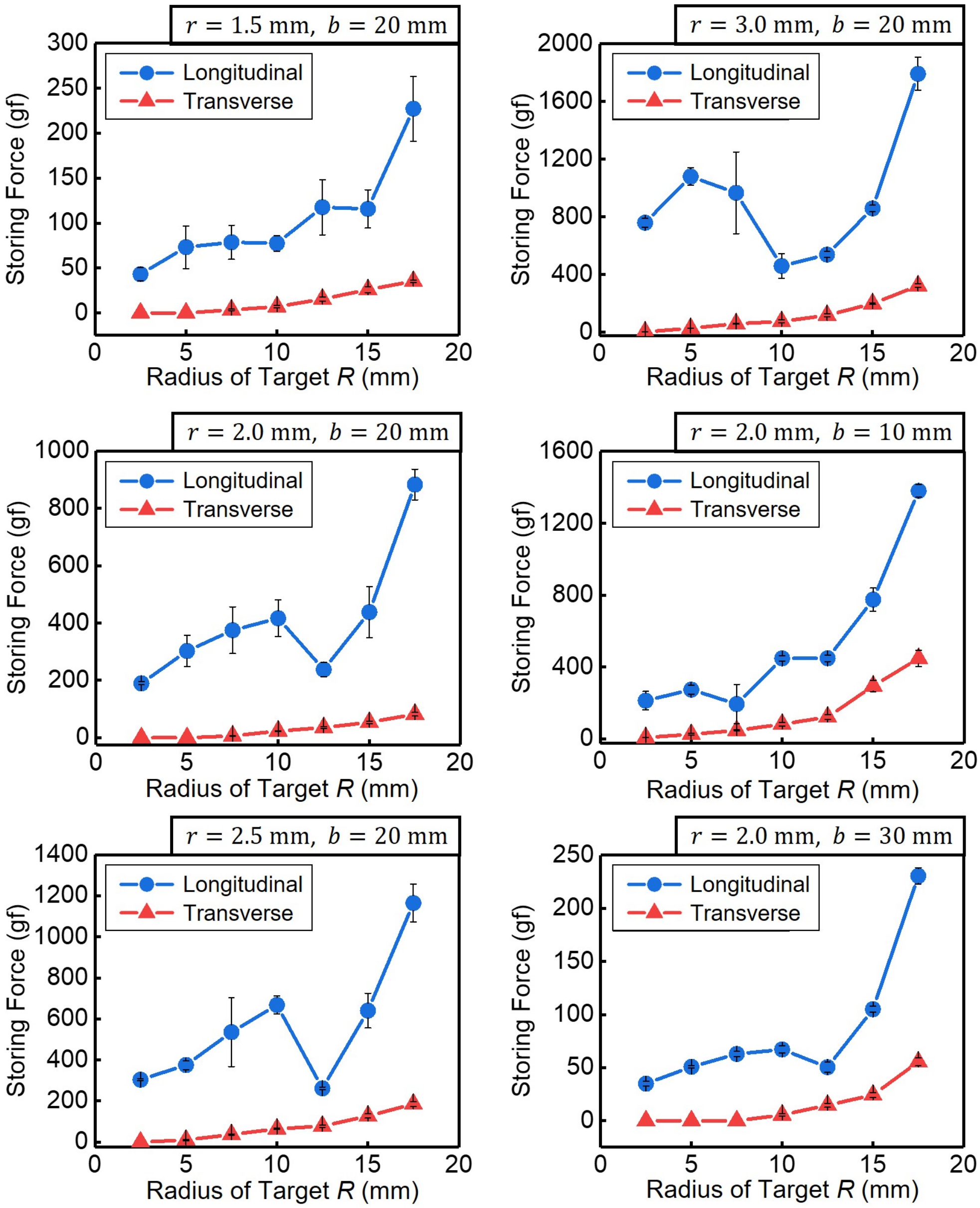

Figure 3.19. Comparison of the transverse storing force and the longitudinal storing force for different conveyor palm designs. In all tested conveyor palm designs, the longitudinal storing force was greater than the transverse storing force.

3.3.5 Storing Force According to Material Parameter

In the last two chapters, the changes in storing force based on the geometric parameters of the conveyor palm were examined. Additionally, in this chapter, the storing force was experimentally measured by varying the material parameters of the conveyor palm. The material parameters of the conveyor palm include Young's modulus of the material and the static friction coefficient between the material and the object. Three different materials were used to fabricate conveyor palms, and the storing force of each conveyor palm was measured. Since the Young's modulus and the static friction coefficient change together depending on the material selection, they are not independent parameters. The selected materials were DragonSkin 30, Smooth-Sil 950, and Smooth-Sil 960 (all by Smooth-On, Inc.), with Shore hardness values of A30, A50, and A60, respectively. In the previous chapters (Chapter 3.3.3 and 3.3.4), the storing force of the palm was defined as the transverse storing force. Therefore, only the transverse storing force was measured in this chapter.

The experimental setup for the storing force test is shown in Figure 3.20, and the experimental method follows the same procedure as the transverse storing force test described in Chapter 3.3.3 (Fig. 3.12). The transverse storing force was measured using a load cell (KTOYO 333FDX) while pulling the object with a linear motor (Actuonix P16-150-256-12-P) at a speed of 4.2 mm/s. To ensure repeatability in the process of inserting the object into the storage, the storage was divided into two halves and placed on either side of a rail (Figure 3.20A). The target object was placed between the storages, which were then moved toward the center to store the object. Each stored object was pulled five times using the linear motor, and the maximum pulling force was recorded as the storing force (Figure 3.20C). The geometric parameters of the conveyor palm, including the hair radius (r, 2 mm) and the distance between the hair (b, 10 mm), were kept constant throughout the experiment. The radii of the objects ranged from 2.5 mm to 17.5 mm, increasing in increments of 2.5 mm.

The storing force and standard deviation measured with varying material parameters are shown in Figure 3.21A. The storing force of all three conveyor palms showed a linear increase as R increased from 2.5 mm to 12.5 mm, followed by a sharp rise when R exceeded 12.5 mm. Additionally, the storing force increased as the stiffness of the material increased. Unlike the results obtained by varying the geometric parameters (Figures 3.14 and 3.16), which showed significant differences in storing force trends for each conveyor palm design, the trends were nearly identical when material parameters were varied. This indicates that the deformation behavior of the hairs resulting from object storage is more influenced by the geometry of the conveyor palm than by its material properties.

To further analyze the experimental results, the ratios of storing force measured with different materials were compared (Fig. 3.21B). The blue line in Figure 3.21B represents the ratio of the storing force of a conveyor palm made of Smooth-Sil 950 to that of one made of DragonSkin 30. Similarly, the green line represents the ratio of the storing force of a conveyor palm made from Smooth-Sil 960 to that of one made from DragonSkin 30. Except for smaller objects ($R = 2.5$ mm and 5.0 mm), the storing force ratios remained nearly constant regardless of object size. Since the geometry of the conveyor palm and objects did not change in this experiment, there was little variation in the hair deformation during object storage. As a result, for the same object, the hair deformation remained similar, resulting in nearly constant storing force ratios regardless of object size.

For small objects, the storing force ratio increased as the hair stiffness increased. This is because the deformation of the hair when storing small objects varies depending on its stiffness. Higher stiffness reduces the influence of gravity on the hairs, causing them to remain less bent before storage. As a result, the hairs align well along the belt's length and exert greater force on the object, similar to the stacking effect discussed in Chapter 3.3.4. In contrast, for materials with lower stiffness, the hairs bend due to gravity before storing the object, and the stacking effect does not occur, resulting in lower storing forces for small objects. For objects with radii larger than 5 mm, the alignment of the hairs is influenced by the object during storage, leading to slippage among the hairs. Consequently, the stacking effect disappears as object size increases, and the hair configuration remains consistent despite material parameter changes, resulting in similar storing force ratios.

The storing force is determined by the hair's modulus and the static friction coefficient between the hairs and the object. Since precise references for the modulus and static friction coefficients of DragonSkin 30, Smooth-Sil 950, and Smooth-Sil 960 were unavailable, these values were measured experimentally (Appendix A). The modulus was determined as the 100% modulus, which represents the modulus at 100% elongation. The results showed that the 100%

modulus of DragonSkin 30, Smooth-Sil 950, and Smooth-Sil 960 were 0.48 MPa, 1.37 MPa, and 2.02 MPa, respectively. The static friction coefficients were 1.10, 0.51, and 0.49, respectively. When the hairs undergo the same bending, a higher 100% modulus increases the normal force exerted on the object, while a higher static friction coefficient increases the frictional force on the object. Since the storing force equals the frictional force exerted by the hairs on the object, the product of the hair's 100% modulus and the static friction coefficient proportionally affects the storing force. Therefore, the ratio of the storing force of conveyor palms made of Smooth-Sil 950 to DragonSkin 30 is predicted to be 1.35, and the ratio for Smooth-Sil 960 to DragonSkin 30 is predicted to be 1.89. These predictions were well-aligned with the experimental results.

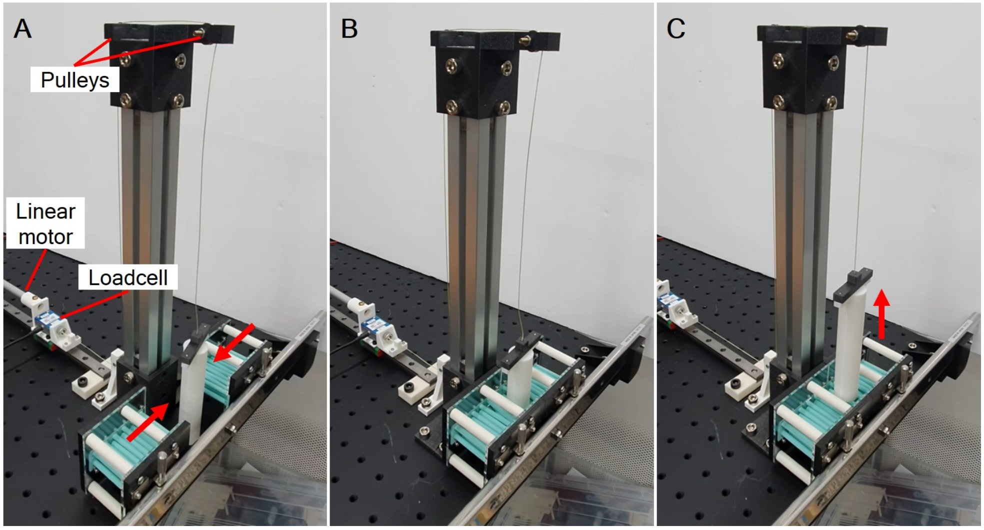
A
Pulleys
Linear motor
Loadcell
B
C

Figure 3.20. Experimental setup for measuring storing force with material variation . (**A**) Position the object between the two halves of the split conveyor palm. (**B**) Move the palms toward the center to store the object. (**C**) Finally, pull the object to measure the pulling force.

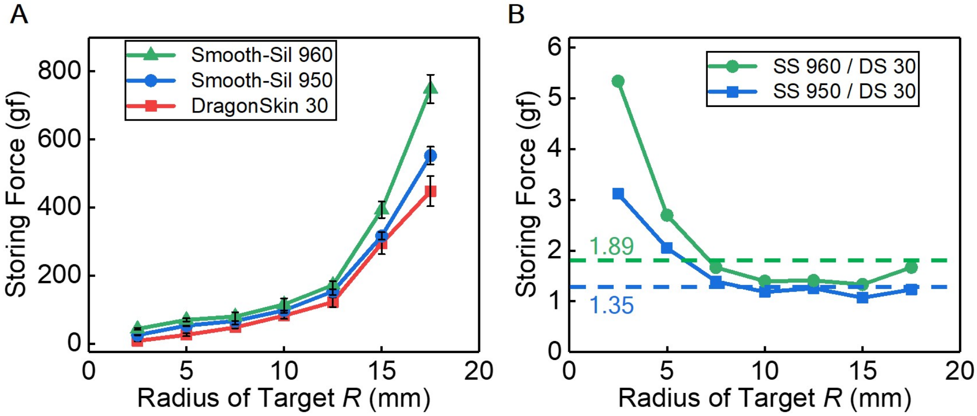

Figure 3.21. Experimental results of storing force measurement with material variation. (**A**) Storing force measured for conveyor palms composed of different materials. (**B**) To further investigate the effects of material properties on storing force, the storing force ratios of two conveyor palms were analyzed according to object size.

3.3.6 Theoretical Analysis of Conveyor Palm Scalability

To verify the scalability of the developed palm design, the change in storing force was simply calculated when all dimensional parameters of the palm and object were scaled by a factor of n. The analytical modeling of the storing force is challenging due to the stochastic contact of hairs when the object is stored in the palm. While determining the exact storing force is difficult, the change in storing force when all dimensions are scaled by n can be predicted under one assumption: since all parameters of the object and palm are scaled by n, the deformed configuration of the hairs and the contact conditions between the hairs remain the same.

The storing force of the conveyor palm can be expressed as the product of the static friction coefficient and the normal force exerted by each hair on the object:

$$F_{\text{store}} = \mu_h \sum F_i \tag{3.52}$$

where F_i is normal force exerted by each hair on the object and μ_h is the static friction coefficient between the object and hair (Fig. 3.22A). In addition, the moment-curvature equation of single hair (Equation (5.12) in [96]) is expressed as:

$$M = \kappa EI = \kappa E \cdot \frac{1}{4}\pi r^4 \tag{3.53}$$

where I is the second moment of inertia of the hair, r is the radius of the hair, E is the Young's modulus of the hair, and κ is the curvature of the hair.

Using the moment-curvature equation (Equation 3.53), F_i can be determined as follows:

$$|\vec{L}_i \times \vec{F}_i| = \kappa E \cdot \frac{1}{4\pi r^4} \tag{3.54}$$

$$F_i = \frac{\kappa E \pi r^4}{4 L_i \sin\theta_i} \tag{3.55}$$

where L_i is the distance from the base of the hair to the contact point with the object, θ_i is the angle between $\vec{L}_i$ and $\vec{F}_i$ (Fig. 3.22B).

If all dimensions are scaled by n, in Equation 3.55, the radius of the hair (r) and L_i both increase by n times, while κ decreases by $1/n$ times. Consequently, F_i increases by a factor of n^2. However, the weight of the object increases by a factor of n^3, resulting in a storing force that becomes relatively smaller compared to the object's weight as dimensions increase, and relatively larger as dimensions decrease. This scenario assumes a constant number of hairs (two hairs) in the width direction of the belt. If the number of hairs also increases by n times, then F_{store} would increase by a factor of n^3, making the conveyor belt scalable.

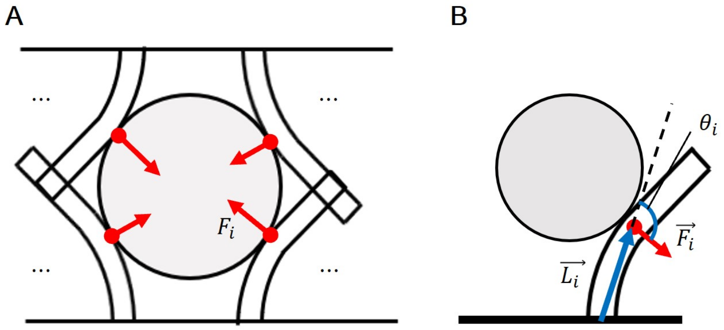
A
B
...
...
...
...
F_i
θ_i
$\overrightarrow{F_i}$
$\overrightarrow{L_i}$

Figure 3.22. Schematic related to the force exerted by hairs on an object. (**A**) The combined restoring force exerted by multiple deformed hairs creates the normal force applied to the object. The product of this normal force and the coefficient of friction is the storing force. (**B**) Schematic of hairs bent due to the storage of the object.

3.3.7 Simultaneous Storing Capability

In order to better understand the simultaneous storing capability of multiple objects, the storing force of the cylindrical object was measured by changing the radius of the additional object (Fig. 3.23). Since the transverse storing force is the weakest direction for the palm, and the longitudinal storing force is expected to have less variation, only the effect of additional objects on the transverse storing force was analyzed. The distance between the two objects was set as 30 mm, and the radii of the additional objects were 7.5 and 17.5 mm (fig. 3.23A).

The storing force was measured using the settings from the previous experiment (Fig. 3.12) to ensure the reliability of the experimental setup. The storage was divided into three parts as shown in Fig. 3.23A. The two objects were placed on both sides of the middle storage (highlighted in green), and the left and right storages (highlighted in orange) were moved to the center to store both objects. The black cylinder was pulled 5 times for each experiment at a speed of 30 mm/min through a tensile testing machine (INSTRON 5948 Microtester), and the maximum pulling force was measured as the storing force (Fig. 3.23B). The storing force without an additional object was also measured for comparison.

As a result, storing additional objects did not decrease the storing force, but rather increased it (Fig. 3.23C). This is because the additional object pushes the hairs between two objects when it is stored, and the pushed hairs apply additional force to the previously stored object. Furthermore, as the size of the additional object increased, the hairs between the two objects became more compressed, resulting in an increase in the storing force. When the radius of the additional object was 7.5 mm and 17.5 mm, the storing force of the black cylinder increased by about 10% and 20%, respectively.

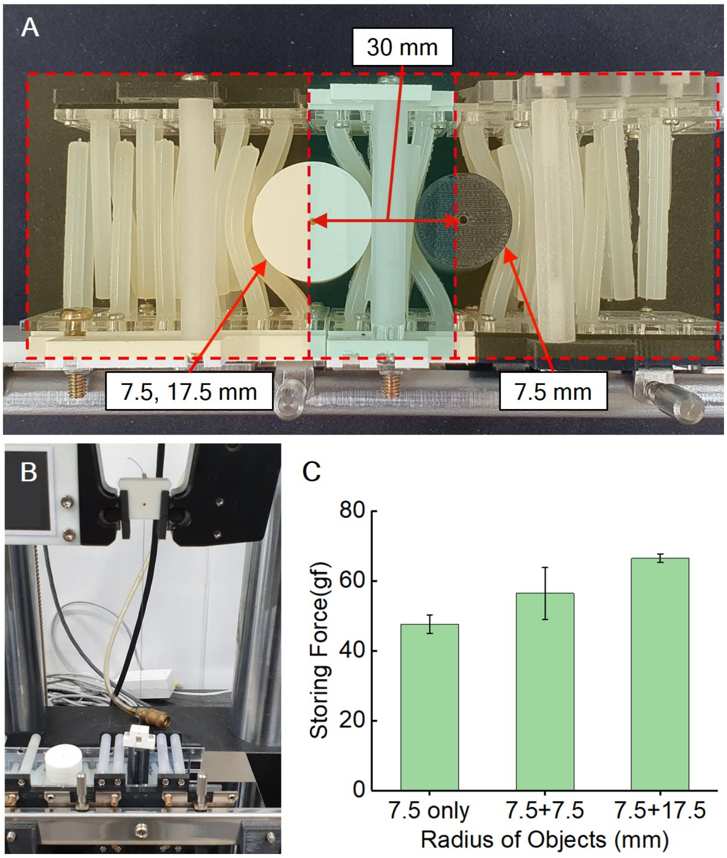

Figure 3.23. Experimental verification of individual storage capability of the hairy belt system. (**A**) Experimental setup. The target (a black cylinder with a 7.5 mm radius) and an additional object (a white cylinder with radii of 7.5 mm and 17.5 mm) were stored together, spaced 30 mm apart. (**B**) The storing force of the target is measured through a tensile testing machine. (**C**) Relationships between the additional object's radius and the storing force of target. The standard deviation of each data point is presented with a black vertical line.

3.3.8 Design Guidelines of Conveyor Palm

In previous chapters, the upper and lower size limits of objects that the conveyor palm can store were theoretically analyzed, and the storing force of the conveyor palm was experimentally evaluated based on object size. Additionally, the scalability of the conveyor palm was theoretically presented. This chapter aims to synthesize these results to propose a design guideline for the conveyor palm.

Let us assume that the size and weight information of a set of target objects, the maximum size of the gripper body, and the materials available for the conveyor palm are given. For tasks such as grasping objects inside a shelf, the maximum size of the gripper body could be constrained to fit within the shelf. According to Equation 3.51, the radius of the largest object in the set of objects must satisfy the following condition:

$$R_{\text{obj,max}} \leq -\left(1 + \frac{SF}{\epsilon_{\text{max}}}\right) r + \sqrt{\left(\frac{SF \cdot r}{\epsilon_{\text{max}}} - \frac{b}{4}\right)^2 + \frac{d_{\text{surf}}^2}{4}} \tag{3.56}$$

where $R_{\text{obj,max}}$ represents the radius of the largest object in the object set. Additionally, the radius of the smallest object must satisfy the following condition:

$$R_{\text{obj,min}} \geq \frac{b}{4} - r \tag{3.57}$$

where $R_{\text{obj,min}}$ represents the radius of the smallest object in the object set. Equations 3.56 and 3.57 serve as geometric and material constraints for designing the conveyor palm. Next, by varying the design parameters of the hairs, we can select a set of conveyor palm designs capable of producing the storing force larger than the weight of the objects in the set. While changes in the geometric parameters of the conveyor palm are difficult to predict theoretically, variations in the material parameters can be estimated with theoretical models. Additionally, the effect of changes in the distance between the two belt surfaces of the conveyor palm (d_{surf}) can be predicted through the scalability model of the conveyor palm. In summary, the storing force of the conveyor palm must be measured experimentally when r and b change, but its variation can be predicted to some extent when d_{surf} and the material change. Therefore, to reduce the number of experiments needed for designing the conveyor palm, the storing force is first measured by varying r and b within the range that satisfies Equations 3.56 and 3.57. Based on this, the storing force is predicted when d_{surf}, and the material change. Through this process, a design can be determined to ensure the conveyor palm's storing force satisfies the weight of all objects.

From the previous experimental results, it can be observed that increasing r or decreasing b tends to increase the storing force, thereby enhancing the likelihood of storing all objects in the set. However, a high storing force is not necessarily optimal for all target tasks. Constraints on the upper limit of the storing force can result from two factors, depending on the target application.

The first constraint is storing safety. The developed conveyor palm passively stores objects through the deformation of hairs, enabling the simultaneous storage of multiple objects with a single motor. However, it lacks the ability to actively control the storing force applied to individual objects. For tasks involving fragile objects, such as food packaging or farming, it is crucial to ensure that excessive force is not applied to the objects. Therefore, when targeting fragile objects, an upper limit on the storing force may be necessary.

The second constraint is the amount of material used to manufacture the conveyor palm. While material usage is not critical at the lab scale, reducing the material costs of the conveyor palm could become important when the proposed gripper is applied in industrial settings. Increasing the hair radius (r) or decreasing the distance between the hair (b) to enhance the storing force results in higher material usage for the conveyor palm, which may be less ideal. Changes in r affect material usage quadratically, whereas changes in b affect it proportionally. However, as shown in Figure 3.14, the rate of increase in storing force due to variations in b is greater than that due to variations in r. Thus, to minimize material use while increasing storing force, reducing the hair spacing (b) may be a more effective solution than increasing the hair radius (r).

3.4 Success Rate and Placement Error

3.4.1 Grasping with Center of Mass

To validate not only the finger and palm but also the integrated gripper system, the robustness of the proposed gripper's manipulation skills (finger-to-palm translation and palm-to-finger translation) was studied through various experiments. First, the success rate and placement error of the proposed multi-object grasping sequence for various objects were studied (Figs. 3.24 and 3.25). The experimental setup is described in Fig. 3.24A. The proposed multi-object grasping sequence consists of grasping, storing, retrieving, and placing processes. Failure of this sequence was defined as cases where the finger or palm failed to properly grasp or store the object during the translation process between the finger and palm. Specifically, if the palm failed to store the object after finger-to-palm translation, or if the finger failed to properly retrieve the object during palm-to-finger translation, the sequence was considered a failure. Failures were particularly frequent during the retrieval process, often due to the object being tilted or rotated in the palm (Fig. 3.24B), preventing all four fingers from grasping it correctly.

The success rate and placement error were hypothesized to have different tendencies based on the curvature of the target objects' surfaces, so the target objects for the two experiments were chosen to be a cylinder and a cuboid (Fig. 3.24C). However, since a cylinder can roll after being placed, making it difficult to accurately measure placement error, a cylinder with one-tenth of its diameter sliced off was used. The diameter/width of the sliced cylinder/cuboid was set at intervals of 5 mm, ranging from 5 mm to 35 mm, and each object was tested 20 times. To measure the placement error of the multi-object grasping sequence, the configuration of the object before grasping and after placement was captured using a camera (ABKO APC900) (Fig. 3.24A). Blue markers were placed at the center of mass of the object and at a point 30 mm along the length from that center. The position changes of the markers were measured using OpenCV. In the storing process of the multi-object grasping sequence, the distance at which each object was stored from the entrance of the storage was set to 30 mm.

The success rates for each object are shown in Figs. 3.25A and B. For the sliced cylinder, the success rate increased until the diameter reached 20 mm, and all objects with a diameter greater than 20 mm had a 100% success rate. Sliced cylinders with smaller diameters often rolled between the adjacent hairs of the conveyor palm, resulting in a lower success rate (Fig. 3.25A). In contrast, the cuboid did not roll along the length of the hairs, resulting in a high success rate regardless of width (Fig. 3.25B). The success rate was 90% when the width was 10 mm because, as shown in Fig.3.24B, the edges of the cuboid sometimes aligned with the intersections of the hairs, causing the cuboid to rotate and not be properly retrieved.

The placement errors for the sliced cylinders and cuboids of various sizes are shown in Figs. 3.25C and D. The placement error of an object is defined by comparing the object's configuration before grasping and after placing, measuring the displacement of the center of mass (d_O) and the object's tilt angle (θ) (Fig. 3.24A). For the sliced cylinder, both the displacement of the object center and the tilt angle decreased as the diameter increased. In the case of the cuboid, the tilt angle was nearly zero regardless of the object size, but the center displacement was around 2 to 4 mm irrespective of the object size.

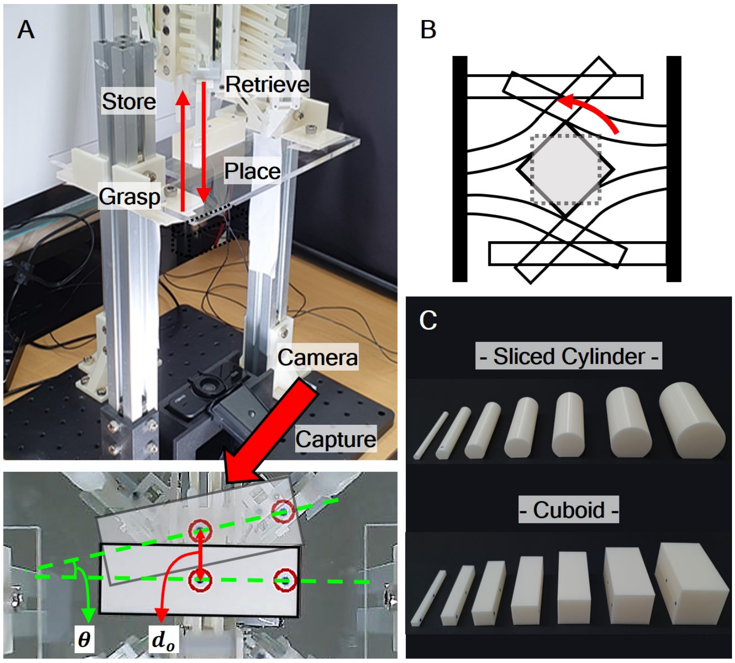

Figure 3.24. Experimental setting for measuring the success rate and placement error of proposed multi-object grasping sequence. (**A**) Experimental setup. The configuration of the object before grasping and after placement is captured using a camera to measure the placement error. The placement error consists of the displacement of the object's center of mass (d_o) and the tilting angle of the object (θ). (**B**) One example of a situation where the gripper fails to retrieve a cuboid occurs when the cuboid rotates during storage. (**C**) The target objects consist of cylinders and cuboids of various sizes. To prevent the cylinder from rolling during the placing process, a cylinder with one-tenth of its diameter sliced off was used. The diameter/width of the sliced cylinder/cuboid was set at intervals of 5 mm, ranging from 5 mm to 35 mm.

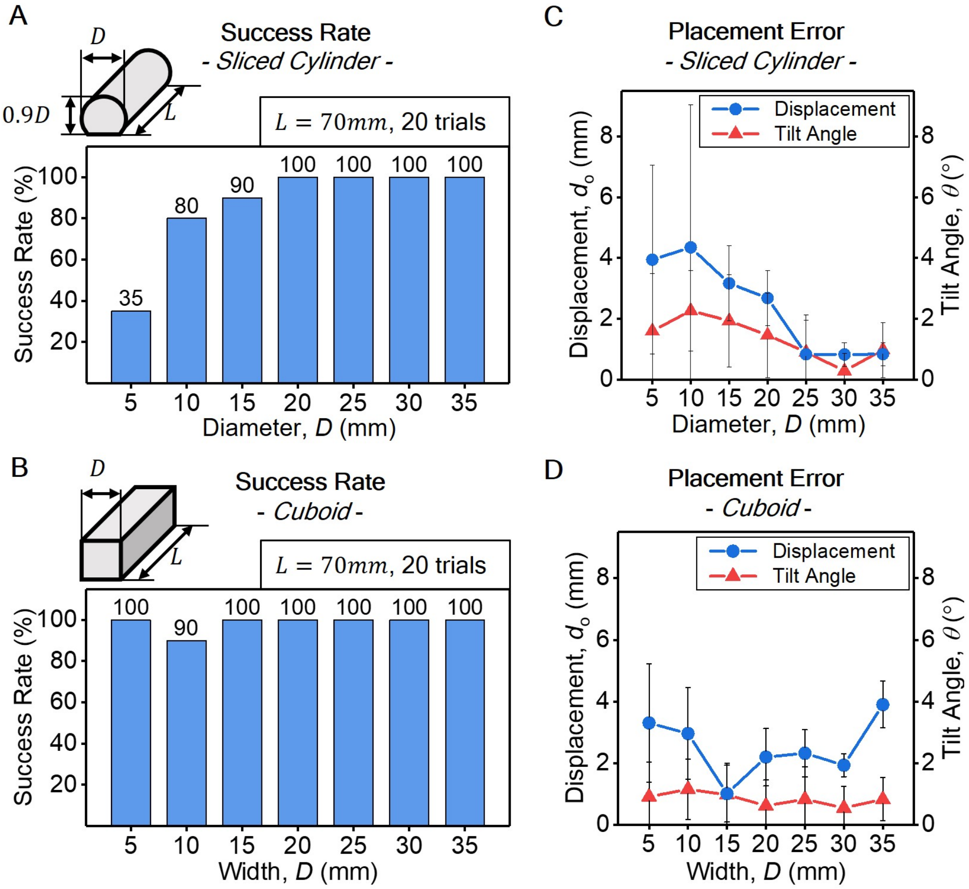

Figure 3.25. Experimental results for the success rate and placement error of the proposed multi-object grasping sequence. (**A** and **B**) The success rate for (A) sliced cylinders and (B) cuboids of various sizes. (**C** and **D**) The placement errors for (C) sliced cylinders and (D) cuboids of various sizes.

3.4.2 Off-Centered Grasping

To further investigate the limitations of the translation process for a grasped object, the success rate and placement error of the multi-object grasping sequence were measured when the object was grasped off-center from its center of mass. The experimental setup was identical to the previous setup used for measuring success rate and placement error (Fig. 3.24A), and the target objects and experimental results are shown in Fig. 3.26. The types of target objects were sliced cylinder and cuboid, as in the previous experiment, with dimensions of 20 mm in diameter and width, and 140 mm in length (Fig. 3.26A). The distance between the target's center of mass and the center of the contact points during grasping was set as 0 mm, 5 mm, 10 mm, and 15 mm. Twenty trials were conducted for each distance to measure the success rate and placement error for each object. In this paper, the distance between the center of mass and the center of contact points is termed the "off-center distance" (Fig. 3.26B). As illustrated in Fig. 3.26C, the greater the off-center distance was, the greater the object tilt was when stored in the palm.

Consequently, in experiments with both objects, when the off-center distance reached approximately 10 mm, failures in retrieving objects began to occur (Fig. 3.27A). For distances of 15 mm or more, retrieval failures occur in all trials. The placement error for each case is shown in Figs. 3.27B and C. In experiments with both types of objects, there was little difference in placement error at off-center distances of 0 mm and 5 mm, and the highest placement error was observed at an off-center distance of 10 mm. In this experiment, the object was placed on a flat surface, indicating that tilting of the object during the storing and retrieving process does not significantly affect placing. However, for tasks requiring high placement accuracy, such as peg-in-hole, it is crucial to grasp the object as close to its center of gravity as possible to minimize placement error.

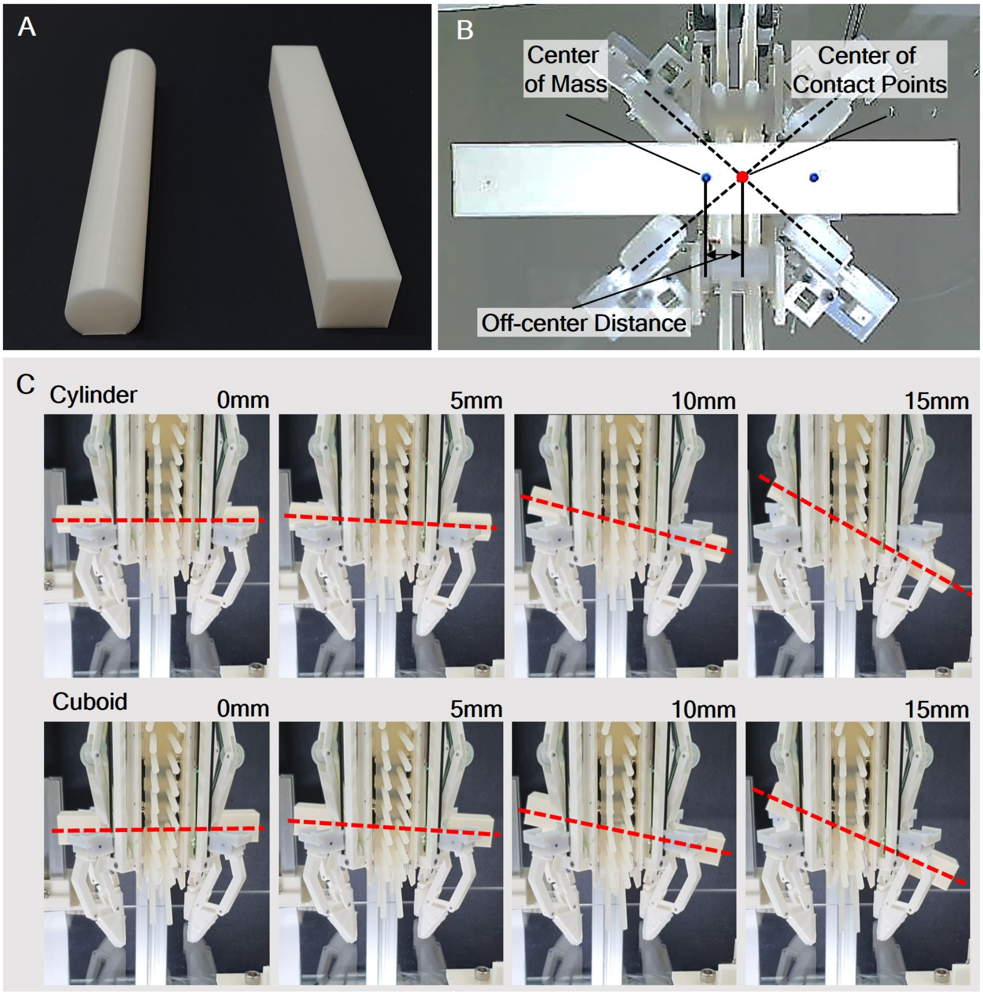
A
B
Center of Mass
Center of Contact Points
Off-center Distance
C
Cylinder
0mm
5mm
10mm
15mm
Cuboid
0mm
5mm
10mm
15mm

Figure 3.26. Experimental setup and qualitative results for measuring the success rate and placement error when a long object is grasped off-center. (**A**) The target objects were a 140 mm long sliced cylinder and a 140 mm long cuboid. The diameter of the sliced cylinder and the width of the cuboid were set to 20 mm, which is the median size of the storable objects. (**B**) The off-center distance is defined as the distance between the center of mass and the center of contact points. (**C**) The degree of tilting of each object when stored, depending on the off-center distance.

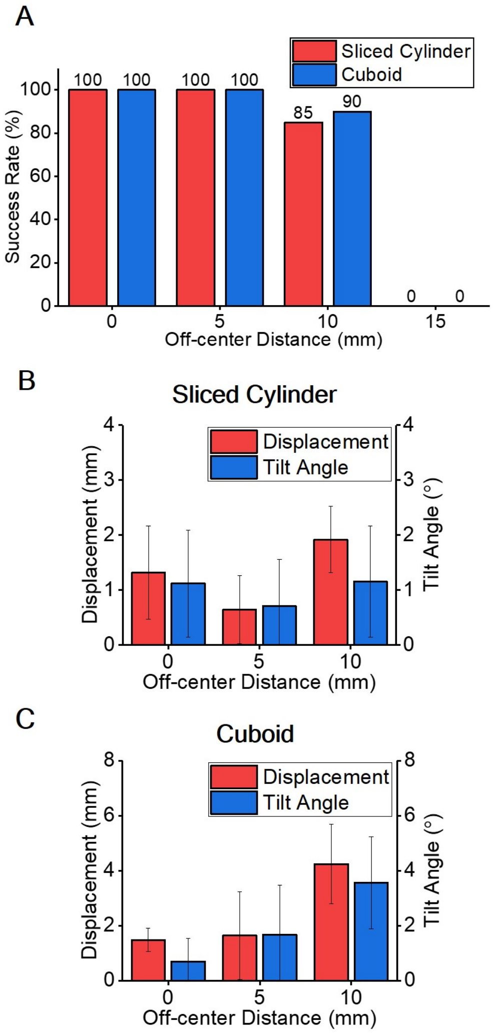

Figure 3.27. Experimental results for measuring the success rate and placement error when a long object is grasped off-center. (**A**) The success rate of the multi-object grasping sequence for each object depending on the off-center distance. (**B**) The placement error of the sliced cylinder depending on the off-center distance. (**C**) The placement error of the cuboid depending on the off-center distance.

3.5 Position Error of Palm-to-Finger Translation

To further investigate the limitations of the translation process for a grasped object, an analysis was also conducted on cases where the translation direction of the object does not align with the direction of gravity (Figs. 3.28 and 3.29). In contrast to the finger-to-palm translation, which is directly driven by the translating tendon, the palm-to-finger translation is accomplished by the restoring force of the spring connected to the slider. This causes the palm-to-finger translation to be affected by changes in external conditions such as the object's weight, friction of the slider, and gripper tilt angle. For example, if the friction between the slider and the linear guide is high, the finger may stop before reaching its initial position during the palm-to-finger translation process. In this paper, the distance between the finger's stopping position after palm-to-finger translation and its initial position is referred to as the retrieval offset of the finger. In the same manner, the distance between the stopping position of the object's center of mass after palm-to-finger translation and its initial position is referred to as the retrieval offset of the object. A theoretical analysis was conducted to determine which parameters affect the retrieval offset of the object, and this was experimentally verified.

First, consider the case where the gripper is tilted while grasping a long object (Fig. 3.28A). Unlike the "Maximum grasping force" section in the supplementary method, this is a more complex and general case as the fingers do not apply force perpendicular to the object. In this scenario, the force exerted

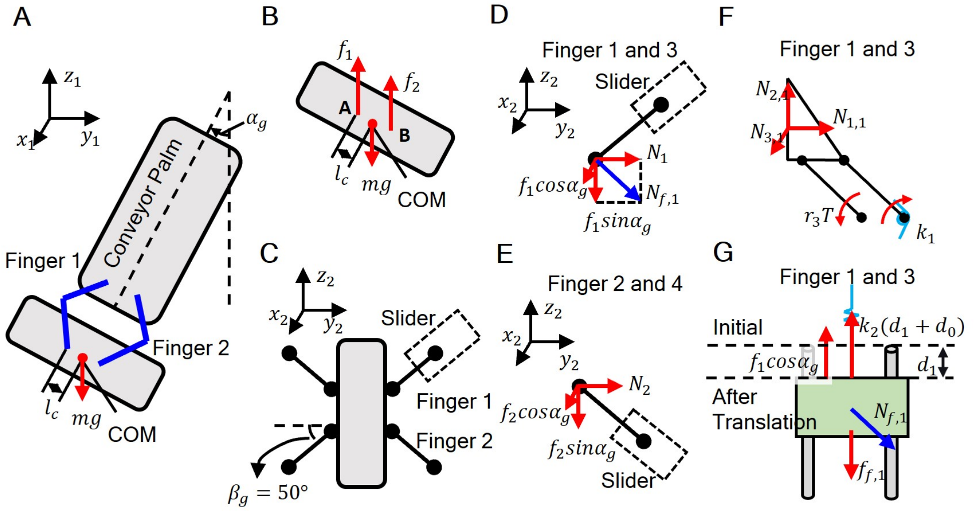
A
z_1
x_1
y_1
α_g
Conveyor Palm
Finger 1
Finger 2
l_c
mg
COM
B
f_1
f_2
A
B
l_c
mg
COM
C
z_2
x_2
y_2
Slider
Finger 1
Finger 2
$\beta_g = 50°$
D
Finger 1 and 3
z_2
x_2
y_2
Slider
N_1
$f_1 cos\alpha_g$
$N_{f,1}$
$f_1 sin\alpha_g$
E
Finger 2 and 4
z_2
x_2
y_2
N_2
$f_2 cos\alpha_g$
$f_2 sin\alpha_g$
Slider
F
Finger 1 and 3
$N_{2,1}$
$N_{1,1}$
$N_{3,1}$
$r_3 T$
k_1
G
Finger 1 and 3
Initial
$k_2(d_1 + d_0)$
$f_1 cos\alpha_g$
d_1
After Translation
$N_{f,1}$
$f_{f,1}$

Figure 3.28. Analysis of the object's retrieval offset after palm-to-finger translation. (**A**) Schematic of a tilted gripper grasping an object. (**B**) Free body diagram of the object. (**C**) Schematic of the finger grasping the object viewed from the gripper's longitudinal direction. (**D**) Free body diagram of fingers 1 and 3. (**E**) Free body diagram of fingers 2 and 4. (**F**) Equilibrium of moments at the fingertip, including the force exerted by the grasping tendon and the moment applied by the torsional spring. (**G**) Free body diagram of the slider connected to finger 1.

by finger 1 on the object is derived as follows (Fig. 3.28B):

$$\sum M_{B,x} = mgl_c \cos\alpha_g - 4f_1 l_c \cos\alpha_g = 0 \tag{3.58}$$

$$f_1 = \frac{1}{4}mg \tag{3.59}$$

where m is the mass of the grasped object, g is the gravitational acceleration, α_g is the tilt angle of the gripper, f_1 is the force exerted by finger 1 on the object, $\sum M_{B,x}$ is the sum of the moments exerting on the object in the x_1 direction about point B, and l_c is the distance between the contact point and the object's center of mass. Since this situation is symmetric about the $y_1 - z_1$ plane, fingers 3 and 4 are omitted in Fig. 3.28: finger 3 exerts the same force as finger 1, and finger 4 exerts the same force as finger 2 on the object. Using the moment equilibrium in the x_1 direction at point A, the force exerted by finger 2 on the object (f_2) can also be derived as follows:

$$f_2 = \frac{1}{4}mg \tag{3.60}$$

The configuration of the object being grasped, viewed from the length direction of the gripper, is illustrated in Fig. 3.28C. The angle between the fingers and the vertical plane of the object's surface is denoted as β_g. The free body diagram for fingers 1 and 3 is shown in Fig. 3.28D. Here, the x_2 axis direction is parallel to the fingertip and aligned with the axis of the linear guide connected to the slider. The forces acting on the fingers are the normal force (N_1) exerted by the object and the frictional force (f_1) lifting the object.

Since the gripper is tilted, the frictional force can be separated into the x_2

and z_2 directions. The x_2 axis component of f_1 is $f_1 \cos\alpha_g$, and the z_2 axis component is $f_1 \sin\alpha_g$. The normal force that generates friction between the slider and the linear guide, $N_{f,1}$, is the resultant force of the applied forces at finger in the $y_2 - z_2$ plane (N_1 and $f_1 \sin\alpha_g$ in Fig. 3.28D). The x_2 directional force, $f_1 \cos\alpha_g$, directly moves the slider and is caused by the weight of the object. The forces exerted on fingers 2 and 4 can also be analyzed in the same manner (Fig. 3.28E).

The force exerted on finger 1 can be divided into three components in the direction exerted on the finger, as shown in Fig. 3.28F ($N_{1,1}$, $N_{2,1}$, and $N_{3,1}$). Among them, $N_{1,1}$ and $N_{2,1}$ are expressed as follows:

$$N_{1,1} = N_1 \cos\beta_g - f_1 \sin\alpha_g \sin\beta_g \tag{3.61}$$

$$N_{2,1} = f_1 \cos\alpha_g \tag{3.62}$$

$N_{1,1}$ and $N_{2,1}$ must balance the moment due to the pulling force of the grasping tendon and the torsional spring. Using the same method as in deriving Equation 3.5, N_1 can be obtained by substituting $N_{1,1}$ for F in Equation 3.1 and $N_{2,1}$ for $\mu_s F$ in Equation 3.2:

$$N_1 = \frac{r_3 T - k_1 \Delta\theta}{l_3 \sin\theta \cos\beta_g} + \left(\frac{\cos\alpha_g}{\tan\theta \cos\beta_g} + \frac{\sin\beta_g \sin\alpha_g}{\cos\beta_g} \right) f_1 \tag{3.63}$$

Since both f and N_1 are known, the normal force and frictional force between the slider and the linear guide can be calculated. Immediately after the palm-to-finger translation, the force equilibrium equation from the free body diagram of the slider (Equation 3.64) and $N_{f,1}$ are derived as follows

(Fig. 3.28G):

$$f_1 \cos \alpha_g + k_2(d_1 + d_0) - f_{f,1} = 0, \quad d_1 > 0 \tag{3.64}$$

$$f_{f,1} = \mu_g N_{f,1} \tag{3.65}$$

$$N_{f,1} = \sqrt{N_1^2 + (f_1 \sin \alpha_g)^2} \tag{3.66}$$

where $f_{f,1}$ is the frictional force between the slider and the guide for finger 1, d_0 is the pretension length of the linear spring, d_1 is retrieval offset of the finger 1 after the palm-to-finger translation, and $_g$ is the static friction coefficient between the slider and the guide. Since the block prevents d_1 from having a negative value, d_1 is always positive (Fig. 2.7A). Substituting Equation 3.65 and 3.66 into Equation 3.64, the following equation is obtained:

$$d_1 = \max\left(\frac{1}{k_2}\left(\mu_g\sqrt{N_1^2 + \left(\frac{1}{4}mg\sin\alpha_g\right)^2} - \frac{1}{4}mg\cos\alpha_g\right) - d_0, 0\right) \tag{3.67}$$

In the same manner, the equation for d_2 can also be obtained as follows:

$$d_2 = \max\left(\frac{1}{k_2}\left(\mu_g\sqrt{N_2^2 + \left(\frac{1}{4}mg\sin\alpha_g\right)^2} - \frac{1}{4}mg\cos\alpha_g\right) - d_0, 0\right) \tag{3.68}$$

Finally, the retrieval offset of the object can be determined as follows:

$$d_{\text{object}} = \frac{d_1 + d_2}{2} \tag{3.69}$$

To validate the model of the object's retrieval offset, experiments were conducted under various conditions to measure the retrieval offset, and the results were compared with the model predictions. The experimental setup and target objects are shown in Fig. 3.29A and B. The gripper's tilt angle was varied from 0 to 180 degrees in 30-degree increments. The mass of the grasped object was 50, 100, 150, and 200 g, which were composed of the combinations of one 50 g weight block and two 100 g weight blocks (Fig. 3.29B). The results of the theoretical model are shown in Fig. 3.29C. The offset increases with larger tilt angles. When the tilt angle is large, the offset is smaller with lighter masses, whereas when the tilt angle is small, the offset is smaller with heavier masses. The differences between the model and the experiment are illustrated in Fig. 3.29D, showing that the modeling properly reflects the experimental results. According to Equations 3.67 and 3.68, increasing the pretension of the spring connected to the slider could reduce the retrieval offset.

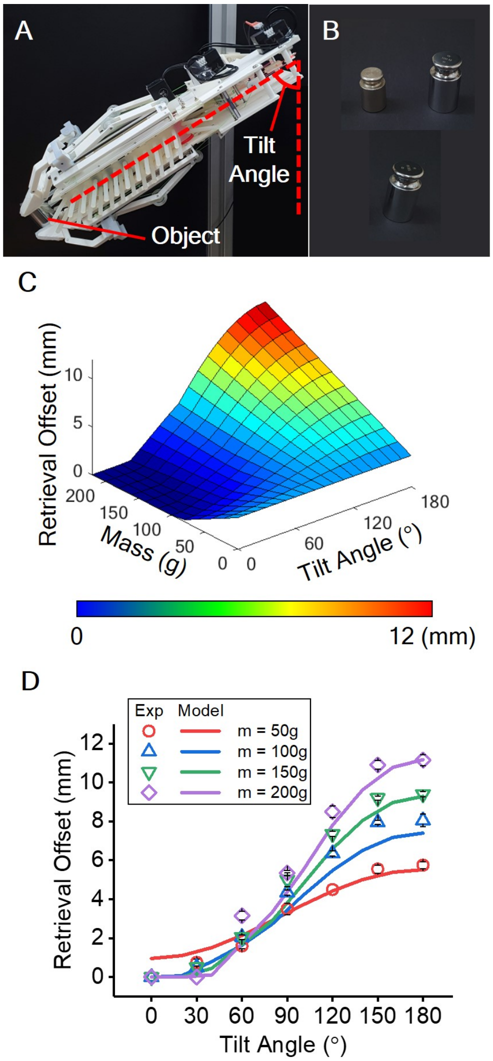

Figure 3.29. Experimental study of the object's retrieval offset after palm-to-finger translation. (**A**) Experimental setup. The tilt angle of the gripper was adjusted from 0 to 180 degrees in 30-degree increments. (**B**) Target objects. (**C**) Theoretical modeling results of retrieval offset varying with the mass of the grasped objects and the tilt angle of the gripper. (**D**) Experimental results of the retrieval offset varying with the tilt angle of the gripper and the mass of the grasped objects.

3.6 Validation through Lab-Scale Demonstrations

3.6.1 Comparison with Single-Object Gripper

To validate that the total pick-and-place process time and travel distance of the robot arm can be reduced through the proposed multi-object gripper, a logistics demonstration was conducted in a laboratory environment (Fig. 3.30A). Using the proposed gripper, the time and travel distance required to place four objects in each of the two boxes were measured for both when the gripper moved a single object at a time and when it moved four objects simultaneously. As a result, when using single-object grasping, the travel distance of the manipulator's end-effector was 29.5 m and the overall process time was 1 minute and 29 seconds; whereas, when using multi-object grasping, the travel distance was 8.5 m, and the process time was 59 seconds (Fig. 3.30B). Therefore, the proposed multi-object gripper can reduce the travel distance by about 71% and the overall process time by about 34% in this demonstration. In this demonstration, the speed of the manipulator was 150 mm/s and the acceleration was 800 mm/s^2.

In order to investigate the effectiveness of multi-object grasping compared to single-object grasping, I also conducted a theoretical comparison of the two methods, focusing on the travel length of the manipulator and overall pick-and-place process time. The grasping and placing sequence of the developed gripper is illustrated in Figs. 3.31A and B. In the process of grasping an object, the fingers grasp the object and then translate it to the palm while storing it simultaneously. Subsequently, the object is stored in the palm, and the fingers

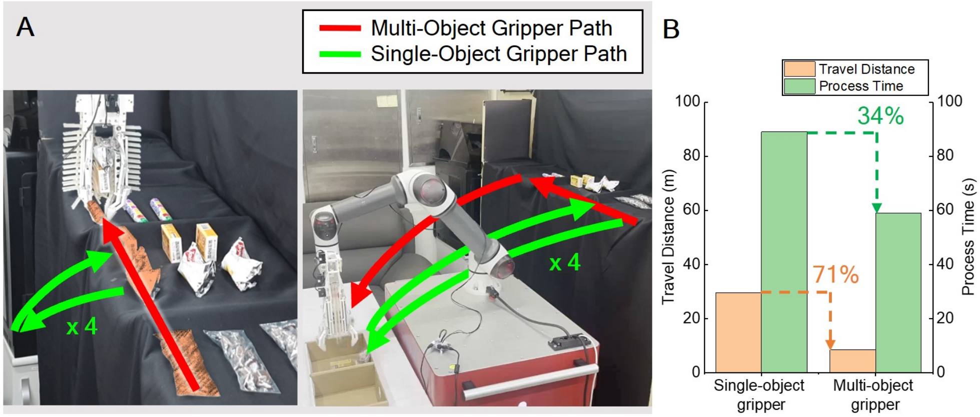

Figure 3.30. Demonstration of the proposed multi-object gripper in a laboratory-scale logistics environment. (**A**) Logistic demonstration to compare the travel distance of the manipulator's end-effector and the overall pick-and-place process time when using single-object grasping and multi-object grasping. (**B**) The comparison of travel distance and process time between single-object and multi-object grippers in a laboratory-scale logistics demonstration. Multi-object gripper can reduce the travel distance by about 71% and the overall process time by about 34% in this demonstration.

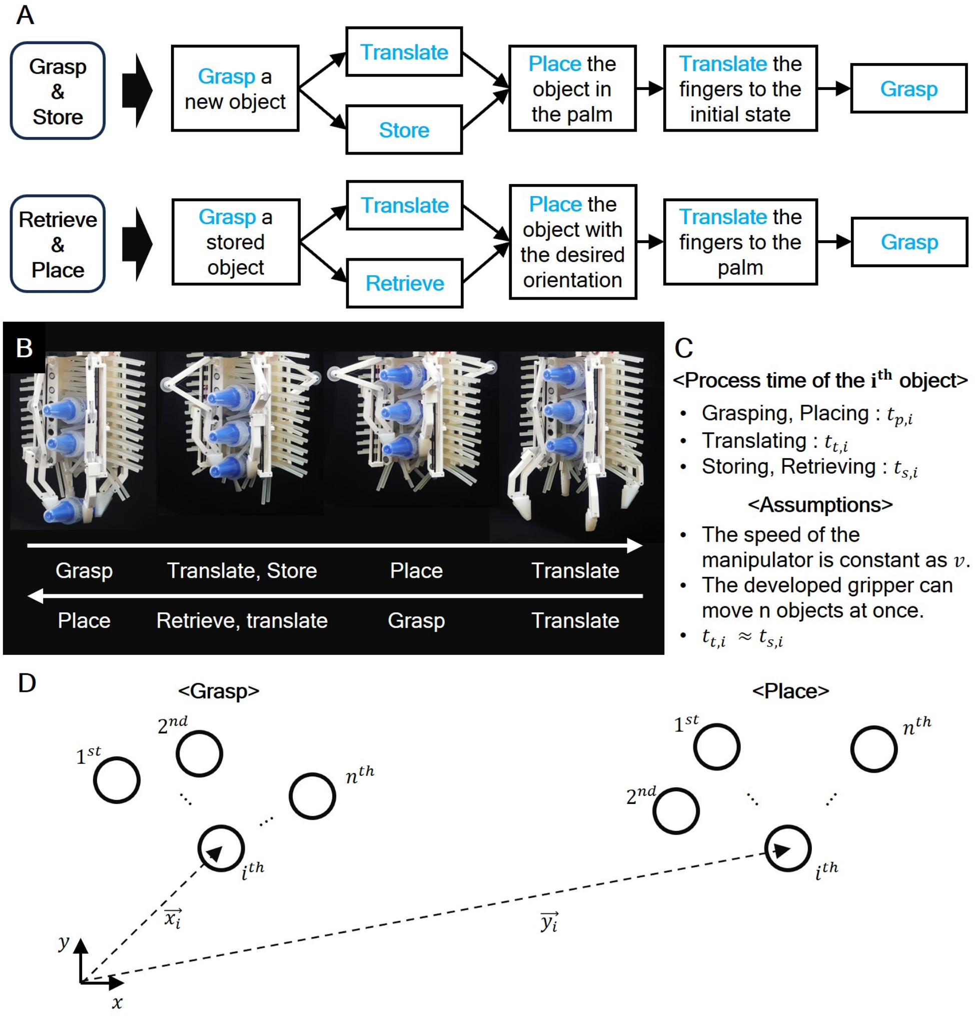
A
Grasp & Store
Grasp a new object
Translate
Store
Place the object in the palm
Translate the fingers to the initial state
Grasp
Retrieve & Place
Grasp a stored object
Translate
Retrieve
Place the object with the desired orientation
Translate the fingers to the palm
Grasp
B
Grasp
Translate, Store
Place
Translate
Place
Retrieve, translate
Grasp
Translate
C
<Process time of the ith object>
Grasping, Placing : $t_{p,i}$
Translating : $t_{t,i}$
Storing, Retrieving : $t_{s,i}$
<Assumptions>
The speed of the manipulator is constant as v.
The developed gripper can move n objects at once.
$t_{t,i} \approx t_{s,i}$
D
<Grasp>
1^{st}
2^{nd}
n^{th}
i^{th}
$\vec{x_i}$
y
x
<Place>
1^{st}
2^{nd}
n^{th}
i^{th}
$\vec{y_i}$

Figure 3.31. Details of the proposed multi-object grasping sequence and a comparison of grasping process efficiency with single-object grasping. (**A**) The grasping and placing sequence of the proposed multi-object gripper. (**B**) A detailed illustration of the proposed grasping and placing sequence. (**C**) Variables and assumptions for the comparison of manipulator's travel length and process time between multi-object and single-object grasping. (**D**) The schematic of the pick-and-place process.

return to their original state. In the placing process, the fingers grasp the stored object, translate it out of the palm, and retrieve it. Then, the object is placed at the desired location, and the fingers translate back towards the palm to grasp another stored object.

Variables and assumptions for calculating the manipulator's travel length and pick-and-place process time are illustrated in Figs. 3.31C and D. Firstly, the time taken to pick and place the i^{th} object is defined as $t_{p,i}$, the time required for translation as $t_{t,i}$, and the time for storing and retrieving as $t_{s,i}$. Additionally, the position of the i^{th} object before grasping in its reference frame is represented as $\vec{x}_i$, and the desired location where it needs to be placed is denoted as $\vec{y}_i$. In this scenario, it is assumed that the speed of the manipulator is constant at v, and the developed gripper can move n objects at once. Additionally, we assume that the time taken to store an object is almost similar to the time for translating it.

Under the aforementioned assumptions, when objects are moved one at a time using single-object grasping, the travel length and total process time of the manipulator are as follows:

$$L_S = \sum_{i=1}^{n} |\vec{x}_i - \vec{y}_i| + \sum_{i=1}^{n-1} |\vec{x}_{i+1} - \vec{y}_i| \tag{3.70}$$

$$T_S = \frac{\sum_{i=1}^{n} |\vec{x}_i - \vec{y}_i| + \sum_{i=1}^{n-1} |\vec{x}_{i+1} - \vec{y}_i|}{v} + 2\sum_{i=1}^{n} t_{p,i} \tag{3.71}$$

where L_S is the travel length of the manipulator when using the single-object grasping method, and T_S is the time taken for the grasping process. Similarly, the travel length (L_M) and total process time (T_M) of the manipulator when applying the multi-object grasping method are derived as follows:

$$L_M = \sum_{i=1}^{n-1} \left(|\vec{x}_{i+1} - \vec{x}_i| + |\vec{y}_{i+1} - \vec{y}_i|\right) + |\vec{x}_n - \vec{y}_n| \tag{3.72}$$

$$\begin{aligned} T_M = \sum_{i=1}^{n-1} \Bigg(& \max\left(t_{p,i} + 2t_{t,i}, \frac{|\vec{x}_{i+1} - \vec{x}_i|}{v}\right) \\ & + \max\left(t_{p,i} + 2t_{t,i}, \frac{|\vec{y}_{i+1} - \vec{y}_i|}{v}\right)\Bigg) + \frac{|\vec{x}_n - \vec{y}_n|}{v} + 2\sum_{i=1}^{n} t_{p,i} \end{aligned} \tag{3.73}$$

In the case of multi-object grasping, as the manipulator's movement and the object's translation and storing process occur simultaneously, the longer of the two will directly influence T_M. Therefore, it is important to design for simplifying the translation and storing process. If these process times are reduced to less than the time taken for the manipulator's movement, then T_M is derived as follows:

$$\min(T_M) = \frac{\sum_{i=1}^{n-1} \left(|\vec{x}_{i+1} - \vec{x}_i| + |\vec{y}_{i+1} - \vec{y}_i|\right) + |\vec{x}_n - \vec{y}_n|}{v} + 2\sum_{i=1}^{n} t_{p,i} \tag{3.74}$$

Comparison of Equations 3.71 and 3.74 indicates that multi-object grasping becomes more efficient as the distance between the objects decreases and the distance between the pick and place locations increases. Consequently, the developed gripper is anticipated to be especially effective in environments like logistics processes, where pick and place locations are distinctly separate. It is also expected to excel in scenarios such as households, where mobile manipulators are utilized to move between pick and place locations that are significantly distanced from each other.

Equation 3.74 also represents the theoretical maximum time efficiency that the developed multi-object grasping method can achieve. The most efficient multi-object grasping can be achieved when the translation and storing process times are shorter than the manipulator's movement time, as these processes occur simultaneously with the manipulator's movement. The theoretical minimum pick-and-place process time, calculated by movie analysis of demonstration (Fig. 3.30), was approximately 55 seconds, which was about 6.8% less than the actual demonstration time. This indicates that the translation and storing processes of the developed multi-object gripper are sufficiently short. To achieve a shorter process time, the use of faster and more powerful translating and storing motors could be considered.

3.6.2 Theoretical Efficiency Comparison with other Multi-Object Grasping Methods

A theoretical analysis was conducted to evaluate the efficiency of the proposed multi-object grasping strategy, compared to other conventional multi-object grasping strategies. All strategies assume the ability to move n objects simultaneously. Among the conventionally developed multi-object grasping strategies, the general approach is to gather objects in one location and then grasp them all at once [29, 38]. Typical methods for gathering objects include sweeping multiple objects at once [38] and pushing each object individually to a designated location [29]. In detail, the sweeping strategy involves sequentially sweeping objects from the first to the n^{th} object, assuming that before gathering the i^{th} object, the previous objects (first to $(i-1)^{\text{th}}$ objects) are moved together. The pushing strategy involves pushing individual objects to a predetermined location (such as the position of the i^{th} object), which results in a longer travel length for the manipulator compared to sweeping. Both sweeping and pushing strategies assume that objects are gathered without being grasped. Additionally, these strategies are not suitable for placing objects individually; therefore, the comparison of efficiency between multi-object grasping strategies is limited to scenarios where objects are placed simultaneously. The manipulator travel length and pick-and-place process time for each strategy were compared. For clarity, the proposed strategy in this paper is referred to as the translation strategy. The time required for picking and placing is assumed to be the same for all strategies, denoted as t_p.

Under the aforementioned assumptions, when objects are gathered by the sweeping strategy and moved together, the travel length and total process time of the manipulator are as follows:

$$L_{\text{sweep}} = \sum_{i=1}^{n-1} |\vec{x}_{i+1} - \vec{x}_i| + |\vec{x}_n - \vec{y}_n| \tag{3.75}$$

$$T_{\text{sweep}} = \frac{\sum_{i=1}^{n-1} |\vec{x}_{i+1} - \vec{x}_i| + |\vec{x}_n - \vec{y}_n|}{v} + 2t_p \tag{3.76}$$

where L_{sweep} is the travel length of the manipulator when using the sweeping strategy, and T_{sweep} is the time taken for the grasping process. Similarly, the travel length (L_{push}) and total process time (T_{push}) of the manipulator when applying the sweeping strategy are derived as follows:

$$L_{\text{push}} = |\vec{x}_2 - \vec{x}_1| + \sum_{i=2}^{n-1} 2|\vec{x}_{i+1} - \vec{x}_1| + |\vec{x}_n - \vec{y}_n| \tag{3.77}$$

$$T_{\text{push}} = \frac{|\vec{x}_2 - \vec{x}_1| + \sum_{i=2}^{n-1} 2|\vec{x}_{i+1} - \vec{x}_1| + |\vec{x}_n - \vec{y}_n|}{v} + 2t_p \tag{3.78}$$

The pushing strategy was assumed to gather the n objects to the location of the first object. Finally, excluding the process of placing each object, the travel length of the manipulator ($L_{\text{M,grasp}}$) and the total process time ($T_{\text{M,grasp}}$) for the translation strategy are derived as follows:

$$L_{M,\text{grasp}} = \sum_{i=1}^{n-1} |\vec{x}_{i+1} - \vec{x}_i| + |\vec{x}_n - \vec{y}_n| \tag{3.79}$$

$$T_{M,\text{grasp}} = \frac{\sum_{i=1}^{n-1} |\vec{x}_{i+1} - \vec{x}_i| + |\vec{x}_n - \vec{y}_n|}{v} + (n+1)t_p \tag{3.80}$$

When calculating the total process time ($T_{\text{M,grasp}}$), it was assumed that the translation and storing process are sufficiently fast (Equation 3.74). Comparing Equations 3.75, 3.77, and 3.79, the manipulator travel length for the translation strategy was the same as that for the sweeping strategy, with the pushing strategy having the longest manipulator travel length. In terms of total process time, the translation strategy had a longer process time than the sweeping strategy due to the time required for picking the objects. The process time for the translation strategy and the pushing strategy depends on the manipulator's speed, the distance between objects, and the time required for picking. The shorter the time required for picking and the higher manipulator's speed, and the greater the distance between objects, the better the pick-and-place time efficiency of the translation strategy compared to the pushing strategy.

Since there is no optimal grasping strategy for all scenarios, an appropriate multi-object grasping strategy should be selected based on the gripper's object manipulation capabilities and the conditions of the target pick-and-place process. For example, in situations where there are obstacles or bumps between objects that make using the sweeping and pushing strategies difficult (Fig. 3.30) or where precise placement of objects is crucial, the translation strategy would be more effective. Conversely, if there are no obstacles between objects and the individual placement of objects is not highly important, the sweeping strategy would be more efficient. If designing a gripper capable of sweeping all objects is challenging, the translation strategy or pushing strategy should be applied according to the pick-and-place environment.

3.6.3 Pick-and-Place Versatility

To verify that the proposed gripper can place the stored objects in their desired locations, we demonstrated a gripper tidying up a cluttered desk in a domestic environment (Fig. 3.32). The proposed gripper grasped a small lotion bottle and a travel toothbrush sequentially, translating them to the palm through finger-to-palm translation. After that, the gripper grasped a razor and transferred three objects simultaneously (Fig. 3.32A). Thereafter, the gripper placed the razor in a cup (Fig. 3.32B) and retrieved the stored objects one by one to hang the toothbrush set on the wall (Fig. 3.32C) and put the lotion bottle on the shelf (Fig. 3.32D). The detailed specifications of the target objects are presented in Table 3.4. All demonstrations (Fig. 3.30 and 3.32) were performed by attaching the gripper to a manipulator (RB5-850, Rainbow Robotics).

Finally, as shown in Fig. 3.33, the gripper successfully grasped, stored, retrieved, and placed 23 different types of objects. In this demonstration, the largest and heaviest target object was an NI myRio (National Instrument, size: 136 × 24 × 88 mm, weight: 195.07 g), the smallest object was a marble (size: 20 × 20 × 20 mm, weight: 12.00 g), and the lightest object was a chocolate packaging vinyl (size: 10 × 25 × 70 mm, weight: 0.15 g). This result shows the gripper's grasping and retrieving abilities for various types of objects.

Object number	**Description**	**Width** (mm)	**Length** (mm)	**Height** (mm)	**Weight** (g)
1	Lotion bottle	33	33	72	38.7
2	Travel toothbrush set	48	220	27	51.8
3	Razor	29	156	27	95.9

Table 3.4. Detailed specifications of objects used in the demonstration of tidying up a cluttered desk.

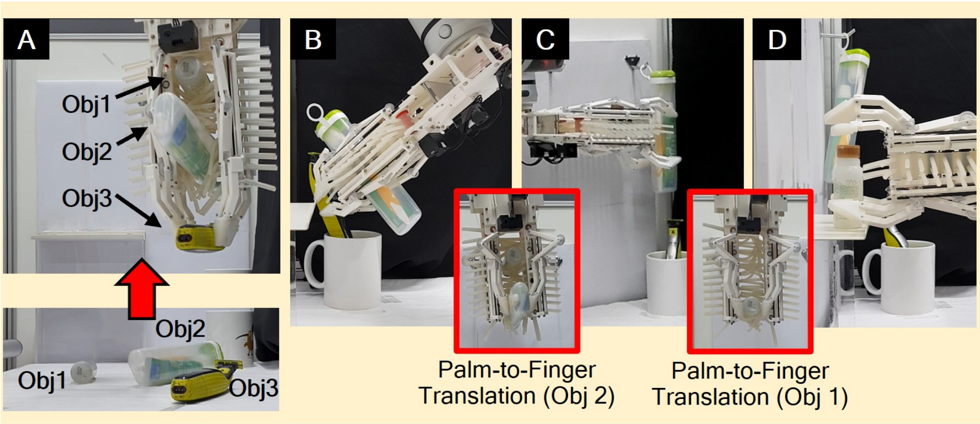
A
Obj1
Obj2
Obj3
Obj2
Obj1
Obj3
B
C
D
Palm-to-Finger Translation (Obj 2)
Palm-to-Finger Translation (Obj 1)

Figure 3.32. Domestic demonstration to verify the placing ability of multi-object gripper. (**A**) The gripper sequentially grasped a small lotion bottle, a travel toothbrush, and razor. And then, the gripper moved them together. After that, the gripper (**B**) placed the razor in a cup and retrieved the stored objects one by one to (**C**) hang the toothbrush set on the wall and (**D**) put the lotion bottle on the shelf.

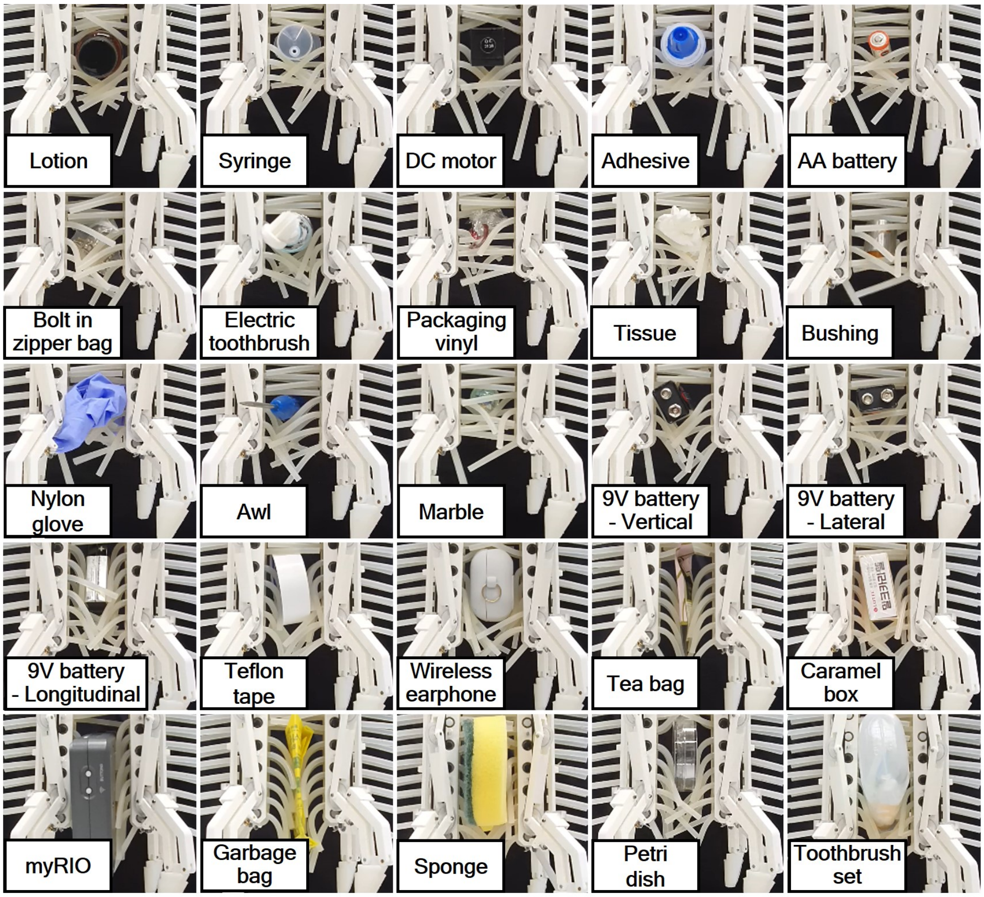
Lotion
Syringe
DC motor
Adhesive
AA battery
Bolt in zipper bag
Electric toothbrush
Packaging vinyl
Tissue
Bushing
Nylon glove
Awl
Marble
9V battery - Vertical
9V battery - Lateral
9V battery - Longitudinal
Teflon tape
Wireless earphone
Tea bag
Caramel box
myRIO
Garbage bag
Sponge
Petri dish
Toothbrush set

Figure 3.33. Grasping and placing capabilities of the proposed multi-object gripper. Proposed gripper can grasp, store, retrieve and place 23 different objects, including the long cylinders, cubes, cuboids, spherical objects, thin objects, and porous objects.

Chapter 4

Path Planning for Proposed Multi-Object Gripper

4.1 Background

In previous lab-scale demonstrations, the proposed multi-object gripper moved objects faster than a single-object gripper and was applicable to various pick-and-place tasks. These tasks included scenarios where obstacles were placed between objects, or where objects needed to be placed individually, making conventional multi-object grippers difficult to utilize. This versatility is achieved because the proposed method allows for sequential grasping and storing of multiple objects, enabling one object to be picked or placed while others are stored.

To use the developed gripper in the real world, it should be able to recognize objects placed in arbitrary positions and calculate efficient pick-and-place paths. In this case, for efficient pick-and-place operations, path planning is necessary for the order in which multiple objects are grasped and stored. Therefore, this chapter aims to propose a path planning method for the multi-object gripper using in-hand translation, outlining key considerations and evaluating the potential efficiency improvements.

The purpose of the path planning presented in this chapter is to support the real-world application of the proposed gripper. To facilitate design modifications based on task requirements, the fabrication method of the conveyor palm was changed from molding to 3D printing (see Appendix B for details). The 3D-printed conveyor palm has a hair radius of 2mm and a 10mm gap between hairs, identical to the conveyor palm produced by molding in Chapters 2 and 3. It was manufactured using an FDM printer (PRUSA MK3S+) with TPU 95A material. The 3D-printed conveyor palm is designed with hairs connected in pairs along the width of the belt (Fig. B.1). Since the current experiments and models are conducted in 2D planes, having the hairs connected along the width of the belt to prevent out-of-plane bending offers the advantage of higher consistency with the model. In previous polymer-based conveyor palms, frequent out-of-plane bending of the hairs made their behavior difficult to predict. By connecting the hairs, out-of-plane bending is minimized, which improves the reproducibility of the experiments. Additionally, this design could facilitate future geometric modeling of the occupied space. However, in terms of storage capacity, reducing out-of-plane bending could be a disadvantage. This is because bent hairs stack neatly within the palm. Consequently, compared to polymer-based conveyor palms, the 3D-printed palm may exhibit slight inefficiencies in storage capacity.

4.1.1 Real World Applications for Multi-Object Grasping

Before implementing path planning with the developed gripper for a specific application, it is important to review existing robotic applications and categorize those suitable for multi-object grasping. As discussed in Chapter 1.1.1, robotic applications can be classified into industrial robots and service robots. When limited to pick-and-place processes, industrial applications include manufacturing and logistics, while service robot applications include hospitality, agriculture, and domestics.

To determine which of these applications are suitable for the developed multi-object grasping, it is necessary to reclassify applications based on goal configurations of manipulator and target objects. Previous research provides detailed methods for categorizing multi-object manipulation problems [97]. This paper defined manipulation tasks as processes that transform the initial states of the robot and objects into states that satisfy specific goal conditions. This paper classified manipulation tasks into seven categories based on criteria such as goal specification, object-to-object contact, object labeling, and prioritization. Goal specification refered to whether the task requires satisfying the configuration of only the robot, a single object, or multiple objects at the end of the task. Object-to-object contact considers whether contact between objects occurs during the task. Object labeling evaluates whether labeling or classification of objects is necessary. Prioritization examines whether there is a priority order for picking objects.

Based on these criteria, manipulation tasks are divided into seven categories: singulation, navigation, declutter, rearrangement, packing, placing, and sorting. However, these manipulation tasks include processes like mobile robot navigation or declutter problems such as cleaning dirt, which do not involve pick-and-place operations. Such tasks that do not include the pick-and-place process are excluded from this dissertation. Additionally, tasks that involve the picking and placing of only one object among many are also excluded. Therefore, the manipulation tasks narrowed down to four pick-and-place tasks: singulation, declutter/packing, rearrangement, and sorting (Fig. 4.1). These tasks were classified based on two criteria: goal specification and object labeling (Table 4.1).

Manipulation Tasks	**Goal Spec.**	**Label**
Singulation	RO	U
Declutter/Packing	A	U
Rearrangement	A	L
Sorting	A	LC

R = robot, O = one object, A = all objects
L = labeled, U = unlabeled, C = classified

Table 4.1. The criteria for classifying manipulation tasks [97].

Next, each of these tasks will be explained in detail, followed by an examination of situations where multi-object grasping proves effective. Multi-object grasping includes not only the translation-based method proposed in this dissertation but also methods like scooping [27], pushing [29], sweeping [38], and swallowing [34]. Each multi-object grasping method is effective for different manipulation tasks, and detailed explanations of their effective scenarios will

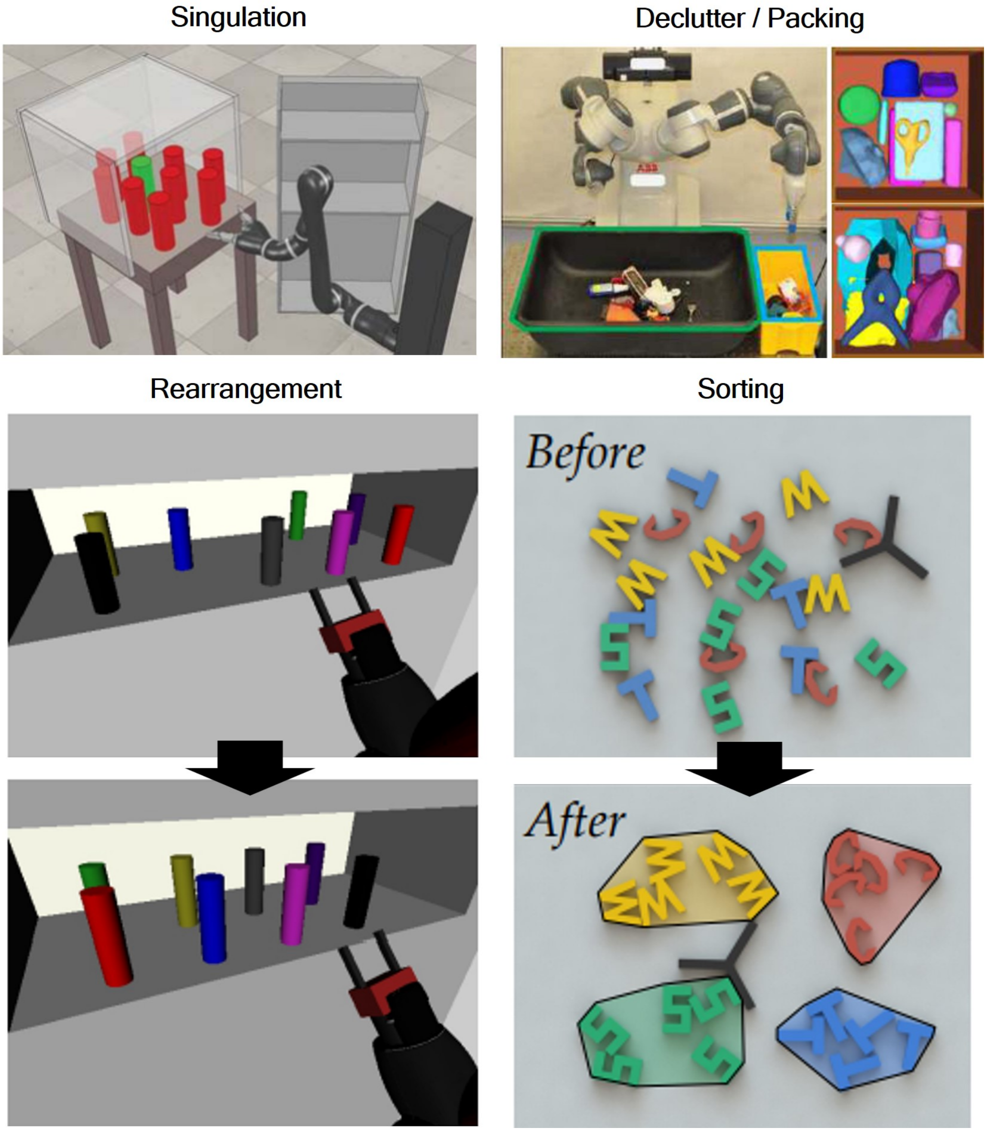
Singulation
Declutter / Packing
Rearrangement
Sorting
Before
After

Figure 4.1. The classification of pick-and-place tasks among various manipulation tasks. They are categorized based on goal specification and the level of labeling.

be discussed. To define the goal of each task, following [97], the robot state space was defined as $x^R \in \mathbb{C}^R$, the state space of each m objects was defined as $x^1(t) \in \mathbb{C}^1, \ldots, x^m(t) \in \mathbb{C}^m$. Additionally, the workspace was defined as X, and the volume of the object being grasped was defined as $O^i(x^i)$.

Singulation refers to tasks where several objects need to be moved beforehand to grasp a specified object, such as retrieving an item located deep inside a shelf or refrigerator [98]. Detailed examples include removing a desired object from a warehouse shelf or a domestic service robot retrieving an item from a refrigerator. Since the target object is positioned behind other objects and the manipulator cannot pick it directly in a single action, a process is required to clear the obstructing objects and create a path for the manipulator. This problem can be mathematically formulated as follows:

$$\mathrm{InGrasp}(x^R, x^1) \tag{4.1}$$

where x^1 represents the target object without loss of generality, and InGrasp is an algorithm that determines the robot arm's state space for grasping the target object. Typically, singulation tasks involve either sequentially grasping and relocating objects [98], or pushing one or multiple objects [99] to clear a path for the manipulator to reach the target object. These methods are effective when the object density on the shelf is low.

However, when the object density on the shelf is high, grasping and relocating objects one by one may lead to inefficiency, as there may be no space on the same shelf to relocate the objects, requiring placement on another shelf [98]. Similarly, methods using pushing can become unstable or slower due to multi-contact interactions between objects. In such cases, applying the in-hand translation-based multi-object grasping method proposed in this dissertation allows the manipulator to temporarily store the obstacles along its path for grasping the target object. This approach eliminates the need to relocate objects to other locations, enabling a more efficient singulation tasks. Therefore, translation-based multi-object grasping is particularly effective for singulation in environments with high object density, where traditional methods prove inefficient.

Decluttering aims to remove all objects from the workspace, while packing focuses on moving all objects to a goal region. Decluttering includes tasks such as wiping away dirt [100], but from a pick-and-place planning perspective, it can be considered similar to packing. Practical applications include tasks where a domestic robot tidies up a cluttered room or agricultural tasks such as picking strawberries and placing them into a basket. The declutter problem and packing problem can be mathematically defined as follows:

$$\text{Declutter} : O^i(x^i) \cap X_{\text{clear}} = \emptyset \quad \text{for all } i = 1, \ldots, m \tag{4.2}$$

$$\text{Packing} : O^i(x^i) \subset X_{\text{pack}}, \quad i = 1, \ldots, m \tag{4.3}$$

Conventional studies on the declutter problem [97, 101] have focused on motion planning to remove objects while avoiding obstacles, rather than finding the minimum time path like multi-goal motion planning, as they typically use grippers that handle only one object at a time.

Recently, studies have been proposed to address the declutter problem more efficiently by grasping and moving multiple objects simultaneously [31, 35]. Research has been conducted to find the optimal gripper posture for grasping clustered objects simultaneously [31], and another study has proposed methods for stacking and removing multiple objects together [35]. However, these studies have limitations regarding the combinations and positioning of objects that can be stably grasped, as contact occurs between objects when grasping multiple items at once. As a result, conventional approaches have focused on grasp planning for grasping multiple objects together, without considering manipulator path planning to improve the overall efficiency of the declutter problem.Therefore, even when the types of objects are arbitrary, path planning can be performed without requiring a delicate grasp plan. Moreover, compared to pushing or sweeping methods, the translation-based method offers greater flexibility in object picking, making it much more efficient for moving objects when obstacles are present between them or when the workspace is three-dimensional.

Rearrangement involves moving a set of objects to a set of specified goal positions [97]. The goal of the problem can be expressed as follows:

$$x^i \in C^i_{\text{goal}}, \quad i = 1, \ldots, m \tag{4.4}$$

Detailed tasks include restocking multiple objects in order at a grocery store [102], a robot organizing household items by placing them in desired locations, setting a dining table, or cleaning a bedroom [103]. Since the goal is to move target objects to specific locations, the individual placement of objects becomes critical. Therefore, compared to other multi-object grasping methods, in-hand translation-based multi-object grasping is more effective for these tasks.

Sorting involves classifying a set of objects and can be defined as follows [97]:

$$O^i(x^i) \subset X_{\text{pack},l} \quad \text{for} \quad l_i = l \tag{4.5}$$

This problem can be seen as an extension of rearrangement, incorporating object classification and encompassing multi-class packing problems. Detailed tasks include stocking grocery shelves according to object types [104] or sorting objects in stackable containers [105]. Since the goal is to classify objects by type and place them in desired locations, object placement is critical to this problem. Therefore, translation-based multi-object grasping is more effective than other multi-object grasping methods for these tasks. However, the developed multi-object gripper can only place objects in the reverse order of storage, requiring careful planning of both picking and placing sequences.

Table 4.2 summarizes the goal conditions, applicable multi-object grasping methods, and scenarios where in-hand translation-based multi-object grasping is advantageous for each manipulation task. For singulation, applicable multi-object grasping methods include in-hand translation, pushing, and sweeping. When object density is high, pushing objects becomes difficult, making in-hand translation a more advantageous approach. For decluttering and packing problems, applicable multi-object grasping methods include pushing, sweeping, swallowing, and in-hand translation. When the set of objects consists of arbitrary objects, planning for grasping multiple objects together becomes difficult, making in-hand translation advantageous. Additionally, when obstacles exist between objects, it becomes challenging to gather objects while avoiding obstacles, further highlighting the advantages of in-hand translation. In both cases, swallowing is also a viable option. For rearrangement and sorting, where placement is critical, in-hand translation, which allows individual object placement, is expected to be the most effective method.

Manipulation Tasks	**Goal Condition**	**Alternative Methods**	**Preferred Cases**
Singulation	InGrasp(x^R, x^1)	Pushing Sweeping	Dense Workspace
Declutter / Packing	Declutter: $O^i(x^i) \cap X_{\text{clear}} = \emptyset$ for all $i = 1, \ldots, m$ Packing: $O^i(x^i) \subset X_{\text{pack}}, i = 1, \ldots, m$	Pushing Sweeping Swallowing	Arbitrary Objects / Obstacles
Rearrangement	$x^i \in C^i_{\text{goal}}, i = 1, \ldots, m$	(-)	(-)
Sorting	$O^i(x^i) \subset X_{\text{pack}}, l_i = l$	(-)	(-)

Table 4.2. Goal conditions and applicable multi-object grasping methods for each manipulation task. The last column indicates cases where the multi-object grasping method proposed in this dissertation is more efficient compared to other methods.

In summary, while the developed translation-based multi-object grasping method is not universally optimal, it can be effectively applied to specific cases within each manipulation task. The detailed tasks where the developed gripper can be utilized are summarized in Table 4.2. As an example of path planning for the developed gripper, this dissertation focuses on the simplest case, a 2D decluttering problem.

4.2 Problem Definition

4.2.1 Declutter Problem

The declutter problem is one of the most representative grasping problems involving the handling of multiple objects [97]. The declutter problem aims to remove all objects from a given workspace. In this chapter, considering the characteristics of the proposed gripper, we present a path planning method that minimizes the manipulator's travel distance when moving multiple objects in declutter problems.

The most straightforward approach is to apply the Traveling Salesman Problem (TSP), which finds the shortest path that visits multiple task points [106, 107]. In conventional multi-goal motion planning problems, the genetic algorithm has been primarily used to solve the TSP [108, 109]. Since genetic algorithms do not require the derivative of the objective function, they can be applied to non-continuous combinatorial optimization problems. Additionally, they offer the advantage of optimizing the path without needing to calculate all possible sequence combinations, allowing for near-optimal route computation in a short time. Although they do not guarantee the absolute optimal solution, genetic algorithms are well-suited for robot arm path planning, where rapid calculation of near-optimal routes is necessary. Therefore, in this thesis, path planning for the multi-object gripper was proposed using a genetic algorithm.

When the conventional TSP is applied to the declutter problem, it provides the shortest path from the home position, passing through all objects, and returning to the goal position, as shown in Fig. 4.2A. In this figure, the home and goal positions are set to be the same. However, this type of path planning is only effective when the gripper has unlimited storage capacity, allowing it to store and move all objects in the workspace simultaneously.

However, in reality, the proposed gripper has a finite storage capacity. Therefore, as shown in Fig. 4.2B, once the storage capacity is full while following the path, the gripper must return to the goal position to unload the stored objects and then return to grasp the remaining objects. Consequently, focusing solely on minimizing the total travel distance, as in the typical TSP, may result in an inefficient path where the gripper makes more trips to the goal position, failing to fully utilize its storage capacity. Therefore, to align with the sequential multi-object grasping method proposed in this thesis, in which objects are grasped and stored sequentially, it is essential to consider the gripper's storage capacity. At the same time, a method must be developed that minimizes the manipulator's travel distance.

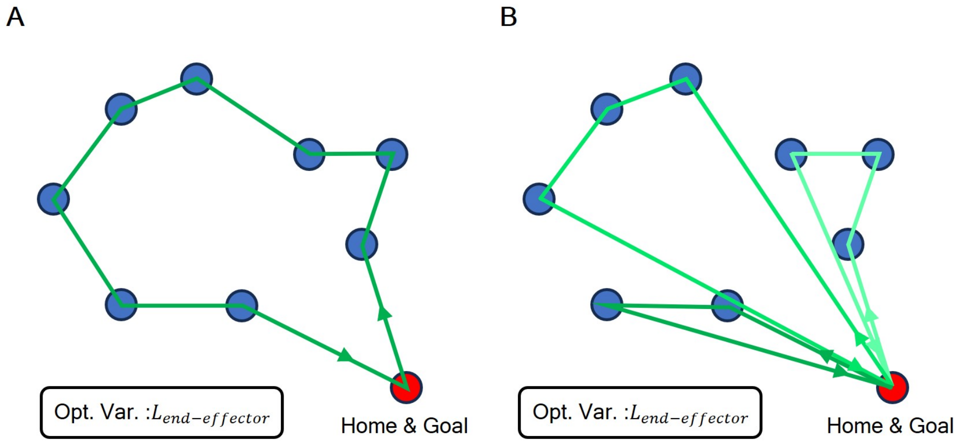
A
B
Opt. Var. :$L_{end-effector}$
Home & Goal
Opt. Var. :$L_{end-effector}$
Home & Goal

Figure 4.2. Comparison of the path for the general TSP problem and the path for declutter problem using multi-object gripper. (**A**) In the general TSP problem, the solution generates the shortest contour connecting the objects and the goal. (**B**) However, the multi-object gripper has a finite storing capacity, meaning it cannot follow the TSP-generated contour directly. Instead, it must return to the goal midway to place the stored objects before continuing.

4.2.2 Storing Capacity

Before formulating the declutter problem using the proposed multi-object gripper, it is necessary to first determine how the gripper's storage capacity will be defined. The configuration of objects and hairs when multiple objects are stored on the proposed conveyor palm is shown in Figure 4.3A. When an object is stored, it deforms the surrounding hairs, which can affect the storage of other objects. This interaction can positively increase the holding force on the objects, but it can also result in storage failures.

Therefore, in this thesis, we defined the minimum space required for each object to be stored without affecting others as the "occupied space." The occupied space was calculated as the length of the region on the conveyor palm where the hairs are deformed when storing an individual object. Examples of occupied spaces for different object sizes are shown in Fig. 4.3B. Since the hairs in contact with both the upper and lower surfaces of the object deform during storage, the occupied space (d_o) is the sum of the length where the hairs deform above (d_{up}) and below (d_{down}) the object. The values of d_{up} and d_{down} for different object sizes were obtained experimentally and are shown in Table 4.3.

Object Diameter (mm)	**5**	**10**	**15**	**20**	**25**	**30**
d_{up} (mm)	7.5	12.5	17.5	17.5	27.5	32.5
d_{down} (mm)	7.5	12.5	17.5	22.5	32.5	37.5

Table 4.3. Experimentally measured d_{up} and d_{down} values for different object sizes.

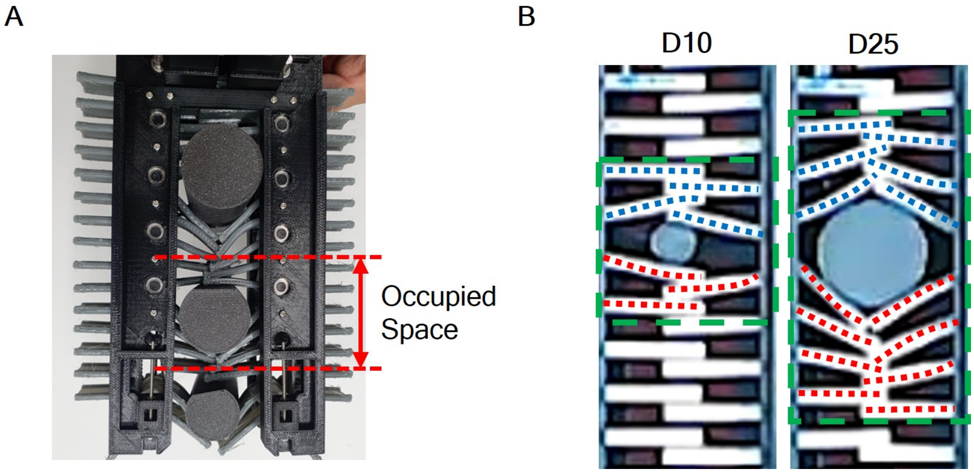

Figure 4.3. Definition of occupied space. (**A**) The configuration of objects and hairs when multiple objects are stored on the proposed conveyor palm. (**B**) Examples of occupied spaces for different object sizes (for objects with diameters of 10 mm and 25 mm, respectively) are illustrated. The occupied space refers to the range of hairs that bend above or below the object when it is stored (green box). The range of hairs bending above the object is denoted as d_{up} (blue hairs), and the range of hairs bending below the object is denoted as d_{down} (red hairs).

When calculate the optimal path, the storage capacity of the conveyor palm must always be greater than or equal to the total occupied space of the objects being stored. The condition for storing n objects together is as follows:

$$C_{\text{store}} \geq \sum_{i=1}^{n} d_o^i \tag{4.6}$$

where C_{store} is storage capacity and d_o^i is the occupied space of the i^{th} stored object. However, Equation 4.6 does not represent the most efficient use of the finite storage capacity. Instead of storing three objects sequentially as in Fig. 4.4A, arranging the first and last objects at the two ends of the conveyor palm allows for more efficient use of space (Fig. 4.4B). Since there are four hairs at the top of the conveyor palm, an object can be stably stored even when placed at the very top of the palm (Fig. 4.4C). Thus, the occupied space of the first stored object is determined by adding object's radius and d_{down}. For objects stored in the middle, the occupied space d_o is the sum of d_{up} and d_{down}. For the last stored object, assuming it is lightweight, it can be stably stored with only two hairs beneath it, meaning that d_o is determined by adding d_{up} and the 10mm distance occupied by the two hairs (Fig. 4.4D). Therefore, the conditions for storing objects greedily to maximize storage capacity are as follows:

$$C_{\text{store}} \geq d_{o,\text{first}}^1 + \sum_{i=2}^{n-1} d_o^i + d_{o,\text{last}}^n \tag{4.7}$$

$$d_{o,\text{first}}^1 = D^1/2 + d_{\text{down}}^1 \tag{4.8}$$

$$d_{o,\text{last}}^n = d_{\text{up}}^n + h_{\text{gap}} \tag{4.9}$$

where D^i is the diameter of i^{th} object, d^i_{up} is d_{up} of i^{th} object, d^i_{down} is d_{down} of i^{th} object, $d_{o,\text{first}}$ is the occupied space of the first stored object, $d_{o,\text{last}}$ is the occupied space of the last stored object, and h_{gap} is the distance between two adjacent hairs on one side of the conveyor palm.

It is important to note that the occupied space of an object may also vary depending on its weight, and if the object is heavy, it might not be possible to store it with only two hairs, meaning that Equation 4.7 could become inaccurate. However, since occupied space is primarily determined by the deformation of the hairs, the most significant factor affecting it is the size of the object. Therefore, in this thesis, the effect of the object's weight is disregarded, and the focus is on proposing a path planning method that accounts for the occupied space of objects of various sizes present in the workspace

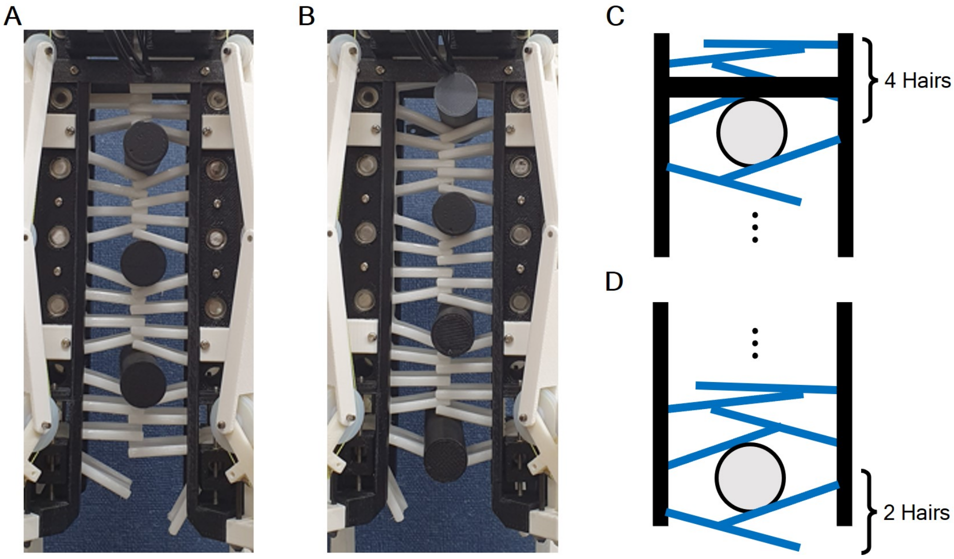

Figure 4.4. Occupied space based on the storage order of objects. (**A**) uses storage capacity less efficiently compared to (**B**). In other words, minimizing the d_{up} and d_{down} of the first and last stored objects increases efficiency. (**C**) The first stored object can be stored stably even when placed near the top of the conveyor palm, as there are 4 hairs above it. (**D**) The last stored object, if light enough, can be supported by only 2 hairs beneath it.

4.2.3 Problem Definition of Declutter Problem using Proposed Multi-Object Gripper

The problem of finding the minimum manipulator travel distance while considering the gripper's storage capacity in the declutter scenario is illustrated in Figure 4.5. In this thesis, the declutter problem was limited to moving objects placed on a desk, with the objects restricted to cylinders of various sizes, for which the occupied space has been experimentally measured. Then, I assumed that there is a set of C objects $\mathcal{C} = \{o_1, \ldots, o_C\}$ along with its visual information. The position of the i^{th} object segmented by vision was represented as (x_i, y_i), and the occupied space of each object was denoted as $(d^i_{\text{up}}, d^i_{\text{down}})$. The grasping sequence of the objects was represented as $f_{\text{path}}(\mathcal{C}) = [o_{\sigma(1)}, \ldots, o_{\sigma(C)}]$ where $\sigma : \{1, 2, \ldots, c\} \rightarrow \{1, 2, \ldots, c\}, \quad \sigma(i) \neq \sigma(j)$. The gripper follows $f_{\text{path}}(\mathcal{C})$, storing objects until its storing section is full. Once the storing section is full, the gripper grasps the last object and moves to the goal. After moving to the goal and placing the objects, the gripper continues to grasp the next object in $f_{\text{path}}(\mathcal{C})$.

During this process, groups of objects that can be moved together were formed along $f_{\text{path}}(\mathcal{C})$, and these groups were denoted as $\mathcal{G}$, i.e. $\mathcal{G} = \{G_k\}_{k=1}^{M}$, where M is the total number of groups. The index of the first object in the k^{th} group was denoted as $g_{k,1}$, and the number of objects in G_k was denoted as n_k, meaning that $G_k = \{o_i\}_{i=g_{k,1}}^{g_{k,n_k}}$. The total distance traveled by the gripper along $f_{\text{path}}(\mathcal{C})$ was denoted as $L_{end-effector}$. The set of objects composing group G was defined as $f_{\text{object}}(G) \subset \mathcal{C}$.

Thus, the goal of the declutter problem, considering storage capacity, is as follows:

$$
\begin{aligned}
&\text{Find } f_{\text{path}}(\mathcal{C}) \arg\min L_{end-effector} \\
&\qquad\qquad \text{s.t.} \quad C_{\text{store}} \geq d_{o,\text{first}}^{g_{k,1}} + \sum_{i=g_{k,2}}^{g_{k,n_k-2}} d_o^i + d_{o,\text{last}}^{g_{k,n_k-1}} \quad \forall G_k \\
&\qquad\qquad f_{\text{object}}(G_j) \cap f_{\text{object}}(G_k) = \emptyset, \quad j \neq k \qquad\qquad (4.10) \\
&\qquad\qquad \bigcup_{G_k \in G} f_{\text{object}}(G_k) = \mathcal{C}
\end{aligned}
$$

$L_{end-effector}$ refers to the travel distance of the manipulator as it follows the object sequence $f_{\text{path}}(\mathcal{C})$ and moves the objects. While storing objects in the order defined by the path, if the condition in Equation 4.7 is not satisfied, the manipulator moves to the goal position to place the stored objects before proceeding to the next one. In this case, even when the storage is full, one additional object can be transported through the gripper's finger. Therefore, when moving the objects in the G_k group, the strategy is to store n_k-1 objects and transport the remaining one using the finger.

To validate the optimal path obtained through Equation 4.10, three baselines were selected. The first baseline was the path for single-object grasping, used to verify the efficiency of multi-object grasping. Additionally, to confirm that the path optimized by considering storage capacity is more efficient, another baseline was established using the solution of general Traveling Salesman Problem (TSP), which only considers object positions. The final baseline was set as a method that considers both storage capacity and object positions.

In this thesis, the grasp path of single-object grasping will be abbreviated as "SOG", and the grasp path along the solution of Traveling Salesman Problem as "TSP". The gripper path generated by the method that considers both storage capacity and object positions is referred to as "TSP_Store."

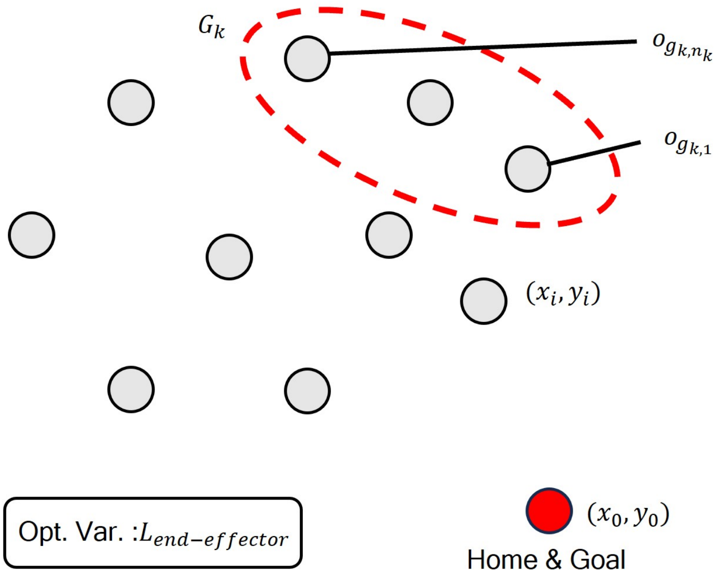

Figure 4.5. Schematic of the declutter problem for the proposed multi-object gripper. As the gripper follows the path and stores objects, groups of objects that can be moved together are formed.

4.3 Results

4.3.1 Path Planning Pipeline

The actual setup for the declutter problem is illustrated in Figure 4.6. As shown in Figure 4.6A, objects were placed on a desk, and the gripper recognizes and moves them using an Intel RealSense D435i camera installed facing the workspace. The camera's view is shown in Fig. 4.6B, and there are a total of 11 objects (Fig. 4.6C). All objects were black cylinders, each 100 mm in length, with diameters ranging from 5 mm to 30 mm in 5 mm intervals. Detailed information about the objects is provided in Table 4.4. The workspace where the objects were located has an x-coordinate range from -300 mm to 300 mm and a y-coordinate range from -750 mm to -350 mm, relative to the manipulator's base coordinate system. These boundaries were set to avoid singularities that might occur as the manipulator moves, and the center of each object must remain within this workspace.

The path planning pipeline is illustrated in Fig. 4.7. First, before moving the gripper and manipulator, the entire workspace was captured by the camera (Figure 4.7A). using OpenCV's boxPoint(rect) function, the cylinders captured by the camera were approximated as rectangles, and the coordinates of the four corners were obtained (Fig. 4.7B). Based on the coordinates of these four corners, the center position of each cylinder can be calculated in pixels, and the tilt angle of the cylinder can also be determined. Additionally, by utilizing the aspect ratio of the rectangle, the size of the object can be identified. Finally, based on the size and position of the objects, a genetic algorithm was applied to find the optimal path that maximizes storage capacity while minimizing travel distance.

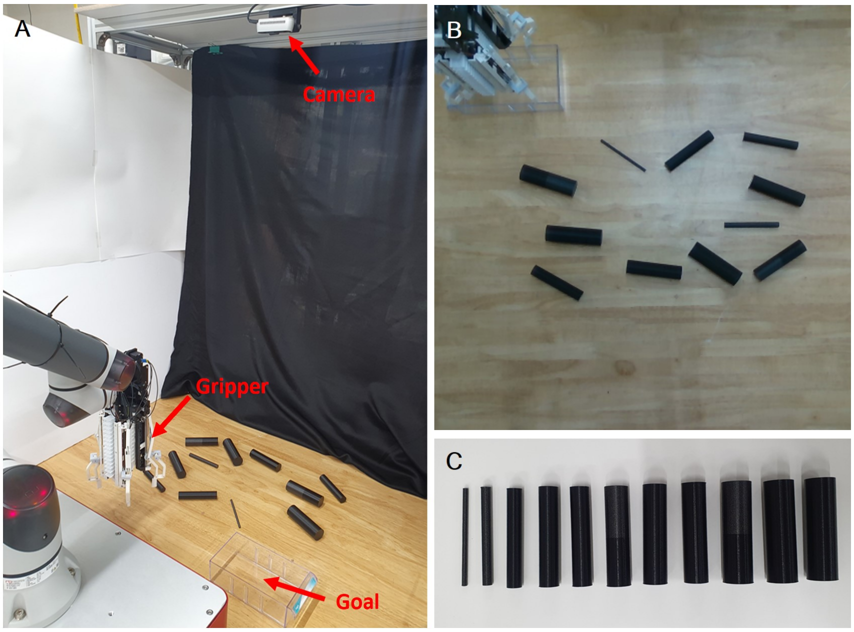

Figure 4.6. The setup for declutter problem. (**A**) Objects are placed on a desk, and the gripper recognizes and grasps them using a camera installed facing the workspace. (**B**). The camera view. (**C**) Target objects. All objects are black cylinders, each 100 in length, with diameters ranging from 5 mm to 30 mm in 5 mm intervals.

Diameter of Objects (mm)	**5**	**10**	**15**	**20**	**25**	**30**
Number of Objects	1	1	1	2	3	3

Table 4.4. Diameter variations of target objects for the declutter problem and the number of objects with each corresponding diameter.

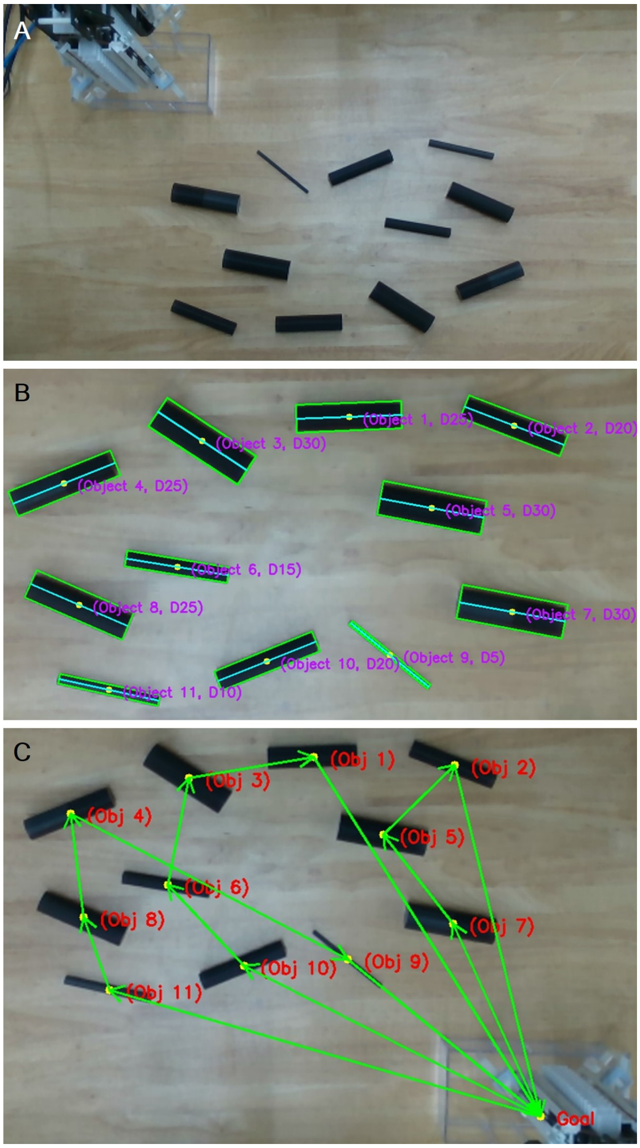
A
B
(Object 1, D25)
(Object 2, D20)
(Object 3, D30)
(Object 4, D25)
(Object 5, D30)
(Object 6, D15)
(Object 8, D25)
(Object 7, D30)
(Object 10, D20)
(Object 9, D5)
(Object 11, D10)
C
(Obj 1)
(Obj 2)
(Obj 3)
(Obj 4)
(Obj 5)
(Obj 6)
(Obj 8)
(Obj 7)
(Obj 10)
(Obj 9)
(Obj 11)
Goal

Figure 4.7. The path planning pipeline of the declutter problem. (**A**) The entire workspace is captured using an overhead camera. (**B**). Using OpenCV, the cylinders are approximated as rectangles, and the position, diameter, and tilt angle of each object are extracted. (**C**) Based on the object information, the manipulator's near-optimal path is obtained.

4.3.2 Path Planning using Genetic Algorithm

To minimize the manipulator's travel length ($L_{end-effector}$) using a genetic algorithm, a random initial population of n_{popul} paths was generated, and the fitness of each path ($L_{end-effector}$) was calculated to find the path with the lowest fitness. While typical genetic algorithms aim to maximize the fitness function, in this thesis, the fitness function was designed to be minimized. Next, $n_(parents)$ pairs of parent combinations were selected using roulette wheel selection, where paths with lower fitness were more likely to be chosen. After that, the sequences of the selected parent generations were combined to produce the same number of offspring generations (crossover). During this process, mutations were applied to prevent the algorithm from getting stuck in a local minimum. The crossover point was randomly chosen between the second and second-to-last indices of the sequence, and mutations were applied with a 5% probability. If any of the newly generated offspring have a lower fitness than the parents, the optimal sequence was updated, and the process was repeated. Initially, 100 random sequences (paths) were generated, with 50 pairs of parents selected and 50 pairs of offspring generated. The genetic algorithm ran for a maximum of 1,000 generations, but it terminated early if there was no change in fitness for 500 generations.

4.3.3 Comparison with Paths Generated by Other Methods

The optimal path obtained through Equation 4.10 was validated via actual demonstrations. To do this, the manipulator's travel distance and process time were compared when performing decluttering using the SOG, TSP, and TSP_Store methods. First, the common object setup is shown in Fig. 4.8A. In the case of SOG, where one object is grasped and moved at a time, the gripper's path consists of straight lines connecting the goal position with each object (Fig. 4.8B). In this scenario, the manipulator performs 11 round trips to move all objects. Next, for the TSP method, the shortest path connecting the goal position with the 11 objects is calculated before determining the gripper's path (Fig. 4.8C). The gripper follows the shortest path determined by TSP, grasping and storing objects sequentially. Once the storing section is full, the gripper returns to the goal position after grasping one additional object. The resulting path is shown in Fig. 4.8D, with the manipulator making 4 round trips in this case. Finally, the gripper path calculated using the TSP_Store method is shown in Fig. 4.8E. In this case, the manipulator completes the task with only 3 round trips.

By comparing Figures 4.8D and 4.8E, it can be observed that the path obtained using the TSP method does not consider the size of the objects. As a result, when larger objects are positioned close to each other, the storage capacity may not be fully utilized, leading to an increased number of round trips for the manipulator. Since the distance between objects and the goal position is greater than the distance between objects themselves, the number of round trips has a direct impact on the travel length and pick-and-place process time. Therefore, the path obtained using the TSP_Store method is more efficient than the one obtained using the general TSP method. To verify the pick-and-place process time for each method, a demonstration was conducted following the paths shown in Fig. 4.8B, D, and E to perform the declutter problem (Fig. 4.8F). In the demonstration using the path from Fig. 4.8B, the gripper repeatedly grasped one object at a time and moved it to the goal position. When following the path from Fig. 4.8D, the gripper moved 3, 3, 4, and 1 objects at a time, respectively, to transfer all 11 objects (Fig. 4.9). Finally, in the demonstration using the path from Fig. 4.8E, the gripper transferred 4, 3, and 4 objects at a time to complete the decluttering process (Fig. 4.10).

The manipulator's travel distance and the process time for the declutter problem for each path are shown in Figure 4.11. In terms of travel distance, the path obtained using the TSP_Store method was 65.7% shorter than the SOG method and 15.9% shorter than the TSP method (Fig. 4.11A). Additionally, for the declutter process time, the path obtained using the TSP_Store method was 40.5% more efficient than the SOG method and 10.3% more efficient than the TSP method.

The reduction in process time is smaller than the reduction in travel distance for two reasons. First, as discussed in Chapter 3.6.1, the multi-object grasping process includes translation and storing processes that do not exist in single-object grasping. If the time spent on translation and storing exceeds the time required for the manipulator to move between objects, the reduction in process time may be smaller than the reduction in travel distance. Second, due to the close distance of the objects, the manipulator may not be able to reach its maximum speed when moving between objects.

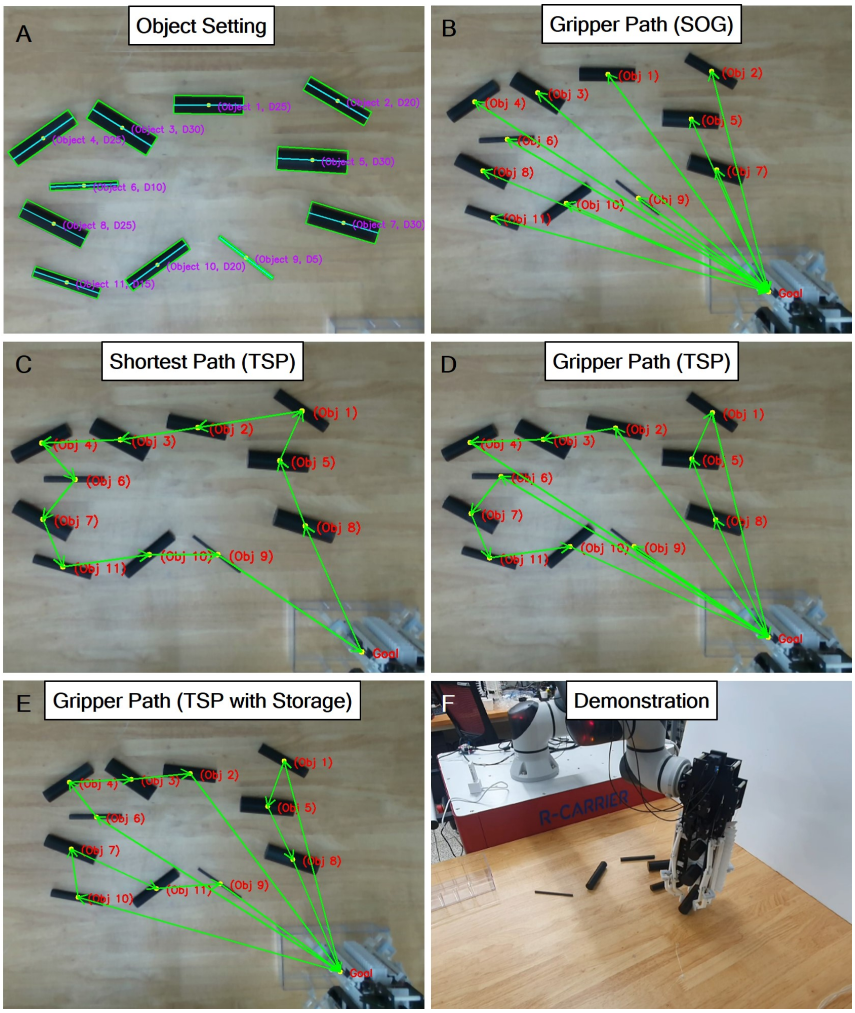
A
Object Setting
B
Gripper Path (SOG)
C
Shortest Path (TSP)
D
Gripper Path (TSP)
E
Gripper Path (TSP with Storage)
F
Demonstration
Goal
R-CARRIER

Figure 4.8. The optimal path obtained through different methods. (**A**) The common arrangement of objects for comparison. (**B**). Gripper path of SOG method. The manipulator performs 11 round trips to move all objects. (**C**) The shortest path obtained by solving the TSP problem. (**D**) Gripper path when grasping objects along the TSP route. The manipulator performs 4 round trips to move all objects. (**E**) Gripper path obtained using the TSP_Store method. The manipulator performs 3 round trips to move all objects. (**F**) Demonstration.

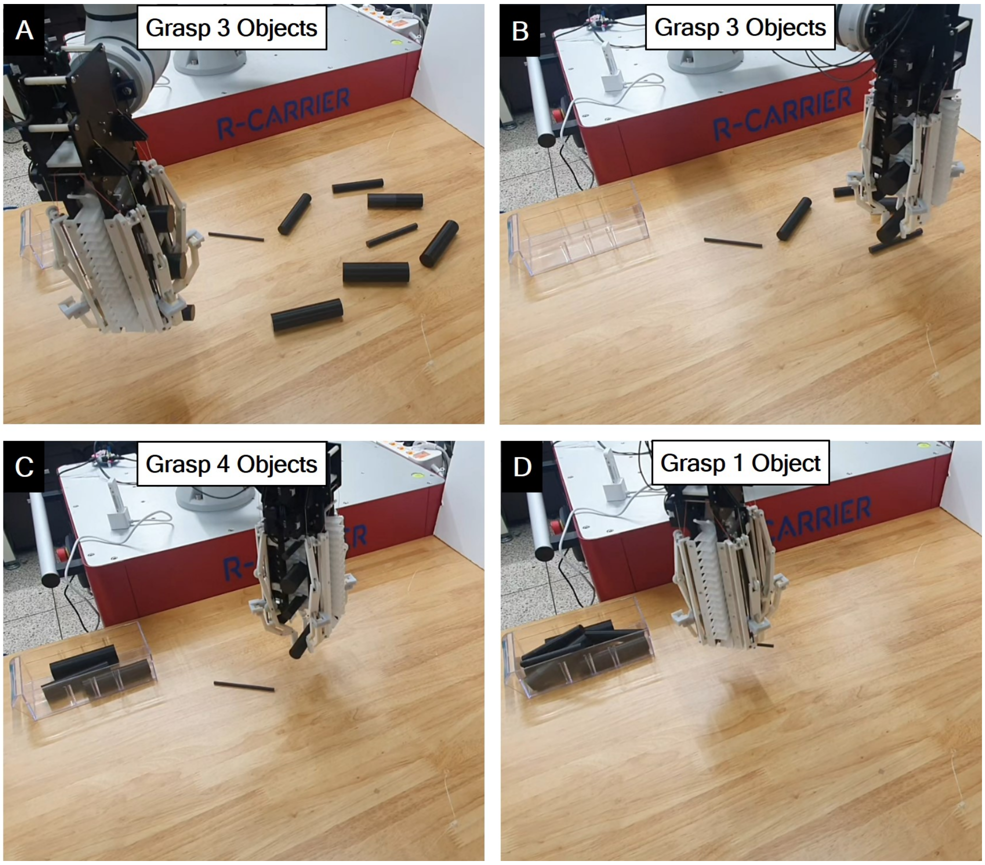
A
Grasp 3 Objects
B
Grasp 3 Objects
C
Grasp 4 Objects
D
Grasp 1 Object
R-CARRIER

Figure 4.9. Declutter demonstration using the path generated by solving the TSP problem. (**A**) The gripper first moves 3 objects together, (**B**) then moves another 3 objects, (**C**) moves 4 objects, and (**D**) finally moves the last object. The manipulator performs 4 round trips to move all objects.

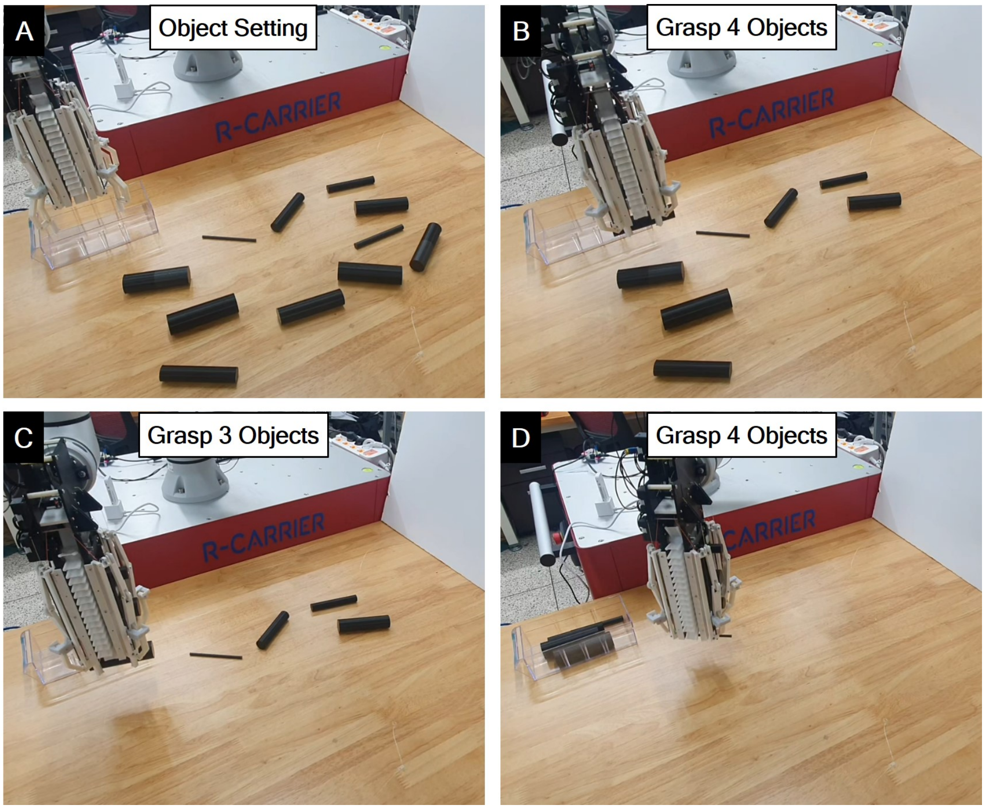
A
Object Setting
B
Grasp 4 Objects
C
Grasp 3 Objects
D
Grasp 4 Objects
R-CARRIER

Figure 4.10. Declutter demonstration using the path generated by solving the TSP_Store method. (**A**) The demonstration setting with 11 objects. (**B**) The gripper first moves 4 objects together, (**C**) then moves another 3 objects, and (**D**) finally moves the last 4 objects. The manipulator performs 3 round trips to move all objects.

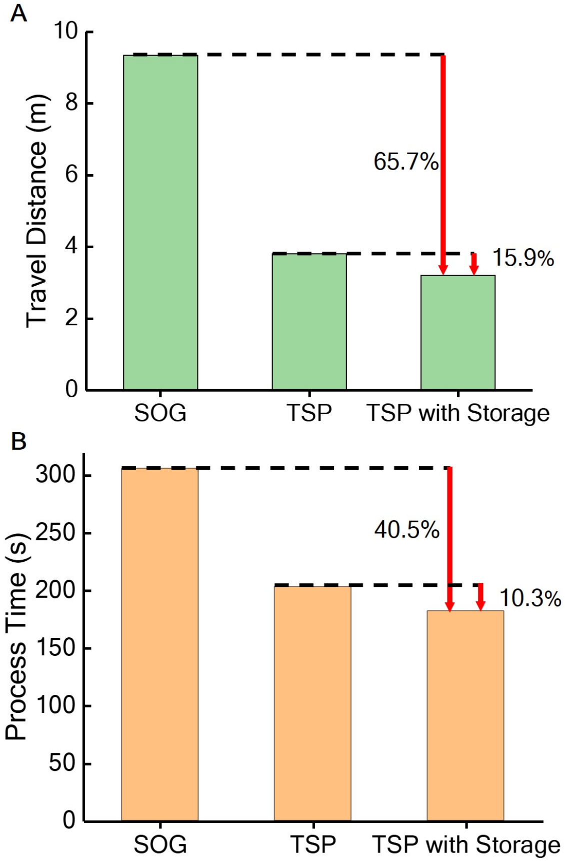

Figure 4.11. Comparison of manipulator travel distance and declutter process time during demonstrations using the paths obtained through the SOG, TSP, and TSP_Store methods. (**A**) The path obtained through the TSP_Store method was 65.7% shorter than the path obtained using the SOG method, and 15.9% shorter than the path obtained using the TSP method. (**B**) In terms of process time, the path obtained through the TSP_Store method reduced the process time by 40.5% compared to the SOG method, and by 10.3% compared to the TSP method.

4.3.4 Comparison of Path Efficiency According to Storage Capacity

In the previous chapters, the efficiency of paths generated by SOG, TSP, and TSP_Store was compared with the gripper's storage capacity fixed at 135 mm. In this chapter, efficiency comparisons of paths generated by TSP_Store and other methods were proposed when the gripper's storage capacity changes.

As the number of objects to be moved increases, the differences between the paths generated by each algorithm become more apparent. Therefore, instead of using the 11 objects from the demo, 16 objects were utilized in this experiment. The diameters and quantities of the objects used are presented in Table 4.5. The 16 objects were arranged as shown in Figure 4.12, and the lengths of the gripper paths planned using TSP_Store, TSP, and SOG methods were compared according to the storage capacity, while maintaining the same object arrangement. The number of round trips in the gripper paths for each algorithm based on storage capacity are illustrated in Figure 4.13.

The experimental results show that, when the storage capacity is small, the number of round trips dramatically decreases as the storage capacity increases. However, when the storage capacity is large, the number of round trips

Diameter of Objects (mm)	5	10	15	20	25	30
Number of Objects	1	1	2	2	5	5

Table 4.5. The diameter and quantity of the target objects for the experiment comparing path efficiency of three different algorithms varying storage capacity.

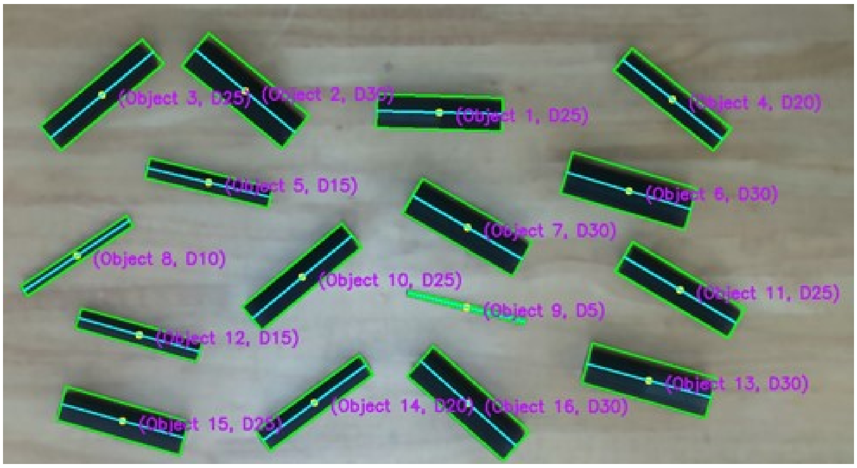
(Object 3, D25)
(Object 2, D35)
(Object 1, D25)
(Object 4, D20)
(Object 5, D15)
(Object 6, D30)
(Object 7, D30)
(Object 8, D10)
(Object 10, D25)
(Object 9, D5)
(Object 11, D25)
(Object 12, D15)
(Object 13, D30)
(Object 15, D25)
(Object 14, D20)
(Object 16, D30)

Figure 4.12. The test setup for comparing the efficiency of paths generated by TSP_Store, TSP, and SOG under varying storage capacities.

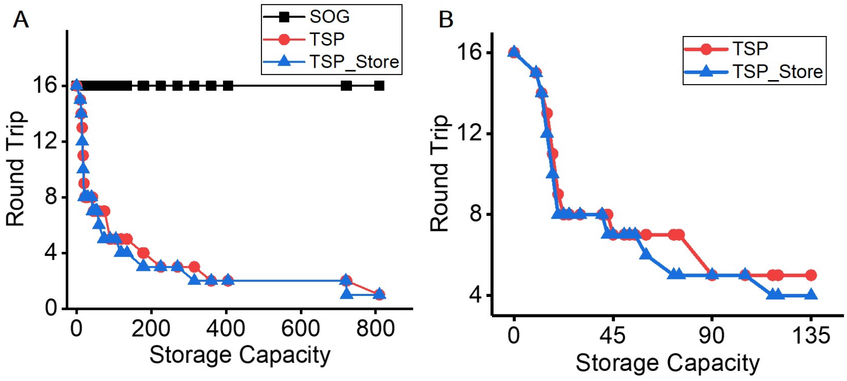

Figure 4.13. Comparison of the number of round trips for each algorithm's path based on storage capacity. (A) Data covering the full range from the smallest storage capacity (0 mm) to the largest storage capacity (810 mm). **(B)** Enlarged graph for detailed comparison between TSP and TSP_Store (the storage capacity range: 0 to 135 mm).

does not decrease significantly with further increases in storage capacity. This phenomenon can be explained with a simple example. If the gripper can grasp two objects simultaneously instead of one, the number of round trips reduces from 16 to 8. However, if the gripper can grasp five objects simultaneously instead of four, the number of round trips remains unchanged at 4. Therefore, the number of round trips decreased sharply as the storage capacity increased, but the rate of decrease gradually reduced.

When the gripper's storage capacity was 0 mm, the paths generated by TSP_Store, TSP, and SOG were identical. This is because the gripper cannot store objects, requiring it to move objects one at a time, following the same path as single-object grasping. In this case, all three methods resulted in the path shown in Figure 4.14A. Furthermore, when the storage capacity is sufficiently large (exceeding 810 mm), enabling the gripper to transport all objects at once, the paths generated by TSP_Store and TSP become identical (Fig. 4.14B). This is because a storage capacity of 810 mm enables the gripper to transport all objects in a single trip, regardless of storage order. In this case, since all objects can be transported in a single round trip without considering storage capacity, the paths generated by TSP_Store and TSP become identical. The specific value of 810 mm corresponds to the worst-case scenario of transporting 16 objects simultaneously. This occurs when the gripper holds a 5 mm diameter object with its fingers and stores a 15 mm object at the topmost position and a 10 mm object at the bottommost position of the conveyor palm (Fig. 4.15A). Since the size of the object held by the fingers is not included in the storage capacity, gripping the largest object is advantageous. Additionally, objects stored at the top and bottommost positions occupy less space (Fig. 4.4), making it optimal to store the largest objects at those positions. Following this optimal solution, the minimum storage capacity required to transport 16 objects simultaneously is 722.5 mm (Fig. 4.15B). In this case, the path generated by TSP_Store allows the gripper to transport all objects in a single round trip, whereas the path generated by TSP requires two round trips. This example highlights the advantage of TSP_Store, which finds the optimal path by fully utilizing the storage capacity, enabling the gripper to store the objects in the best sequence. In contrast, TSP generates a path without considering storage capacity, failing to achieve the optimal solution and resulting in an increased number of manipulator round trips. Therefore, TSP_Store can produce a solution that is less influenced by the arrangement of object sizes compared to TSP.

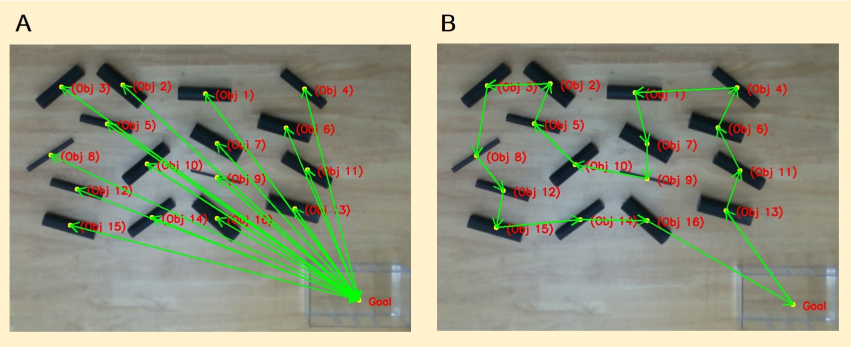
A
(Obj 3)
(Obj 2)
(Obj 1)
(Obj 4)
(Obj 5)
(Obj 6)
(Obj 7)
(Obj 8)
(Obj 10)
(Obj 9)
(Obj 11)
(Obj 12)
(Obj 13)
(Obj 15)
(Obj 14)
(Obj 16)
Goal
B
(Obj 3)
(Obj 2)
(Obj 1)
(Obj 4)
(Obj 5)
(Obj 6)
(Obj 7)
(Obj 8)
(Obj 10)
(Obj 9)
(Obj 11)
(Obj 12)
(Obj 13)
(Obj 15)
(Obj 14)
(Obj 16)
Goal

Figure 4.14. Paths under extreme storage capacities. (A) When the storage capacity is 0 mm, all three algorithms, TSP_Store, TSP, and SOG, generate the same path. **(B)** When the storage capacity is 810 mm, allowing all objects to be transported in a single trip, there is no difference between the paths generated by TSP_Store and TSP.

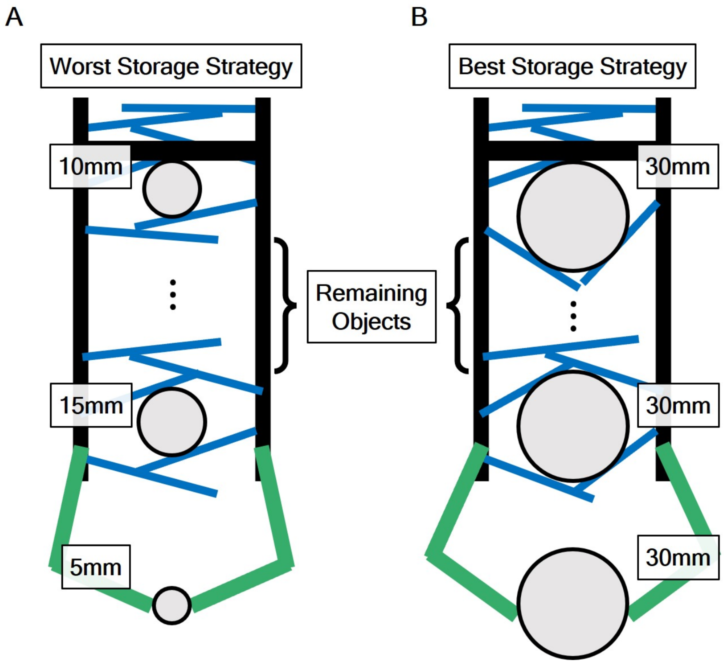

Figure 4.15. The cases of using storage most inefficiently and most efficiently when transporting 16 objects at once. (A) Most inefficient case. The smallest object is grasped by the fingers, and the next smallest objects are stored at the very top and bottom of the storage. **(B)** Most efficient case. The largest object is grasped by the fingers, and the next largest objects are stored at the very top and bottom of the storage.

The advantage of TSP_Store is also evident when the storage capacity is 15 mm (Fig. 4.16). With this storage capacity, the gripper can store objects with diameters of 5, 10, and 15 mm respectively. Since there are four objects with diameters of 15 mm or less, only 12 trips are theoretically required to transport all 16 objects. However, if 5 mm and 15 mm diameter objects are located close to each other in the TSP path, they are transported together, resulting in 13 trips, as the two objects are moved simultaneously. In contrast, TSP_Store completes the task in 12 trips. Therefore, within the storage capacity range of 10 mm to 722.5 mm, TSP_Store generates paths with the same or fewer trips compared to TSP.

The number of trips correlates strongly with the total path length. As a result, the total distance traveled by the manipulator also exhibits a similar trend to the number of trips (Fig. 4.17). In the range of 10 mm to 722.5 mm storage capacity, TSP_Store generates paths with shorter travel distances than TSP. The most efficient case occurs when the storage capacity is 75 mm, where the path generated by TSP_Store is approximately 17.1% shorter than that of TSP. However, this result is based on the arrangement of objects shown in Figure 4.12, and the specific values will change with different object arrangements. Nevertheless, TSP_Store is expected to produce more efficient paths than TSP. Moreover, given a specific set of objects, TSP_Store can be used to determine the design of the optimal storage capacity.

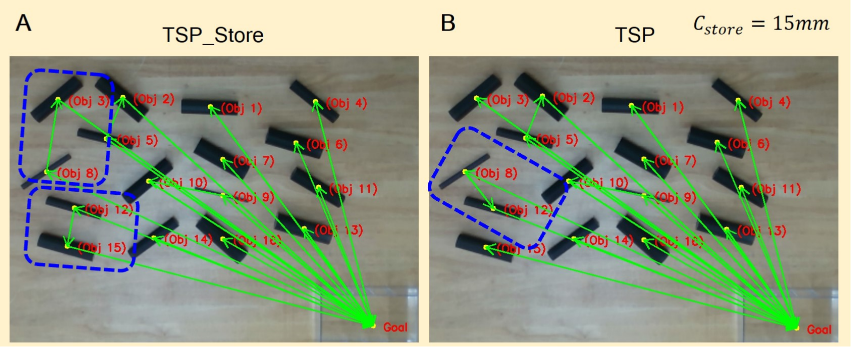
A
TSP_Store
B
TSP
$C_{store} = 15mm$
(Obj 1)
(Obj 2)
(Obj 3)
(Obj 4)
(Obj 5)
(Obj 6)
(Obj 7)
(Obj 8)
(Obj 9)
(Obj 10)
(Obj 11)
(Obj 12)
(Obj 13)
(Obj 14)
(Obj 15)
(Obj 16)
Goal

Figure 4.16. Comparison of paths generated by TSP_Store and TSP when the storage capacity is 15 mm. (A) TSP_Store matches a small object with a larger object to create an optimal path. **(B)** TSP suggests a path that grasps two small objects close to each other simultaneously. If the gripper follows the TSP path, it transports one of the storable objects without storing it, resulting in a higher number of round trips compared to when following the TSP_Store path.

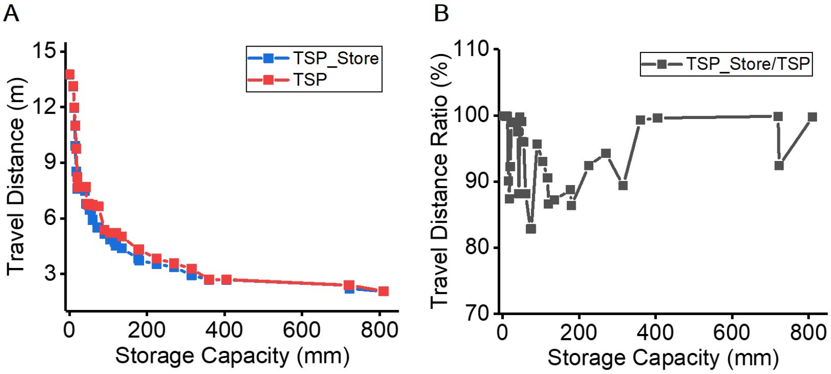

Figure 4.17. Comparison of travel lengths for paths generated by TSP_Store and TSP varying storage capacity. (A) Absolute values of the travel lengths are compared. **(B)** The ratio between the travel lengths of the two paths is analyzed.

4.4 Summary

In this chapter, the path planning method was presented for multi-object grasping that sequentially repeats object grasping and storing through finger-to-palm translation. To demonstrate this, the declutter problem, a well-known pick-and-place problem, was selected for solving. Conventional research on solving the declutter problem using multi-object grasping has primarily focused on how to simultaneously grasp multiple objects, while the overall manipulator path planning for decluttering has not been extensively studied. In contrast, the proposed gripper has the advantage of grasping objects one by one, which reduces the constraints on the combinations of objects to be grasped. This advantage makes the manipulator's path planning problem similar to solving the Traveling Salesman Problem (TSP), where the goal is to find the shortest distance between points. However, if the objective is only to minimize the distance of the path connecting the objects without considering the size of the objects, the gripper's storing capacity cannot be fully utilized. Therefore, in this chapter, the concept of occupied space was defined based on object size. In addition, the TSP with Storage method was proposed, which takes object size and storage capacity into account when solving the TSP. The efficiency of decluttering was compared in three cases: using single-object grasping, through the optimal path for decluttering using the TSP, and through the path generated by the proposed method. The results showed that the TSP with Storage method effectively utilized the storing capacity and minimized the travel length, confirming its efficiency in generating an optimal path.

Chapter 5

Conclusion

5.1 Summary

This dissertation proposed a multi-object gripper for versatile pick-and-place operations in unstructured environments. The developed gripper increases the time efficiency of pick-and-place processes, by reducing the robot arm's travel distance when moving the target objects. The segmentation into a grasping section and a storing section and their synergistic use, along with their synergistic use enabled by in-hand translation, allows the gripper to grasp and place objects relatively freely while moving multiple objects together. This expands the pick-and-place versatility of multi-object gripper. By repeating grasping and storing, the developed gripper can grasp distant objects sequentially and move them simultaneously. The developed gripper can also individually place objects in the desired position by retrieving the stored objects.

Chapter 1 introduced pick-and-place tasks where robotic grippers are currently being used, categorizing tasks based on industrial domains. Pick-and-place tasks are increasingly transitioning from structured environments to unstructured ones. In structured environments, multi-object grasping methods are employed to improve the efficiency of pick-and-place tasks by moving multiple objects simultaneously. However, existing multi-object grasping methods are challenging to apply in unstructured environments. Consequently, various multi-object grasping methods suitable for unstructured environments are being developed. Recent methods are classified into scooping, pushing, sweeping, and swallowing, with their advantages and disadvantages summarized in Table 1.1. This dissertation explored human manipulation strategies for moving multiple objects at once while precisely placing a single object in the desired position. Hand segmentation and in-hand translation were identified as key principle in multi-object grasping for various pick-and-place tasks.

Chapter 2 presented the design of fingers and palm inspired by human strategies. To decouple the grasping and translational movements of the fingers, a decoupling linkage was developed. Additionally, a conveyor palm was designed to store multiple objects at once, simplifying the translating and storing processes required by the proposed multi-object grasping method. Comparisons of alternative finger and palm designs were also provided. Finally, the design of a separable palm was explained to enable easy swapping based on task requirements.

Chapter 3 presented analyses of the proposed fingers and palm. The design conditions of the decoupling linkage were investigated through kinematic and kinetic analyses and were experimentally validated. Grasping force analysis was conducted, including tests on how it changes with repeated operations. For the conveyor palm, analytical modeling and experiments were proposed to determine the size and weight limits of storable objects. Theoretical limits for storable object sizes were presented, and the storing force was measured with varying design parameters, such as object size, hair radius, distance between the hairs, and the materials of hair. Furthermore, the issues related to integrating the developed finger and palm were analyzed. The success rate of object transfer between the fingers and palm was measured, and retrieval offsets during palm-to-finger translation were evaluated by varying object weight and gripper angle. Finally, a laboratory-scale logistics demonstration showcased the gripper's ability to improve the time efficiency of pick-and-place processes. Additional demonstrations validated the feasibility of placing objects one by one in desired orientations and handling 23 different types of objects.

Chapter 4 classified the robotic pick-and-place tasks discussed in Chapter 1 into four categories based on goal specification and the degree of object labeling: singulation, decluttering/packing, rearrangement, and sorting. For each category, the environmental conditions where the developed gripper could be effectively utilized were proposed. Next, a path-planning algorithm for decluttering, one of the manipulation categories, is introduced. The TSP_Store algorithm, which incorporates the gripper's storage capacity into the conventional Traveling Salesman Problem (TSP) algorithm for finding the minimum distance between objects, is presented. Additionally, comparisons between the paths generated by TSP_Store and TSP were conducted and validated through actual demonstrations. The Appendix summarizes additional experimental results. The proposed multi-object grasping technique is expected to be suitable for unorganized environments and those with placement critical tasks. Therefore, I believe that the proposed approach provides extended applications of multi-object grasping, not only in logistics, domestic, and declutter problems, but also in unconstructed industrial settings like bin picking.

5.2 Limitation and Future Work

In Chapter 4, the manipulation tasks were divided into four categories, with scenarios presented where the developed multi-object grasping method could be effectively applied. However, the problem definition and path planning were only developed for the declutter problem. To utilize the developed gripper in more various situations, it is necessary to define and address the other tasks, particularly rearrangement and sorting, where the proposed multi-object grasping method is especially effective. Examples of rearrangement tasks where the developed gripper can be effectively utilized include tidying up a house, while an example of sorting is batch picking in a warehouse. The feasibility of both tasks was demonstrated in this dissertation already, and with proper problem definitions, planning optimal paths will be possible. For rearrangement and sorting tasks, placement plays a crucial role and should be carefully considered during the planning process. This means that path planning needs to account not only for the sequence in which objects are grasped but also for the order in which they are placed. Rearrangement tasks often involve organizing objects in a way that satisfies specific spatial or functional requirements. On the other hand, sorting tasks typically involve classification, where objects must be sorted into distinct categories. In many cases, sorting tasks may also require objects to be placed in a predetermined order or location, which adds an additional layer of complexity to the planning process. By addressing both grasping and placement sequences, these tasks can be executed more efficiently and effectively.

To address tasks where placement is crucial, such as rearrangement and sorting, improving the retrieval process of the developed multi-object grasping gripper should also be considered. Currently, the gripper retrieves objects in the reverse order of storage, which means the order of grasping affects the order of placement. This limitation can result in the inefficient path planning for placement-critical tasks. For example, if it is efficient to grasp objects 1, 2, and 3 in sequence but place them as 2, 3, and 1, the current gripper design cannot achieve the optimal path. Enabling retrieval of specific objects on demand could enhance the gripper's efficiency.

The decluttering problem, as formulated in this dissertation, needs increased complexity to better simulate real-world scenarios. Introducing obstacles between objects or expanding the workspace into a 3D environment, such as shelves, could enable planning for tasks like tidying up a house.

While design guidelines for the conveyor palm were provided, its scalability has only been analyzed theoretically. Since scalability is a critical feature when the size of target objects changes, experimental validation of this characteristic would provide more robust design guidelines for future designs. Additionally, improving the fabrication process by using 3D printing for conveyor palms could simplify design modifications, allowing for the development of conveyor palm tailored to specific target objects.

Finally, further exploration of greedy storing strategies is needed. The storing strategy is crucial in determining the gripper's overall efficiency, making it an essential factor to consider. In this dissertation, the storing strategy was designed to ensure a minimum distance where stored objects do not interfere with each other. However, objects could potentially be stored closer, even influencing each other's storage. Furthermore, with an infinitely rotating belt, objects could even be stored in direct contact with one another. Such greedy strategies are discussed in detail in the appendix and require further analysis in future work.

References

[1] International Federation of Robotics. Executive summary wr 2024 industrial robots, 2024. Accessed: 2024-12-23.

[2] Precedence Research. Service robotics market size, share, and trends 2024 to 2034, 2024. Accessed: 2024-12-23.

[3] Yangmin Li and Qingsong Xu. Kinematic analysis of a 3-prs parallel manipulator. *Robotics and Computer-Integrated Manufacturing*, 23(4):395–408, 2007.

[4] Han Sung Kim and Lung-Wen Tsai. Design optimization of a cartesian parallel manipulator. *J. Mech. Des.*, 125(1):43–51, 2003.

[5] Dan Zhang, Zhuming Bi, and Beizhi Li. Design and kinetostatic analysis of a new parallel manipulator. *Robotics and Computer-Integrated Manufacturing*, 25(4-5):782–791, 2009.

[6] Vincent Nabat, Olivier Company, Francois Pierrot, and Philippe Poignet. Dynamic modeling and identification of par4, a very high speed

parallel manipulator. In *2006 IEEE/RSJ International Conference on Intelligent Robots and Systems*, pages 496–501. IEEE, 2006.

[7] Clement M Gosselin, Sylvain Lemieux, and J-P Merlet. A new architecture of planar three-degree-of-freedom parallel manipulator. In *Proceedings of IEEE international conference on robotics and automation*, volume 4, pages 3738–3743. IEEE, 1996.

[8] Ping Jiang, Junji Oaki, Yoshiyuki Ishihara, and Junichiro Ooga. Multiple-object grasping using a multiple-suction-cup vacuum gripper in cluttered scenes. *arXiv preprint arXiv:2304.10693*, 2023.

[9] Aude Billard and Danica Kragic. Trends and challenges in robot manipulation. *Science*, 364(6446):eaat8414, 2019.

[10] Federico Vicentini. Collaborative robotics: a survey. *Journal of Mechanical Design*, 143(4):040802, 2021.

[11] Takafumi Taketomi, Hideaki Uchiyama, and Sei Ikeda. Visual slam algorithms: A survey from 2010 to 2016. *IPSJ transactions on computer vision and applications*, 9:1–11, 2017.

[12] Jeffrey Ichnowski, Yahav Avigal, Vishal Satish, and Ken Goldberg. Deep learning can accelerate grasp-optimized motion planning. *Science Robotics*, 5(48):eabd7710, 2020.

[13] Jun-Young Lee, Jaemin Eom, Sung Yol Yu, and Kyujin Cho. Customization methodology for conformable grasping posture of soft grippers by stiffness patterning. *Frontiers in Robotics and AI*, 7:114, 2020.

[14] Zhongkui Wang, Ryo Kanegae, and Shinichi Hirai. Circular shell gripper for handling food products. *Soft robotics*, 8(5):542–554, 2021.

[15] Woongbae Kim, Junghwan Byun, Jae-Kyeong Kim, Woo-Young Choi, Kirsten Jakobsen, Joachim Jakobsen, Dae-Young Lee, and Kyu-Jin Cho. Bioinspired dual-morphing stretchable origami. *Science robotics*, 4(36):eaay3493, 2019.

[16] Zhenishbek Zhakypov, Florian Heremans, Aude Billard, and Jamie Paik. An origami-inspired reconfigurable suction gripper for picking objects with variable shape and size. *IEEE Robotics and Automation Letters*, 3(4):2894–2901, 2018.

[17] Clark B Teeple, Theodore N Koutros, Moritz A Graule, and Robert J Wood. Multi-segment soft robotic fingers enable robust precision grasping. *The International Journal of Robotics Research*, 39(14):1647–1667, 2020.

[18] Thierry Laliberte, Lionel Birglen, and Clement Gosselin. Underactuation in robotic grasping hands. *Machine Intelligence & Robotic Control*, 4(3):1–11, 2002.

[19] Yong-Jae Kim, Hansol Song, and Chan-Young Maeng. Blt gripper: An adaptive gripper with active transition capability between precise pinch and compliant grasp. *IEEE Robotics and Automation Letters*, 5(4):5518–5525, 2020.

[20] Zeyu Lu, Haotian Guo, Wensi Zhang, and Haoyong Yu. Gtac-gripper: A

reconfigurable under-actuated four-fingered robotic gripper with tactile sensing. *IEEE Robotics and Automation Letters*, 7(3):7232–7239, 2022.

[21] Matteo Laffranchi, Nicolo Boccardo, Simone Traverso, Lorenzo Lombardi, Michele Canepa, Andrea Lince, Marianna Semprini, Jody A Saglia, Abdeldjallil Naceri, Rinaldo Sacchetti, et al. The hannes hand prosthesis replicates the key biological properties of the human hand. *Science robotics*, 5(46):eabb0467, 2020.

[22] Lionel Birglen, Thierry Laliberté, and Clément M Gosselin. *Underactuated robotic hands*, volume 40. Springer, 2007.

[23] Yu Sun, Eliza Amatova, and Tianze Chen. Multi-object grasping-types and taxonomy. In *2022 International Conference on Robotics and Automation (ICRA)*, pages 777–783. IEEE, 2022.

[24] Werner Friedl. Evaluation of different robotic grippers for simultaneous multi-object grasping. *Frontiers in Robotics and AI*, 11:1351932, 2024.

[25] Chengjun Wang, Changhong Linghu, Shuang Nie, Chenglong Li, Qianjin Lei, Xiang Tao, Yinjia Zeng, Yipu Du, Shun Zhang, Kaixin Yu, et al. Programmable and scalable transfer printing with high reliability and efficiency for flexible inorganic electronics. *Science advances*, 6(25):eabb2393, 2020.

[26] John R Amend, Eric Brown, Nicholas Rodenberg, Heinrich M Jaeger, and Hod Lipson. A positive pressure universal gripper based on the

jamming of granular material. *IEEE transactions on robotics*, 28(2):341–350, 2012.

[27] Wai Tuck Chow et al. Wiring-claw gripper for soft-stable picking up multiple objects. *IEEE Robotics and Automation Letters*, 2023.

[28] Adheesh Shenoy, Tianze Chen, and Yu Sun. Multi-object grasping-efficient robotic picking and transferring policy for batch picking. In *2022 IEEE/RSJ International Conference on Intelligent Robots and Systems (IROS)*, pages 2741–2747. IEEE, 2022.

[29] Wisdom C Agboh, Jeffrey Ichnowski, Ken Goldberg, and Mehmet R Dogar. Multi-object grasping in the plane. In *The International Symposium of Robotics Research*, pages 222–238. Springer, 2022.

[30] Yuyang Li, Bo Liu, Yiran Geng, Puhao Li, Yaodong Yang, Yixin Zhu, Tengyu Liu, and Siyuan Huang. Grasp multiple objects with one hand. *IEEE Robotics and Automation Letters*, 2024.

[31] Wisdom C Agboh, Satvik Sharma, Kishore Srinivas, Mallika Parulekar, Gaurav Datta, Tianshuang Qiu, Jeffrey Ichnowski, Eugen Solowjow, Mehmet Dogar, and Ken Goldberg. Learning to efficiently plan robust frictional multi-object grasps. In *2023 IEEE/RSJ International Conference on Intelligent Robots and Systems (IROS)*, pages 10660–10667. IEEE, 2023.

[32] Caio Mucchiani and Mark Yim. A novel underactuated end-effector for planar sequential grasping of multiple objects. In *2020 IEEE Inter-*

national Conference on Robotics and Automation (ICRA), pages 8935–8941. IEEE, 2020.

[33] Haili Li, Xingzhi Li, Bo Wang, Xiaoyang Shang, and Jiantao Yao. A fault-tolerant soft swallowing robot capable of grasping delicate structures underwater. *IEEE Robotics and Automation Letters*, 2023.

[34] Dongbao Sui, Yanhe Zhu, Sikai Zhao, Tianshuo Wang, Sunil K Agrawal, He Zhang, and Jie Zhao. A bioinspired soft swallowing gripper for universal adaptable grasping. *Soft robotics*, 9(1):36–56, 2022.

[35] Kishore Srinivas, Shreya Ganti, Rishi Parikh, Ayah Ahmad, Wisdom Agboh, Mehmet Dogar, and Ken Goldberg. The busboy problem: Efficient tableware decluttering using consolidation and multi-object grasps. In *2023 IEEE 19th International Conference on Automation Science and Engineering (CASE)*, pages 1–6. IEEE, 2023.

[36] Zihe Ye and Yu Sun. Only pick once–multi-object picking algorithms for picking exact number of objects efficiently. *arXiv preprint arXiv:2307.02662*, 2023.

[37] Shrey Aeron, Edith LLontop, Aviv Adler, Wisdom C Agboh, Mehmet Dogar, and Ken Goldberg. Push-mog: Efficient pushing to consolidate polygonal objects for multi-object grasping. In *2023 IEEE 19th International Conference on Automation Science and Engineering (CASE)*, pages 1–6. IEEE, 2023.

[38] Yuwen Zhao, Jie Zhang, Siyuan Zhang, Peng Zhang, Guixin Dong, Jian-

ing Wu, and Jinxiu Zhang. Transporting dispersed cylindrical granules: An intelligent strategy inspired by an elephant trunk. *Advanced Intelligent Systems*, 5(10):2300182, 2023.

[39] Yiting Chen, Xiao Gao, Kunpeng Yao, Loïc Niederhauser, Yasemin Bekiroglu, and Aude Billard. Differentiable robot neural distance function for adaptive grasp synthesis on a unified robotic arm-hand system. *arXiv preprint arXiv:2309.16085*, 2023.

[40] Kunpeng Yao and Aude Billard. Exploiting kinematic redundancy for robotic grasping of multiple objects. *IEEE Transactions on Robotics*, 2023.

[41] Pho Van Nguyen, Dhyan Bohra Sunil, and Wai Tuck Chow. Soft-stable interface in grasping multiple objects by wiring-tension. *Scientific Reports*, 13(1):21537, 2023.

[42] Takumi Sakamoto, Weiwei Wan, Takao Nishi, and Kensuke Harada. Efficient picking by considering simultaneous two-object grasping. In *2021 IEEE/RSJ International Conference on Intelligent Robots and Systems (IROS)*, pages 8295–8300. IEEE, 2021.

[43] Tianze Chen and Yu Sun. Multi-object grasping–experience forest for robotic finger movement strategies. *IEEE Robotics and Automation Letters*, 2024.

[44] Francis Tsow, Tianze Chen, and Yu Sun. Counting objects in a robotic hand. *arXiv preprint arXiv:2404.06631*, 2024.

[45] Makoto Kaneko and Kensuke Harada. Grasp and manipulation of multiple objects. In *Robotics Research: The Ninth International Symposium*, pages 33–39. Springer, 2000.

[46] Kensuke Harada, Makoto Kaneko, and T Tsujii. Rolling-based manipulation for multiple objects. *IEEE Transactions on robotics and automation*, 16(5):457–468, 2000.

[47] Takayoshi Yamada, Manabu Yamada, and Hidehiko Yamamoto. Stability analysis of multiple objects grasped by multifingered hands with revolute joints in 2d. In *2012 IEEE International Conference on Mechatronics and Automation*, pages 1785–1792. IEEE, 2012.

[48] Charlotte E Exner. In-hand manipulation skills. *Development of hand skills in the child*, pages 35–45, 1992.

[49] Karina Pont, Margaret Wallen, and Anita Bundy. Conceptualising a modified system for classification of in-hand manipulation. *Australian occupational therapy journal*, 56(1):2–15, 2009.

[50] Marieta Visser, Mariette Nel, Carla du Plessis, Shame Jacobs, Amor Joubert, Martli Muller, Bianco Smith, Tania van Heerden, and Renette van Soest. In-hand manipulation (ihm) in children 6 and 7 years of age: a follow-up study. *South African Journal of Occupational Therapy*, 46(2):52–58, 2016.

[51] Hanna Yousef, Mehdi Boukallel, and Kaspar Althoefer. Tactile sensing

for dexterous in-hand manipulation in robotics—a review. *Sensors and Actuators A: physical*, 167(2):171–187, 2011.

[52] CE Exner. Evaluation and interventions to develop hand skills. *Occupational therapy for children*, 6:275–324, 2010.

[53] II Charles Long, PW Conrad, EA Hall, and SL Furler. Intrinsic-extrinsic muscle control of the hand in power grip and precision handling: an electromyographic study. *JBJS*, 52(5):853–867, 1970.

[54] Cosimo Della Santina, Giorgio Grioli, Manuel Catalano, Alberto Brando, and Antonio Bicchi. Dexterity augmentation on a synergistic hand: The pisa/iit softhand+. In *2015 IEEE-RAS 15th International Conference on Humanoid Robots (Humanoids)*, pages 497–503. IEEE, 2015.

[55] Cosimo Della Santina, Cristina Piazza, Giorgio Grioli, Manuel G Catalano, and Antonio Bicchi. Toward dexterous manipulation with augmented adaptive synergies: The pisa/iit softhand 2. *IEEE Transactions on Robotics*, 34(5):1141–1156, 2018.

[56] Manuel G Catalano, Giorgio Grioli, Edoardo Farnioli, Alessandro Serio, Cristina Piazza, and Antonio Bicchi. Adaptive synergies for the design and control of the pisa/iit softhand. *The International Journal of Robotics Research*, 33(5):768–782, 2014.

[57] Aaron M Dollar and Robert D Howe. Simple, robust autonomous grasping in unstructured environments. In *Proceedings 2007 IEEE Interna-*

tional Conference on Robotics and Automation, pages 4693–4700. IEEE, 2007.

[58] Lael U Odhner and Aaron M Dollar. Stable, open-loop precision manipulation with underactuated hands. *The International Journal of Robotics Research*, 34(11):1347–1360, 2015.

[59] Raymond Ma and Aaron Dollar. Yale openhand project: Optimizing open-source hand designs for ease of fabrication and adoption. *IEEE Robotics & Automation Magazine*, 24(1):32–40, 2017.

[60] Minas Liarokapis and Aaron M Dollar. Deriving dexterous, in-hand manipulation primitives for adaptive robot hands. In *2017 IEEE/RSJ International Conference on Intelligent Robots and Systems (IROS)*, pages 1951–1958. IEEE, 2017.

[61] Irfan Hussain, Federico Renda, Zubair Iqbal, Monica Malvezzi, Gionata Salvietti, Lakmal Seneviratne, Dongming Gan, and Domenico Prattichizzo. Modeling and prototyping of an underactuated gripper exploiting joint compliance and modularity. *IEEE Robotics and automation letters*, 3(4):2854–2861, 2018.

[62] Aaron M Dollar and Robert D Howe. Joint coupling design of underactuated grippers. In *International Design Engineering Technical Conferences and Computers and Information in Engineering Conference*, volume 42568, pages 903–911, 2006.

[63] Gwang-Pil Jung, Je-Sung Koh, and Kyu-Jin Cho. Underactuated adap-

tive gripper using flexural buckling. *IEEE Transactions on Robotics*, 29(6):1396–1407, 2013.

[64] Mathieu Baril, Thierry Laliberté, Clément Gosselin, and François Routhier. On the design of a mechanically programmable underactuated anthropomorphic prosthetic gripper. *Journal of Mechanical Design*, 135(12):121008, 2013.

[65] Yedige Tlegenov, Kuat Telegenov, and Almas Shintemirov. An open-source 3d printed underactuated robotic gripper. In *2014 IEEE/ASME 10th International Conference on Mechatronic and Embedded Systems and Applications (MESA)*, pages 1–6. IEEE, 2014.

[66] Bin Gao, Shuai Yang, Haiyang Jin, Ying Hu, Xiaojun Yang, and Jianwei Zhang. Design and analysis of underactuated robotic gripper with adaptive fingers for objects grasping tasks. In *2016 IEEE International Conference on Robotics and Biomimetics (ROBIO)*, pages 987–992. IEEE, 2016.

[67] Toshihiro Nishimura, Kaori Mizushima, Yosuke Suzuki, Tokuo Tsuji, and Tetsuyou Watanabe. Variable-grasping-mode underactuated soft gripper with environmental contact-based operation. *IEEE Robotics and Automation Letters*, 2(2):1164–1171, 2017.

[68] Amir Firouzeh and Jamie Paik. Grasp mode and compliance control of an underactuated origami gripper using adjustable stiffness joints. *Ieee/asme Transactions on Mechatronics*, 22(5):2165–2173, 2017.

[69] Jihao Li, Tingbo Liao, Hassen Nigatu, Haotian Guo, Guodong Lu, and Huixu Dong. Under-actuated robotic gripper with multiple grasping modes inspired by human finger. *arXiv preprint arXiv:2403.12502*, 2024.

[70] Matei Ciocarlie, Fernando Mier Hicks, and Scott Stanford. Kinetic and dimensional optimization for a tendon-driven gripper. In *2013 IEEE International Conference on Robotics and Automation*, pages 2751–2758. IEEE, 2013.

[71] Matei Ciocarlie, Fernando Mier Hicks, Robert Holmberg, Jeffrey Hawke, Michael Schlicht, Jeff Gee, Scott Stanford, and Ryan Bahadur. The velo gripper: A versatile single-actuator design for enveloping, parallel and fingertip grasps. *The International Journal of Robotics Research*, 33(5):753–767, 2014.

[72] Amir Firouzeh and Jamie Paik. An under-actuated origami gripper with adjustable stiffness joints for multiple grasp modes. *Smart Materials and Structures*, 26(5):055035, 2017.

[73] Long Kang, Jong-Tae Seo, Sang-Hwa Kim, Wan-Ju Kim, and Byung-Ju Yi. Design and implementation of a multi-function gripper for grasping general objects. *Applied Sciences*, 9(24):5266, 2019.

[74] Si-Hwan Heo, Cheolgyu Kim, Taek-Soo Kim, and Hyung-Soon Park. Human-palm-inspired artificial skin material enhances operational functionality of hand manipulation. *Advanced Functional Materials*, 30(25):2002360, 2020.

[75] Clark B Teeple, Buse Aktaş, Michelle C Yuen, Grace R Kim, Robert D Howe, and Robert J Wood. Controlling palm-object interactions via friction for enhanced in-hand manipulation. *IEEE Robotics and Automation Letters*, 7(2):2258–2265, 2022.

[76] Yunquan Li, Ren Tao, Yingtian Li, Yang Yang, Jianshu Zhou, and Yonghua Chen. A highly adaptive robotic gripper palm with tactile sensing. In *2022 IEEE International Conference on Real-time Computing and Robotics (RCAR)*, pages 130–135. IEEE, 2022.

[77] Maria Pozzi, Monica Malvezzi, Domenico Prattichizzo, and Gionata Salvietti. Actuated palms for soft robotic hands: Review and perspectives. *IEEE/ASME Transactions on Mechatronics*, 2023.

[78] Jeongwon Lee, Jaehee Kim, Sungwoo Park, Donghyun Hwang, and Sungwook Yang. Soft robotic palm with tunable stiffness using dual-layered particle jamming mechanism. *IEEE/ASME Transactions on Mechatronics*, 26(4):1820–1827, 2021.

[79] Aaron M Dollar and Robert D Howe. The highly adaptive sdm hand: Design and performance evaluation. *The international journal of robotics research*, 29(5):585–597, 2010.

[80] Raymond R Ma, Lael U Odhner, and Aaron M Dollar. A modular, open-source 3d printed underactuated hand. In *2013 IEEE International Conference on Robotics and Automation*, pages 2737–2743. IEEE, 2013.

[81] Aaron M Dollar and Robert D Howe. Simple, robust autonomous grasp-

ing in unstructured environments. In *Proceedings 2007 IEEE International Conference on Robotics and Automation*, pages 4693–4700. IEEE, 2007.

[82] Ryuta Ozawa, Hiroaki Kobayashi, and Kazunori Hashirii. Analysis, classification, and design of tendon-driven mechanisms. *IEEE transactions on robotics*, 30(2):396–410, 2013.

[83] Divya Shah, Alberto Parmiggiani, and Yong-Jae Kim. Constant length tendon routing mechanism through axial joint. In *2020 IEEE/ASME International Conference on Advanced Intelligent Mechatronics (AIM)*, pages 753–758. IEEE, 2020.

[84] Shigeo Hirose and Shugen Ma. Coupled tendon-driven multijoint manipulator. In *Proceedings. 1991 IEEE International Conference on Robotics and Automation*, pages 1268–1269. IEEE Computer Society, 1991.

[85] Yong-Jae Kim, Younbaek Lee, Jiyoung Kim, Ja-Woo Lee, Kang-Min Park, Kyung-Sik Roh, and Jung-Yun Choi. Roboray hand: A highly backdrivable robotic hand with sensorless contact force measurements. In *2014 IEEE International Conference on Robotics and Automation (ICRA)*, pages 6712–6718. IEEE, 2014.

[86] Muhammad E Abdallah, Robert Platt Jr, and Charles W Wampler. Decoupled torque control of tendon-driven fingers with tension management. *The International Journal of Robotics Research*, 32(2):247–258, 2013.

[87] Zhihao Liang, Bin Wang, Yaowei Song, Tao Zhang, Chaoqun Xiang, and Yisheng Guan. Design of a novel cable-driven 3-dof series-parallel wrist module for humanoid arms. In *2021 IEEE International Conference on Mechatronics and Automation (ICMA)*, pages 709–714. IEEE, 2021.

[88] Zhihao Liang, Yisheng Guan, Chaoqun Xiang, and Yaowei Song. Design and modeling of a novel cable-driven elbow joint module for humanoid arms. In *2021 IEEE International Conference on Robotics and Biomimetics (ROBIO)*, pages 1264–1269. IEEE, 2021.

[89] Xiongdun Xie, Dezhu Xiong, and James Zhiqing Wen. A wrist-inspired suspended tubercle-type tensegrity joint with variable stiffness capacity. *Bioinspiration & Biomimetics*, 18(1):016010, 2022.

[90] Yong-Jae Kim. Anthropomorphic low-inertia high-stiffness manipulator for high-speed safe interaction. *IEEE Transactions on robotics*, 33(6):1358–1374, 2017.

[91] Qiujie Lu, Nicholas Baron, Angus B Clark, and Nicolas Rojas. Systematic object-invariant in-hand manipulation via reconfigurable underactuation: Introducing the ruth gripper. *The International Journal of Robotics Research*, 40(12-14):1402–1418, 2021.

[92] Yilin Cai and Shenli Yuan. In-hand manipulation in power grasp: Design of an adaptive robot hand with active surfaces. In *2023 IEEE International Conference on Robotics and Automation (ICRA)*, pages 10296–10302. IEEE, 2023.

[93] Vinicio Tincani, Manuel G Catalano, Edoardo Farnioli, Manolo Garabini, Giorgio Grioli, Gualtiero Fantoni, and Antonio Bicchi. Velvet fingers: A dexterous gripper with active surfaces. In *2012 IEEE/RSJ International Conference on Intelligent Robots and Systems*, pages 1257–1263. IEEE, 2012.

[94] Shenli Yuan, Austin D Epps, Jerome B Nowak, and J Kenneth Salisbury. Design of a roller-based dexterous hand for object grasping and within-hand manipulation. In *2020 IEEE International Conference on Robotics and Automation (ICRA)*, pages 8870–8876. IEEE, 2020.

[95] Shenli Yuan, Lin Shao, Connor L Yako, Alex Gruebele, and J Kenneth Salisbury. Design and control of roller grasper v2 for in-hand manipulation. in 2020 ieee. In *RSJ International Conference on Intelligent Robots and Systems (IROS)*, pages 9151–9158. IEEE, 2020.

[96] James M Gere. Mechanics of materials, thomson learning. *Inc. http://dx. doi. org/10.1007/978-1-4899-3124-5*, 2004.

[97] Zherong Pan, Andy Zeng, Yunzhu Li, Jingjin Yu, and Kris Hauser. Algorithms and systems for manipulating multiple objects. *IEEE Transactions on Robotics*, 39(1):2–20, 2022.

[98] Jinhwi Lee, Younggil Cho, Changjoo Nam, Jonghyeon Park, and Changhwan Kim. Efficient obstacle rearrangement for object manipulation tasks in cluttered environments. In *2019 International Conference on Robotics and Automation (ICRA)*, pages 183–189. IEEE, 2019.

[99] Jochen Stüber, Claudio Zito, and Rustam Stolkin. Let's push things forward: A survey on robot pushing. *Frontiers in Robotics and AI*, 7:8, 2020.

[100] Sarah Elliott and Maya Cakmak. Robotic cleaning through dirt rearrangement planning with learned transition models. In *2018 IEEE international conference on robotics and automation (ICRA)*, pages 1623–1630. IEEE, 2018.

[101] Ajay Kumar Tanwani, Nitesh Mor, John Kubiatowicz, Joseph E Gonzalez, and Ken Goldberg. A fog robotics approach to deep robot learning: Application to object recognition and grasp planning in surface decluttering. In *2019 international conference on robotics and automation (ICRA)*, pages 4559–4566. IEEE, 2019.

[102] Athanasios Krontiris and Kostas E Bekris. Dealing with difficult instances of object rearrangement. In *Robotics: Science and Systems*, volume 1123, 2015.

[103] Dhruv Batra, Angel X Chang, Sonia Chernova, Andrew J Davison, Jia Deng, Vladlen Koltun, Sergey Levine, Jitendra Malik, Igor Mordatch, Roozbeh Mottaghi, et al. Rearrangement: A challenge for embodied ai. *arXiv preprint arXiv:2011.01975*, 2020.

[104] Haoran Song, Joshua A Haustein, Weihao Yuan, Kaiyu Hang, Michael Yu Wang, Danica Kragic, and Johannes A Stork. Multi-object rearrangement with monte carlo tree search: A case study on planar

nonprehensile sorting. In *2020 IEEE/RSJ international conference on intelligent robots and systems (IROS)*, pages 9433–9440. IEEE, 2020.

[105] Shuai D Han, Nicholas M Stiffler, Kostas E Bekris, and Jingjin Yu. Efficient, high-quality stack rearrangement. *IEEE Robotics and Automation Letters*, 3(3):1608–1615, 2018.

[106] Paraskevi Th Zacharia, Elias K Xidias, and Nikos A Aspragathos. Task scheduling and motion planning for an industrial manipulator. *Robotics and computer-integrated manufacturing*, 29(6):449–462, 2013.

[107] Christian Wurll and Dominik Henrich. Point-to-point and multi-goal path planning for industrial robots. *Journal of Robotic Systems*, 18(8):445–461, 2001.

[108] P Th Zacharia and NA Aspragathos. Optimal robot task scheduling based on genetic algorithms. *Robotics and Computer-Integrated Manufacturing*, 21(1):67–79, 2005.

[109] Mitul Saha, Tim Roughgarden, Jean-Claude Latombe, and Gildardo Sánchez-Ante. Planning tours of robotic arms among partitioned goals. *The International Journal of Robotics Research*, 25(3):207–223, 2006.

Appendix A

Experiments for Analyzing Material Properties

To calculate the stroke margin of the tendon-driven system during repeated grasping, as discussed in Chapter 3.2.2, a cyclic loading test was conducted. Two types of tendons were used in the study: Dyneema (SAPA) size 2 and size 4. Tendons 3 and 4 were Dyneema size 2, while tendons 1 and 2 were Dyneema size 4. Since the process of grasping and placing objects involves applying and releasing loads on the tendons, cyclic loading tests are suitable for measuring the permanent deformation of tendons during repeated grasping.

Thus, a cyclic loading test was conducted 5,000 times for each tendon, and the experimental setup is shown in Fig. A.1. The load conditions for each tendon were identical to those used in the cyclic pulling test conducted in Chapter 3.2.2. One end of the tendon was fixed to a load cell (KTOYO 333FDX), while the other end was fixed to the ground. The load cell was connected to a linear guide and slider and moved using a linear motor (Actuonix P16-150-256-12-P).

The cyclic loading test consisted of two steps. First, the tendon was pulled using the linear motor, and when the tension value measured by the load cell reached the target load condition, the motor paused at that position for 1 second. Next, the linear motor pushed the tendon back to its initial position and pauses for 1 second. This process was repeated 5,000 times to conduct the cyclic loading test for each tendon. The gripper's tendon actuation system consisted of four tendons, each subjected to different loads. When the motor was current controlled at 220 mA, the tension applied to tendon 1 was 2.9 kgf, tendon 2 experienced 1.45 kgf, and tendons 3 and 4 were subjected to 0.725 kgf. The experiment was conducted under these load conditions to ensure realistic and accurate results.

The results of the experiment are shown in Fig. A.2. Fig. A.2A presents the results of the cyclic loading test for Dyneema size 4 under a load of 2.9 kgf. It was observed that the elongation converged as the number of cycles increased from the first to the 5000th cycle. Fig. A.2B illustrates the deformation ratios of the tendons over 5,000 cycles. In all cases, the deformation rate of the tendons increased initially and then converged, with the converged values varying depending on the type of tendon and the magnitude of the load. For tendon 1, under a 2.9 kgf load, the permanent deformation converged to 7.56% after 5,000 cycles (blue line in Fig. A.2A). This indicates that repeatedly applying and releasing a 2.9 kgf load to Dyneema size 4 increases the initial length of the tendon, which converges at 7.56% deformation. Similarly, for tendon 2, under a load of 1.45 kgf, the deformation converged to 3.45% (red line in Fig.

A.2A), and for tendons 3 and 4, under a load of 0.725 kgf, the deformation converged to 4.54% (green line in Fig. A.2A).

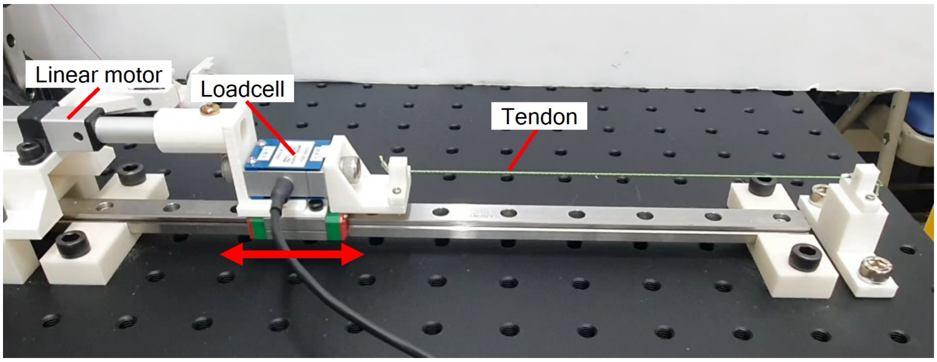

Figure A.1. Experimental setting for cyclic loading test of tendon.

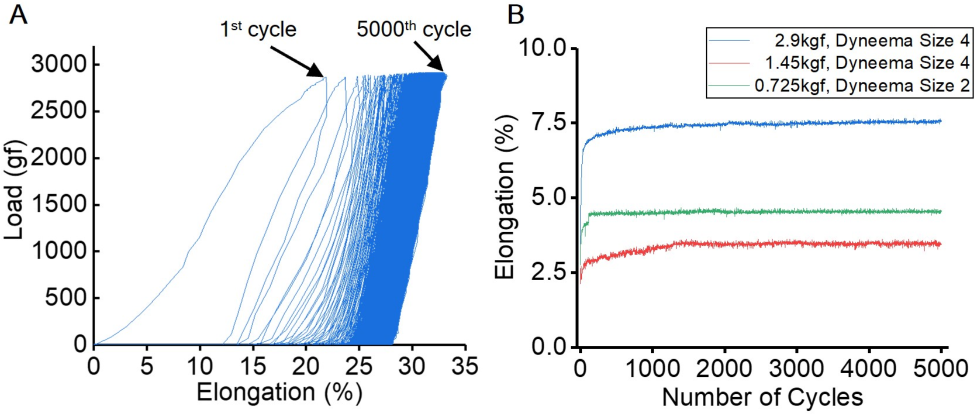

Figure A.2. Cyclic loading test results of tendon. (**A**) The results of the cyclic loading test for Dyneema size 4 under a load of 2.9 kgf. (**B**) The degree of permanent deformation of each tendon based on the number of cycles.

To interpret the results of the storing force measurements based on the material parameter variations of the conveyor palm, the 100% modulus of the materials used was measured. The tested materials were DragonSkin 30, Smooth-Sil 950, and Smooth-Sil 960. The experiment followed ASTM D412, the standard test method for determining the mechanical properties of elastomers. Specimens corresponding to Type C of ASTM D412 were prepared (Fig. A.3A). The colors of the specimens were transparent for DragonSkin 30, blue for Smooth-Sil 950, and green for Smooth-Sil 960. All specimens had a uniform thickness of 2 mm.

The experimental setup is illustrated in Figure A.3B. One end of the prepared specimen was fixed to a load cell, while the other end was anchored to the ground. The specimen was stretched using a linear motor, and the pulling force was measured according to the elongation of the specimen. The initial gauge length of the specimen was 33 mm, and since the goal of the experiment was to measure the 100% modulus, the specimen was stretched to a gauge length of 66 mm and then released. This process was repeated five times to measure the average pulling force. Prior to the experiment, the specimen was preconditioned by stretching it to 100% strain five times.

The experimental results are shown in Figure A.3C to E. Figure A.3C shows the stress-strain curve for DragonSkin 30, Figure A.3D for Smooth-Sil 950, and Figure A.3E for Smooth-Sil 960. All five repeated test data are included in the figures. The results show slight hyperelasticity and hysteresis, but these were considered negligible within the 100% strain range. Accordingly, the modulus was calculated by assuming the stress-strain curve to be linear.

The calculated 100% moduli were as follows: DragonSkin 30 had a modulus of 0.48 MPa, Smooth-Sil 950 had a modulus of 1.37 MPa, and Smooth-Sil 960 had a modulus of 2.02 MPa.

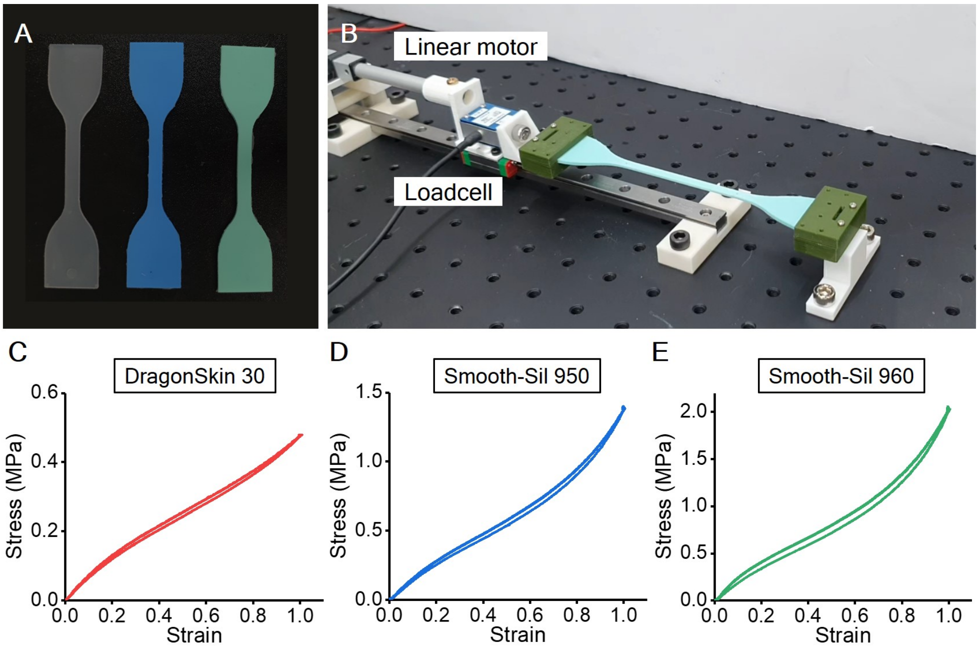

Figure A.3. Measurement of 100% modulus for DragonSkin 30, Smooth-Sil 950, and Smooth-Sil 960. (**A**) Specimens prepared according to ASTM D412 Type C standards. (**B**) Experimental setup for modulus measurement. (**C to E**) Stress-strain curves for (C) DragonSkin 30, (D) Smooth-Sil 950, and (E) Smooth-Sil 960.

To analyze the results of the conveyor palm storing force measurements based on material parameter variations, the static friction coefficients of the corresponding materials were also measured. The tested materials were DragonSkin 30, Smooth-Sil 950, and Smooth-Sil 960. For the friction measurement experiment, flat square plates were fabricated using each material, with a thickness of 3 mm and dimensions of 50 mm × 50 mm (Fig. A.4A).

The experimental setup is illustrated in Figures A.4B and A.4C. A flat tray made of the same material as the cylindrical objects used in the storing force experiments was placed on top of the square elastomer plates. Weight blocks were then added on the tray to vary the normal force between the tray and elastomer plate for measuring the friction force.

The results are shown in Figures A.4D to A.4F. Figure A.4D shows the friction measurement results for DragonSkin 30, Figure A.4E for Smooth-Sil 950, and Figure A.4F for Smooth-Sil 960. The pulling force was measured proportionally to the applied normal force, and the gradient of the graph was calculated as the static friction coefficient. The calculated static friction coefficients were 1.10 for DragonSkin 30, 0.51 for Smooth-Sil 950, and 0.49 for Smooth-Sil 960.

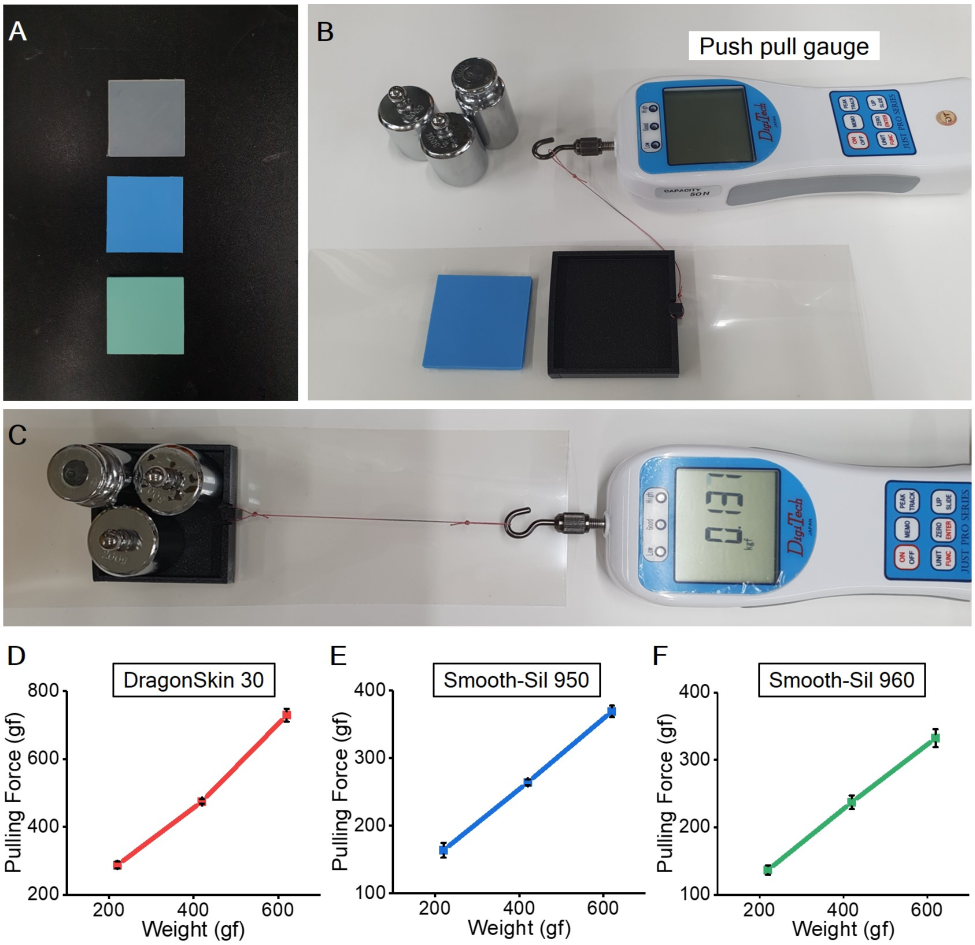

Figure A.4. Measurement of static frictional coefficients for DragonSkin 30, Smooth-Sil 950, and Smooth-Sil 960. (**A**) Prepared specimens. (**B to C**) Experimental setup for measuring the static frictional coefficients for each material. (**D to F**) Graphs of friction force versus normal force for (D) DragonSkin 30, (E) Smooth-Sil 950, and (F) Smooth-Sil 960.

Appendix B

Another Fabrication Method: 3D Printed Conveyor Palm

The original molding method for the conveyor palm allowed the use of highly flexible materials (e.g., DragonSkin 30, Smooth-On. Inc), but it had the drawback of requiring mold redesigns whenever the conveyor palm design was changed. To address this limitation, a fabrication method using a 3D printer (PRUSA MK3S+) was introduced (Fig. B.1). The conveyor palm was produced via FDM 3D printing with TPU 95A material. As shown in Fig. B.1A, due to the limitations of FDM printing, two hairs are connected during the printing process, resulting in the conveyor palm seen in Fig. B.1B. By everting this structure, the final conveyor palm is obtained, as shown in Fig. B.1C. This 3D-printed conveyor palm, like the one fabricated through molding, retains the ability to store and translate multiple objects simultaneously (Fig. B.1D).

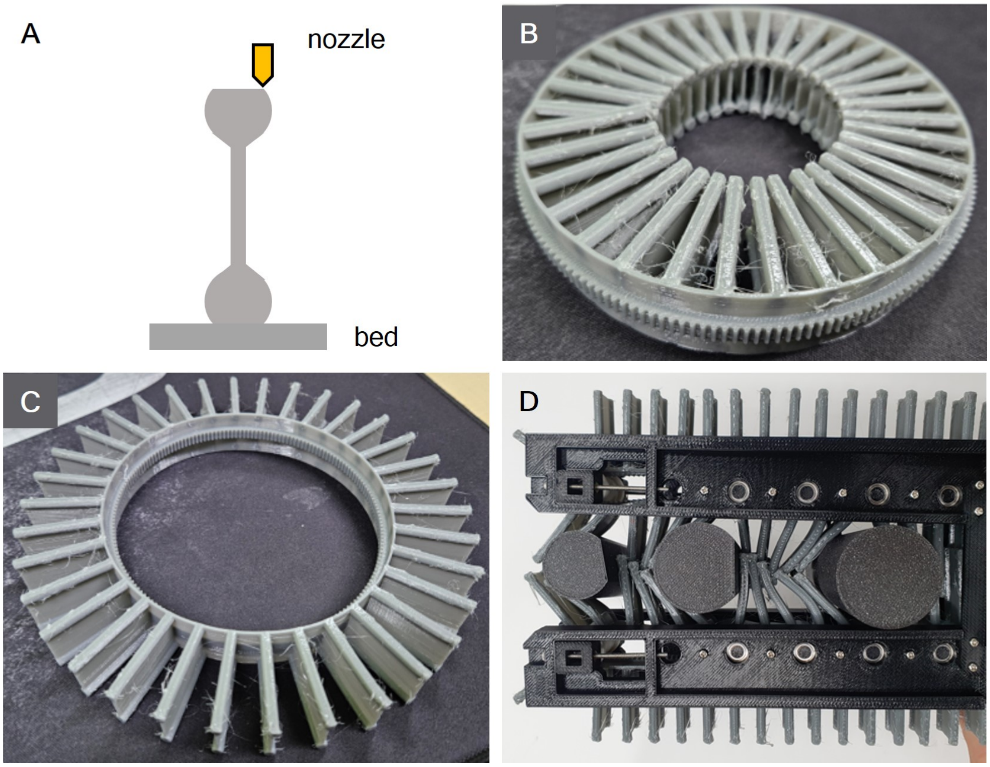

Figure B.1. 3D printed conveyor palm. (**A**) Cross-sectional view of the conveyor palm during the printing process. (**B**). The conveyor palm immediately after printing. (**C**) The printed conveyor palm can be everted for use. (**D**) Feasibility of storing multiple objects.

Appendix C

Methods for Storing Objects More Greedily

In this chapter, methods for storing objects more greedily compared to the conventional approach in Chapter 4.2.2 will be discussed. First, a method utilizing the "tolerable storing distance," which is the minimum distance required for storing objects between others, is introduced.

The conventional storage method involves determining the storage distance between objects to ensure that stored objects do not interfere with the storage of other objects. This distance is defined as the "non-interfering storing distance" and can be calculated using the occupied space of each object listed in Table 4.3. For example, the non-interfering storing distance between the i^{th} stored object and the $(i+1)^{\text{th}}$ stored object can be calculated as follows:

$$d_{\text{non-inter}}^{(i,i+1)} = d_{\text{down}}^{i} + d_{\text{up}}^{(i+1)} \tag{C.1}$$

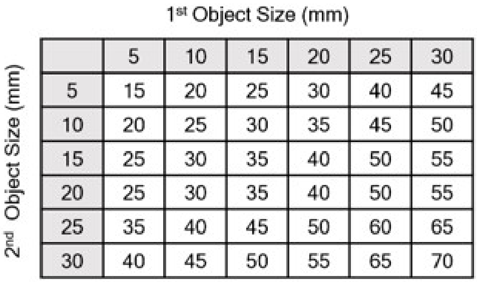

		1st Object Size (mm)					
		5	10	15	20	25	30
2nd Object Size (mm)	5	15	20	25	30	40	45
	10	20	25	30	35	45	50
	15	25	30	35	40	50	55
	20	25	30	35	40	50	55
	25	35	40	45	50	60	65
	30	40	45	50	55	65	70

Figure C.1. Non-interfering storing distance between two objects: The minimum distance that allows objects to be stored without interfering with each other's storage.

The value of $d_{\text{non-inter}}$ varies depending on the diameters of the previously stored object and the subsequently stored object. Using the occupied space and Equation C.1, the calculated $d_{\text{non-inter}}$ is illustrated in Figure C.1.

The tolerable storing distance (d_{toler}) also varies with the diameters of the previously stored and next objects, and it should be determined experimentally. The experimental setup and method are shown in Figure C.2. Initially, the first object was stored, and then the second object was stored while gradually increasing the number of hairs located at the bottom of the first object from 2. As a result, the number of hairs between two objects required for the second object to achieve a 100% storage success rate was measured. The reason for setting the minimum number of hairs to 2 is that at least two hairs are required to store a single object. The gripper's grasping force was assumed to be 200 gf. To apply this condition during the experiment, an external force of 200 gf was added using a weight block to assist in storing the second object. Consistent with the previous occupied space experiments, the diameter varia-

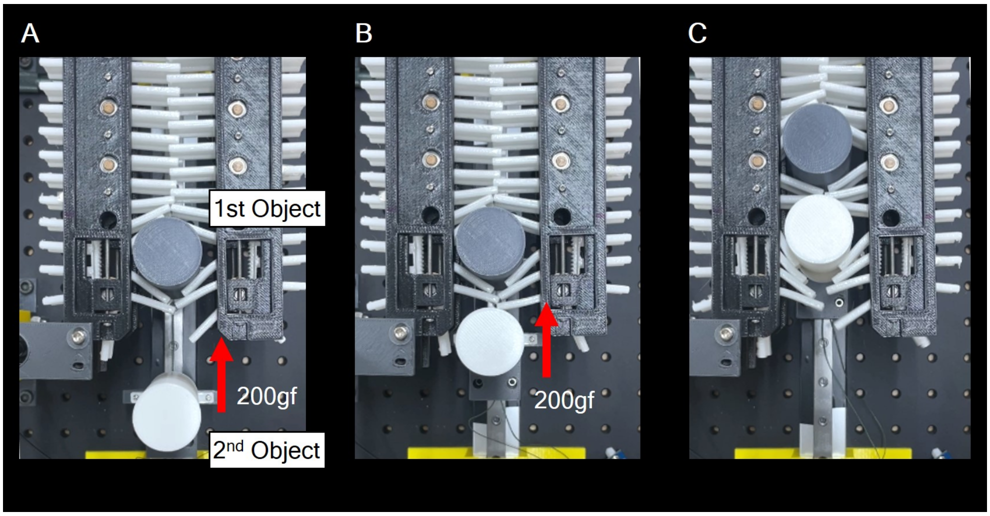

Figure C.2. Experiment to determine the tolerable storing distance. **(A)** The first object is stored, and the number of hairs beneath the object is adjusted. **(B)** The second object is brought into contact with the conveyor palm under a force of 200 gf. **(C)** The conveyor palm is rotated to verify if the second object can be successfully stored.

tions of the stored objects were set from 5 mm to 30 mm in 5 mm increments. Experiments were conducted for all 36 pairs of diameters, with five trials for each pair. Storing failures occurred when the distance between objects was too small, causing the second object to be ejected.

The experimental results about the tolerable storing distance are shown in Figure C3, where the tolerable storing distance (d_{toler}) wwas observed to be smaller than the non-interfering storing distance ($d_{\text{non-inter}}$). This indicates that applying d_{toler} allows for a greedier storage approach compared to the conventional method. To verify whether the tolerable storing distance can be applied to the actual gripper's storing plan, additional experiments were

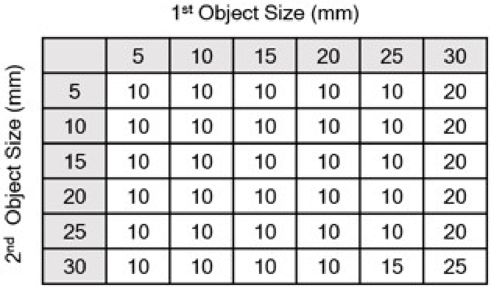

1st Object Size (mm)

2nd Object Size (mm)

	5	10	15	20	25	30
5	10	10	10	10	10	20
10	10	10	10	10	10	20
15	10	10	10	10	10	20
20	10	10	10	10	10	20
25	10	10	10	10	10	20
30	10	10	10	10	15	25

Figure C.3. Tolerable storing distance between two objects: The minimum distance at which two objects can be experimentally stored successfully, even if they interfere with each other's storage.

conducted for the most challenging case, where both objects have a diameter of 30 mm. First, it was confirmed that the gripper could successfully store two objects while satisfying d_{toler}. Next, the storing force of each object stored at d_{toler} was measured (Fig. C.4). The results confirmed that the storing force for each object was greater than the storing force observed when storing a single object. Therefore, objects that can be stored while satisfying $d_{\text{non-inter}}$ can also be stored more greedily by satisfying d_{toler}.

Although the applicability of the tolerable storing distance (d_{toler}) has been confirmed, there are significant challenges due to the increased number of experiments required to determine d_{toler}. For obtaining $d_{\text{non-inter}}$, it is sufficient to measure the occupied space of each object, requiring approximately [number of objects] × [5 repetitions] experiments. This approach offers the additional advantage of determining the optimal storage design for new sets of objects based solely on individual storage test results. In contrast, calculating d_{toler} involves considering all possible object pairs and gradually increasing the num-

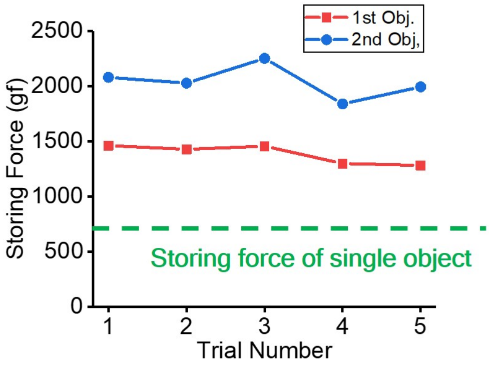

Figure C.4. Storing force measurements for each object when two objects are stored based on the tolerable storing distance. This result shows that they are stored with greater force compared to storing each object individually (green line).

ber of hairs beneath the first stored object during experiments. Therefore, a substantially larger number of experiments is required compared to those conducted for measuring $d_{\text{non-inter}}$.

Moreover, as the storing force changes compared to single-object storage, it becomes necessary to experimentally measure the storing force for each object stored at d_{toler} (Fig. C.4). Another issue is the inconsistency between tolerable storing distances for consecutive object pairs. For instance, the tolerable storing distance between the first and second objects may differ from that between the second and third objects due to differences in the configuration of hairs beneath the stored objects (Fig. C.5).

Thus, relying on d_{toler} as the basis for determining the storage design for new object sets is experimentally demanding. Instead, it is recommended to use occupied space to design the storage system for a set of objects and then

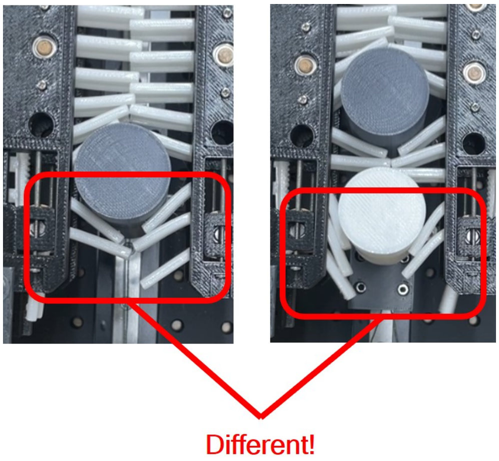

Figure C.5. The differences in the configuration of hairs beneath the first and second stored objects. The tolerable storing distance between the first and second objects may differ from that between the second and third objects due to differences in the configuration of hairs beneath the stored objects.

fine-tune the storing strategy using d_{toler}. However, since d_{toler} can result in increased storing forces, it may not be suitable for fragile objects, such as those used in food packaging. In such cases, higher storing forces could damage the objects, as the conveyor palm design would be based on single-object storing forces. Therefore, in applications dealing with fragile objects, it is better to adopt the non-greedy approach based on $d_{\text{non-inter}}$. In summary, the selection of storing distances should align with the nature of the object set and the specific task requirements.

Another greedy method for storing objects is to continuously rotate the conveyor palm after storing each object. With this approach, the first object is stored at the top of the conveyor palm, and the next object is stored directly below the first one, in contact with it. This method maximally utilizes the conveyor palm's storage capacity, as all objects are stacked by contacting each other.

For the conveyor palm to rotate infinitely while storing an object, it must be able to rotate even if the first stored object is stuck and remains stationary at the top of the palm. This situation is the exact opposite of the experimental situation for measuring longitudinal storing force (Fig. 3.15). Therefore, the total resistance force applied by the stuck object on the palm's hairs is equal to the longitudinal storing force, and the belt must rotate with a force stronger than this. If the stiffness of the hairs is too high, the motor requires excessive force to rotate. This can cause slippage during power transmission, preventing the conveyor palm from rotating. However, if the stiffness of the hairs is sufficiently small, the belt can rotate indefinitely, and this condition will be determined by the longitudinal storing force of the target objects.

손가락-손바닥 이동 동작 구현을 통해 다양한 파지 및 정렬 작업이 가능한 다물체 파지 그리퍼

서울대학교 대학원
기계공학부
엄 재 민

요 약

인간은 다양한 상황에서 여러 물체를 효율적으로 이동시키기 위해 여러 물체를 한 번에 파지해 옮기는 다양한 다물체 파지 전략을 사용하며, 이때 손가락의 높은 자유도와 손바닥의 적응성을 활용한다. 개별 물체의 파지와 정렬이 중요한 환경에서 인간은 물체를 하나씩 잡고 손바닥의 척골 측면에 임시로 저장한 후, 이 저장된 물체를 하나씩 꺼내 원하는 위치에 배치하는 전략을 채택한다. 즉, 이 방법은 손을 두 개의 기능적 구역으로 나눠 사용하는 방법으로, 손은 물체를 집고 놓는 작업을 담당하는 ‘파지 구역’과 임시로 물체를 저장하는 ‘저장 구역’으로 나뉜다. 파지 구역은 엄지를 포함한 검지 및 중지 손가락으로 구성되며, 저장 구역은 손바닥과 파지 구역에 속하지 않은 나머지 손가락들로 구성된다. 이러한 구분은 여러 물체를 동시에 운반하면서도 개별 물체를 정밀하게 집고 놓는 작업을 수행할 수

있도록 돕는다. 손의 기능적 구분이 효과적으로 작동하기 위해서는 파지 구역과 저장 구역 간 물체를 이동시키는 방법이 필요하다. 인간은 손 안에서 물체를 이동시키는 기술, 예를 들어 손가락에서 손바닥으로, 또는 손바닥에서 손가락으로 물체를 옮기는 기술을 사용하여 두 구역들 간에 물체를 이동시킨다. 이 기술들을 각각 손가락–손바닥 이동 동작, 손바닥–손가락 이동 동작으로 부른다. 손가락–손바닥 이동 동작은 파지 구역에서 잡은 물체를 저장 구역으로 옮겨 임시로 저장할 수 있게 하며, 파지 구역이 다양한 물체를 집고 놓는 작업을 자유롭게 수행하는 동안 저장 구역이 다수의 물체를 저장할 수 있도록 한다. 또한, 손바닥–손가락 이동 동작은 저장 구역에서 저장된 물체를 파지 구역으로 하나씩 옮겨 파지 구역이 각 물체를 꺼내 원하는 위치에 배치할 수 있도록 한다. 이와 다르게 기존의 다물체 파지 그리퍼들은 여러 물체를 동시에 운반할 수는 있었지만, 저장 구역의 임시 저장 기능과 파지 구역의 정밀한 파지 및 정렬 기능을 결합한 통합 기능이 부족하여 물체를 하나씩 잡거나 놓는 데에 한계가 있었다.

본 학위 논문에서는 다물체 파지 그리퍼의 파지 및 정렬 기능을 향상시키기 위해 손의 구역 분할과 손 안에서의 물체 이동 기능을 적용한 다물체 파지 그리퍼를 제안한다. 제안된 그리퍼는 네 개의 손가락으로 이루어진 파지 구역과 두 쌍의 적응형 컨베이어 벨트로 구성된 저장 구역으로 구성된다. 손가락은 다양한 방향에서 개별 물체를 집을 수 있으며, 이를 손가락–손바닥 이동 동작을 통해 저장 구역으로 옮겨 저장하고 함께 이동시킬 수 있다. 물체를 이동시킨 후, 손바닥–손가락 이동 동작을 통해 손가락이 저장 구역에 저장된 물체를 하나씩 꺼내 원하는 위치와 방향으로 배치한다. 기존의 단일 물체를 집는 방식에 비해, 추가적인 물체 이동 과정 및 저장 과정은 전체 파지 및 정렬 과정을 느리게 만들 수 있다. 따라서 간단한 손가락–손바닥 및 손바닥–손가락 이동 동작을 위한 파지 구역 설계와 다수의 물체를 동시에 저장하고 이동시킬 수 있는 저장 구역 설계가

제안되고 분석되었다. 실험적 비교 결과, 제안된 다물체 파지 그리퍼는 단일 물체를 파지하는 과정에 비해 파지 및 정렬 과정에 걸리는 시간을 약 34% 단축할 수 있음을 확인하였다. 또한, 개발된 다물체 파지 그리퍼의 파지 및 정렬 기능의 다양성은 실험실 규모의 가정 환경 시연 (책상 치우기)을 통해 검증되었다. 나아가, 다물체 파지 그리퍼의 응용을 위한 최적 경로 생성 알고리즘이 개발되었으며, 이 알고리즘을 책상 치우기 문제 (declutter problem)에 적용하여 제안된 그리퍼의 파지 및 정렬 효율을 향상시킬 수 있음을 확인하였다.

본 논문에서 제안된 다물체 파지 그리퍼는 손의 구역 분할과 손 안에서의 물체 이동 기능이 다물체 파지 그리퍼의 파지 및 정렬 기능을 향상시킬 수 있는 가능성을 강조하며, 다물체 그리퍼의 적용 범위를 넓힐 수 있음을 보였다.

주요어: 다물체 파지 그리핑, 사람 손, 로보틱 그리퍼, 소프트 로보틱스, 적응형 메커니즘

학 번: 2017-23593